25 October 2017
Submitted to Pure and Applied Geophysics

Seiches in the Eastern Caribbean

Philip L. Woodworth

National Oceanography Centre, Joseph Proudman Building, 6 Brownlow Street, Liverpool L3 5DA, United Kingdom

Email:plw@noc.ac.uk, Tel: +44-151-795-4860, ORCID: 0000-0002-6681-239x

Abstract

Data from a network of tide gauges in the eastern Caribbean have been used to investigate the periods and amplitudes of seiches at each station, and the coherence in seiche activity between stations. Seiches in this area have very small amplitudes, but they can be readily identified in the sea level spectra obtained from high-quality, high-frequency tide gauges. Most of their periods are found to be determined by the quarter-wavelength response of the adjacent shelf, and their Q values are generally consistent with them being relatively undamped. At several stations, the forcing responsible for the seiches is clear. At others, the forcing is harder to pin down, seiches appearing seemingly randomly, and resulting in what has been called 'continuous seiche'. Overall, it is demonstrated that seiches (or at least their statistics) need to be better understood and to be included effectively in studies of extreme sea levels. Also related to shelf resonance, two possible examples of 'tidal ringing' have been identified.

Keywords: Coastal seiches; Shelf resonance; Tidal ringing; Tide gauge networks

1. Introduction

Seiches are high frequency oscillations of sea level with periods of minutes to hours. They can be found in almost all tide gauge records with amplitudes at some locations that are comparable to those of the tide. And yet, seiches are a much under-studied aspect of sea level science. There have been many investigations of seiches in one, or a small number of, individual records (for a partial list, see chapter 7 of Pugh and Woodworth 2014, or Rabinovich 2009). However, there has been almost no consideration of seiches on a regional basis.

Seiches are a type of resonance in which the sea level oscillates at a natural period of a harbour, bay or continental shelf (Rabinovich 2009). They are particularly evident when set in motion by the impulse of an incoming tsunami wave, or by a landslide following a large local earthquake, following which the amplitude of the seiche reduces over several cycles (Kulikov et al. 1996). However, they can also be energised by rapid changes in the winds (Heaps et al. 1982), or by abrupt changes in air pressure gradient (Donn and Wolf 1972), sometimes associated with 'meteotsunamis' following thunderstorms (Sibley et al. 2016). Seiches can also result from rapid changes in barotropic tidal elevations and currents (Golmen et al. 1994; Park et al. 2016), by internal tides that can have travelled a considerable distance from their origin (Chapman and Giese 1990; Giese et al. 1990; Wijeratne et al. 2010), and by wave energy impinging on a harbour (Okihiro et al. 1993). Conceivably, they could also occur due to rapid changes in the coastal ocean circulation.

Therefore, there are many possible reasons for seiches, and there may be more than one reason at any one time and location. Consequently, it is not surprising that seiches at some places are present almost continuously, or at least for a large fraction of the time. In these cases, the seiche amplitudes tend not to decrease smoothly, as in the example of an impulse, but appear to be near-continuously

re-energised. The origin of 'continuous seiche' at particular locations has exercised several previous investigators (e.g. Park et al. 2016).

The present paper describes a regional study of the occurrence of seiches, making use of an extensive set of tide gauge records from Puerto Rico and the Leeward and Windward Islands in the eastern Caribbean. A large network of gauges allows the spatial coherence of variations in seiche amplitude to be studied and the reasons for seiches to be better understood. In each case, the main seiche periods can be readily determined by spectral analysis of the sea level records, and the character of the seiches (near-continuous or otherwise) can be investigated. It will be seen that seiches occur at almost all locations and almost continuously, although they may have very small amplitudes.

Section 2 provides details of the tide gauge and meteorological data sets. Section 3 then provides a description of the seiches observed through the region. Sections 4-6 are concerned with explaining the frequencies and widths of the seiche peaks observed at each location, what the reasons might be for them, and why some station records display no evidence for seiches. Section 7 presents the evidence for 'tidal ringing' at certain sites. Conclusions are given in Section 8. A 'postscript' for 2017 follows in Section 9.

2. Data Sets

Most sea level records used here are 1-minute values during 2015-16 obtained from the Sea Level Station Monitoring Facility (SLSMF) of the Intergovernmental Oceanographic Commission (IOC) (http://www.ioc-sealevelmonitoring.org). Many of these 24 records come from either radar or acoustic tide gauges that have been installed in recent years as part of the Caribbean Tsunami Warning Programme of IOC (http://www.ioc-tsunami.org) with data transmitted in near real-time to the SLSMF by either satellite or internet (IOC 2016). Table 1 provides a list of stations while Figure 1(a) shows their locations.

The SLSMF was established to support IOC tsunami programmes in several regions, and also the Global Sea Level Observing System (GLOSS) (IOC 2012), by providing a means for operators to check that their gauges were functioning correctly. Its data archive was not intended to be a resource for scientific research, although some investigators of sea level variability have taken advantage of it (e.g. Vilibić and Šepić 2017).

The SLSMF records are without any kind of quality control (QC), and a first task, therefore, was to remove as many as possible of the instrumental anomalies in the 1-minute values using standard QC procedures (IOC 2016). Most of these anomalies take the form of large positive or negative data spikes that one suspects result primarily from transmission errors. However, several of the records, from northern stations, in particular, were found to have more spikes than could be handled in this way, requiring special software to be written to remove them. Such software is not without its dangers, by removing genuine high-frequency variability such as seiches along with any instrumental errors. Nevertheless, visual inspection of the original and final records suggests that the method used was an efficient one. A final problem concerned some records containing regular short transmission gaps, different for each station, which needed to be identified and filled to provide continuous time series for spectral analysis.

Five additional sea level records between Grenada and St. Vincent in the south of the region were acquired from the UK Hydrographic Office (UKHO) (Figure 1b). These short records were obtained during hydrographic surveys and span only several weeks each. Radar and pressure sensors were used that were set to record in 40-second bursts every 10 minutes. Although these records are short, they

should be long enough to identify if seiches exist at a location, even if their time dependence cannot be investigated in any detail.

Meteorological station records containing hourly wind speeds and directions and air pressures were obtained from the US National Centers for Environmental Information (https://www.ncdc.noaa.gov/cdo-web/datatools/lcd), Center for Operational Products and Services (https://tidesandcurrents.noaa.gov/), and National Buoy Data Center (NDBC) (http://www.nbdc.gov.uk), Météo France (https://donneespubliques.meteofrance.fr), the St. Lucia Meteorological Department, and Barbados Meteorological Services. The NDBC also provides higher-frequency meteorological station data. ERA-Interim reanalyses from the European Centre for Medium-Range Weather Forecasts (Dee et al. 2011) provided 6-hourly winds, air pressures and waves during 2015-16 on a 0.75° grid.

3. Seiches at Each Location

3.1 Data Processing

Power spectral densities (PSDs) were produced for each of the 1-minute time series. As an example, Figure 2 shows the spectrum for Magueyes Island, indicating a peak at 1.175 cph (51 min period). In many cases, there was a single peak, standing out clearly above the background, as in Figure 2. However, in other cases, there were two or more peaks indicating more than one seiche modes. In each case, a main frequency was selected from the spectrum on the basis of greater power and/or lower frequency. Each main frequency and, in some cases, a secondary one are listed in Table 1; the selection of these frequencies can be understood by inspection of the spectra in the Supplementary Material (Figures SM1.1-43).

For each station, a 'seiche band' was defined to span the main seiche peak. In the example of Figure 2, the band was defined to span 0.95-1.45 cph; those for all other stations are given in Table 1. The exact choice of limits for each band is not a critical one, given that the peaks always have a considerably greater power than any background near to the band limits.

Band-pass filtering between the two limits of the band was made using the IDL 'digital_filter' function (IDL, 2017), thereby obtaining a time series of the sea level seiche. The application of such a filter has the desirable aspect of providing a seiche time series that is largely insensitive to the data spikes described above. Figure 3 provides an example for Magueyes Island. Figure 3(a) shows the original record (and note the small data spike just before 2300 hours), and Figure 3(b) shows the band-pass filtered time series.

At each point in the record (i.e. the time of each 1-minute value), an estimate of the instantaneous seiche magnitude can be defined by the standard deviation of the filtered variability, within a window with a width equal to the period of the low-frequency limit of the band (i.e. 63 min in this example). This standard deviation is denoted as σ_s and Figure 3(b) provides an example.

As seiche amplitudes vary considerably between sites, it was useful to also define the normalised instantaneous quantity $\sigma_n = {\sigma_s}/{\overline{\sigma_s}}$, where $\overline{\sigma_s}$ is the average of σ_s through the record. σ_n then allows temporal variations in σ_s to be compared between sites.

Table 1 provides a summary of the standard deviations of each filtered record; this is essentially the same as $\overline{\sigma_s}$. It also shows the median and maximum values of seiche range (maximum minus minimum values of sea level) calculated on a daily basis; these quantities are more suitable than the standard deviation for giving a general impression of seiche magnitude. For several stations with peaks at high

frequencies, the seiche is manifested in the spectrum only and is too small to be readily apparent from inspection of the observed sea level time series by eye.

3.2 Eastern Caribbean Setting

Before discussing the seiches obtained at each location shown in Figure 1, it will be useful to point out some aspects of the regional geography, climate and oceanography.

Several stations to be investigated are located on the south coasts of Puerto Rico, the US Virgin Islands and the British Virgin Islands. These are separated from the deep ocean by a continental shelf ~10 km wide, and are sheltered locations in comparison to sites on the north (Atlantic) coasts of the islands (VIPO 1997; Cambers 2005). Most of our other stations are located on the coasts of the southern Leeward and Windward Islands, which are mostly aligned north-south, with a narrow continental shelf to their west (sometimes only a few km wide), and a wider one to their east. Many of the harbours and bays with tide gauges are also on the west coasts, which are relatively sheltered compared to sites on the east coasts, where there are more energetic wave regimes (see discussion in Section 6, Figure SM2.1(a,b), and Cambers 2005). This west-east bias in gauge distribution has occurred partly due to the development of the regional tsunami monitoring network, which has given priority to the installation of new gauges on Caribbean-facing (west) coasts.

The trade winds are a major feature of the regional climate. These winds blow almost continuously from the east, with some reduction in average wind speed during the last few months of the year (September-November) and, to a lesser extent, in April-May (Figure SM2.1(c)). An amplification of the circulation called the Caribbean Low-Level Jet (CLLJ) contributes to the semiannual cycle in zonal wind peaking around February and July. The jet has an axis centred on ~15° N and is strongest towards the western part of the Caribbean Basin (Whyte et al. 2008; Martin and Schumacher 2011). Mean sea level air pressure also reduces during September-November by ~5 mbar and by about half of that amount during April-May. Hurricanes can occur at any time during June-November, with most in August-September (Saunders et al. 2017; Wikipedia 2017a). As a result, storm surges of magnitude ~1 m can occur during times of bad weather (e.g. see Daniel 1996; Zahibo et al. 2007; Krien et al. 2015 for discussion of storm surges in Guadeloupe and Martinique). A number of 'meteotsunami'-type events have been documented around the coasts of Puerto Rico, especially in summer months, which could readily generate seiches (Alfonso-Sosa 2015).

Semidiurnal and diurnal variations in the local meteorology are particularly interesting. Air pressure has a predominantly semidiurnal cycle, as is common throughout the tropics (Pugh and Woodworth 2014, Section 5.5), with an amplitude of more than 1 mbar, peaking at about 1000 and 2200 local time (0200 and 1400 UT). Small diurnal variations in wind speed occur in the synoptic trades (e.g. Cook and Vizy 2010) and are best measured *in situ* by ocean buoys well away from land. However, much larger diurnal cycles in wind speed are found in data from some coastal land stations. These occur due to local sea and land breeze effects, which at locations in the tropics can extend 10s of km from the coast (Miller et al. 2003; Gille et al. 2005), and can affect many physical and biological processes including the local ocean circulation (e.g. Walter et al. 2017). Inevitably, the sea and land breezes are not represented well in large-scale meteorological products such as ERS-Interim.

In all the meteorological records we have inspected from coastal land stations in the northern part of the eastern Caribbean (from the sources mentioned in Section 2), there is a large diurnal cycle in wind speed. Winds are almost absent other than in the middle of the day (0900-1600 local time) and peak at about 1300 local time (1700 UT). By contrast, while there is a similar diurnal cycle in ocean buoy data, it is not the predominant component of wind speed. Figure 4 presents an example from the

south coast of Puerto Rico. Air pressure changes at the Magueyes Island tide gauge are almost identical to those at a buoy located near to the shelf edge. However, the diurnal variation in wind speed is now superimposed on a much larger average wind speed through the day. The semidiurnal cycle in air pressure is much the same as in Figure 4 for stations in the south of the region (close to Castries airport in the NW of St. Lucia and Bridgetown airport in SE Barbados). Wind speed has a diurnal cycle at St. Lucia more like that for the ocean buoy in Figure 4, while that at Barbados is more like that of the Magueyes Island land station.

The ocean tides have small range (several decimetres at most) throughout the region, but are primarily diurnal or mixed on the Caribbean sides of the islands, whereas they are primarily semidiurnal in the southeast of the region, on the Atlantic sides of the Windward Islands. A considerable amount of semidiurnal tidal dissipation occurs on the shelf areas around the Virgin Islands, and in the passages between the Windward Islands (Ray and Egbert 2017), with some tidal energy converted into semidiurnal internal tides in the SE Caribbean (Ansong et al. 2017).

A northern branch of the Caribbean Current passes around the Grenadine Islands and St. Vincent and is seasonally intensified towards the end of the year following freshwater inflow into the region from the Orinoco and Amazon rivers (Chérubin and Richardson 2007; Johns et al. 2014). Upper ocean water temperatures also peak around October (Jury 2011). As a consequence, seasonal thermosteric and, to a lesser extent, halosteric effects result in a strong seasonal cycle in Mean Sea Level (MSL) with a minimum in March and maximum in October. Figure 5 shows time series of daily MSL for 2015-16 for the stations in Table 1, indicating a range of about 20 cm. The cycle is almost the same in all records. All are shown in black, except for the two in colour: Port St. Charles in Barbados, which is located somewhat to the east of the others, and Le Prêcheur which, unlike most other sites, is equipped with a differential (vented) pressure tide gauge. Figure 5 shows that a slightly larger seasonal cycle took place in 2015 than in 2016, and that 2016 also contained a short-term rise in MSL in April-May. A similar (but inverted) time series was found in regional air pressure, and perhaps ~20% of this seasonal MSL variation can be explained by the inverse barometer. This conclusion is consistent with the wider study of the seasonal cycle of MSL in the Caribbean by Torres and Tsimplis (2012).

In summary, there are many meteorological and oceanographic processes that potentially could energise the observed seiches.

3.3 Magueyes Island

Seiches in the eastern Caribbean were first discovered by Harris (1907) in tide gauge charts from Puerto de Guánica on the south-west coast of Puerto Rico. They were investigated later in detail by Giese et al. (1990) in data from Magueyes Island, 14 km west of Guánica. Those authors identified a 1.2 cph (50 minute) seiche that tended to occur approximately 6-7 days following new and full moon. In brief, the interpretation (more recently discussed by Alfonso-Sosa 2015) is that internal tides generated by large semidiurnal tidal currents in the St. Lucia and St. Vincent Passages are scattered in the area of the Aves ridge in the SE Caribbean (Figure 1a), taking several days to travel to the Puerto Rico shelf, where they break, thereby generating coastal seiches. The shelf has a width of approximately 12 km at this point.

Although there have been alternative suggestions for a more local origin of these seiches (Huang et al. 2000; Teixeira and Capella 2000), the Giese et al. interpretation has remained the preferred one, and has recently been supported by the observation from space of internal waves approaching the coast near to Magueyes Island (Alfonso-Sosa 2015).

Giese et al. (1990) had over 10 years of data available for analysis from Magueyes Island (1976-86), whereas we have only two (2015-16). Nevertheless, the findings here are completely consistent with theirs. They identified seiches with a typical height around 10 cm, and their Figure 9 shows their largest example with a height of 23 cm in June 1982. That height can be compared to the tidal range on that day of 12 cm. The present data set has a comparable example with a height of 19 cm on 6 September 2015 (Figure 3b). Neither of these examples is anywhere near as large as the 'super-seiche' with a height of 67 cm that occurred in November 2006 (Alfonso-Sosa 2015).

The peak at 1.175 cph in Figure 2 using data for 2015-16 has almost the same frequency as that found by Giese et al. (1990). If one selects times for which σ_s is large (more than 1.5 times $\overline{\sigma_s}$), and computes the interval since the last new or full moon (syzygy) then one obtains Figure 6. This figure is almost identical to Figure 4 of Giese et al. (1990), confirming that the largest seiche activity occurs approximately 6 days after syzygy.

Therefore, the internal tidal origin of the seiches at Magueyes Island appears to be understood. Giese et al. (1990) obtained identical findings from Guánica Harbor, confirming the earlier work of Harris (1907) at the same location. Evidence had been presented in an earlier paper (Giese et al. 1982) that similar seiches occurred on the SW section of coast from Punta Cabo Rojo in the west (the SW corner of Puerto Rico) to Punta Salinas in the east (close to Guánica Harbor). However, as will be shown below, the same explanation does not apply for seiches with a comparable period that occur at Caja de Muertos, a further 40 km to the east along the south coast. Neither does it apply to the complicated set of seiches observed at Mayagüez on the west coast of Puerto Rico, the next major tide gauge west of Magueyes Island (as shown in the Supplementary Material).

3.4 Northern Group

The 'northern group' of six stations includes (east to west, and as named by the SLSMF): Tortola in the British Virgin Islands; Lameshur Bay and Charlotte Amalie in the US Virgin Islands; and Vieques Island, Yabucoa Harbor and Caja de Muertos in Puerto Rico (Figure 1a). All except Caja de Muertos are located on the south (Caribbean-facing) side of their islands, separated from the deep ocean by a continental shelf that varies between 4-18 km. Caja de Muertos is a small island nearer to the shelf edge than to the Puerto Rico mainland coast. There are large differences between the seiches observed at each station, some sites having simple peaks, others having multiple ones. For example, the main seiches at Charlotte Amalie have periods of 45 and 24 minutes (Figure SM1.21 and Table 1), which are identical to the seiche periods estimated by Rabinovich et al. (2006) for this station using data from the days following the Sumatra tsunami.

The frequencies of the main peaks for the northern group stations vary between 0.975-3.675 cph (Table 1). The seiche amplitudes also differ between sites, with no obvious spatial dependence, and most are small. In spite of these differences, all sites display much the same temporal behaviour. Figure 7 shows time series of seiche activity when σ_n is averaged into daily values. The most obvious aspect of this figure is that each of the six sites has near-constant values of daily average σ_n. There are relatively few examples of days with σ_n being considerably larger than 1.0. This can be expressed quantitatively in terms of skewness values for the six time series of between 0.82-1.56, which contrasts to 3.27 for Magueyes Island, shown for comparison in Figure 7.

Although seiche activity at the six stations is largely continuous, there is some variability in daily average σ_n which is coherent between sites. Some of the peaks in each record are clearly to do with major storms or hurricanes. For example, it can be seen that a peak occurs in Figure 7 in Tortola, Charlotte Amalie, Vieques and Caja de Muertos on 31 July-1 August 2016 that coincides with the

precursor of Hurricane Earl (Wikipedia 2016). Coherent variability, due to meteorology or other processes, is demonstrated to some extent by the correlation coefficients between pairs of daily average values in the records given in Table 2(a). (A correlation coefficient as small as 0.11 would be considered significantly different from zero at 95% confidence level given a year of data in common, if the daily values are assumed to have little serial correlation, and as small as 0.073 for two years in common.)

The six time series can be combined into one average record for the region (Figure 8) indicating values that were ~20% larger around October 2015 and ~10% larger in April-May and October 2016. These were times of higher MSL as shown in Figure 5, suggesting that the magnitude of seiches could depend at least partly upon hydrographic conditions. Figure 8 also shows a trend in addition to the seasonal cycle, with σ_n increasing by ~9% over the two years. MSL (Figure 5) also has a positive trend in this period.

Some of the positive correlation in Table 2(a) will stem from this seasonality. However, if the time series are high-pass filtered to keep variability on timescales of less than a month only, much the same coefficients are obtained (Table 2b). In addition, autocorrelation of the time series in Figure 8 has a width of 1-2 days, which is a timescale consistent with at least some of the seiche variation having a source such as tides, meteorology or waves. A similar conclusion is drawn from using 1-minute values of σ_n instead of the daily average values. For example, the largest 1-minute values of σ_n at Charlotte Amalie and Tortola (somewhat smoothed out by daily averaging) occurred on 29 September 2016 during Hurricane Matthew. Values of 1-minute σ_n are correlated moderately, with a correlation coefficient of 0.2 and a lag of less than an hour.

The 1-minute values of σ_n at each station, when averaged in terms of hour in the solar, lunar or sidereal day, show no evidence for diurnal or tidal modulation, which could suggest that tides or sea breezes do not play a major part in generating the seiches. However, this conclusion could be misleading, and will depend on the rate of dissipation of seiche energy, as discussed in Section 6.

In summary, Figures 7 and 8 and Table 2 show that there is some correlation between the magnitude of seiches at the six stations and at Magueyes Island. Giese et al. (1990) demonstrated that higher seiche activity occurs at Magueyes Island around May and in September-November, similar to that at the six stations. However, none of the six stations (including Caja de Muertos) have as many large values of σ_n, or exhibit a peak in seiche activity with respect to syzygy, as does Magueyes Island in Figure 6. Altogether, this suggests that the contribution of internal tides to seiches is largely confined to the west end of the south coast of Puerto Rico, and results in the large seiches. But that there is also another mechanism, probably of meteorological origin but with some seasonal dependence, that is responsible for a background of low-amplitude seiches along the entire south coasts of Puerto Rico and the Virgin Islands.

3.5 St. Croix Island

St. Croix Island is administratively part of the US Virgin Islands. However, it is located to the south, on the St. Croix Ridge that is separated from the islands in the northern group by the Virgin Islands Trough (>4000m deep). The SLSMF has two records from St. Croix Island. One is from Christiansted Harbor at the eastern end of the north coast: this station is called 'St. Croix' by the SLSMF, so we denote it similarly. The second is from Lime Tree Bay which is a port located in the middle of the south coast.

The St. Croix power spectrum has one seiche peak at high frequency at about 11 cph (and a hint of one just below 1 cph). Lime Tree Bay has many peaks in its spectrum between 1.8-5.9 cph and above, of which the strongest is at 3.775 cph. Band-pass filtering for this peak gives the time series of σ_n in

Figure 9 which is similar to those of the northern group in Figures 7 and 8. In addition to a seasonal cycle, the record shows an increase of 28% in σ_n during the two years, similarly positive but larger than that for the northern group.

3.6 West Coast Stations

The Leeward Islands are the northern islands of the Lesser Antilles chain, from the Virgin Islands in the north as far south as Montserrat. The southern Leeward Islands are separated from the Virgin Islands by the Anegada Passage. The Windward Islands comprise Guadeloupe and the islands to its south. As shown by Figure 1, stations on the west coast of the southern Leeward and Windward Islands are located next to a continental shelf that can be only a few km wide. The seiche amplitudes are comparable to those of the northern group (i.e. they are small, see Table 1) in the cases of the west coast stations at Basseterre (St. Kitts) and Deshaies (Guadeloupe). To their south, Roseau (Dominica) has a high-frequency/low-amplitude peak around 17.4 cph. At Le Prêcheur (NW Martinique), any seiches have amplitudes that are either too small to be detected or their frequencies are higher than 1-minute sampling can resolve. At Fort-de-France (SW Martinique), there is a detectable seiche but its amplitude is sub-cm (Table 1).

Figure 10 shows the time series of σ_n at Basseterre, Deshaies and Fort-de-France. Peaks in common are around 20 April 2015 for Fort-de-France and Deshaies, and 19 October 2016 for Deshaies and Basseterre, which could be associated with storms (although no hurricanes are reported at those times, Wikipedia 2015, 2016). Overall, the time series for Basseterre is uncorrelated with the other two. Deshaies and Fort-de-France exhibit a weak correlation (coefficient 0.284). None of the time series have similarities to those of the northern group, and exhibit little or no seasonal variation in σ_n.

The next tide gauge station to the south is at Ganter's Bay, which is located on the north side of Castries Harbour in NW St. Lucia. The harbour is an inlet approximately 2 km long and 0.5 km wide, opening onto the narrow continental shelf. The main peak in the power spectrum is at 3.775 cph (similar to that at Lime Tree Bay) and is discussed below. Smaller peaks are found at 2.775 and 5.275 cph and there is a broad plateau in the spectrum between 12-16 cph.

It is arguable whether Calliaqua and Prickly Bay should be called west coast stations. Calliaqua is located on the south coast of St. Vincent. The only plausible peak in the spectrum is around 7.7 cph (there are suggestions of others around 1.72 and 2.9cph). On the other hand, Prickly Bay, on the south coast of Grenada, has twin peaks at 1.725 and 2.025 cph (the former the stronger) with amplitudes comparable to those of the northern group (Table 1).

Finally, there is Port St. Charles on the NW coast of Barbados, much further to the east than the other Windward stations. The only plausible peak in the spectrum is around 6.4 cph.

3.7 Castries Harbour

Special mention can be made of the seiche with a frequency of 3.775 cph (16 min period) at Ganter's Bay, Castries Harbour, St. Lucia. These seiches were found to occur around 1100 and 2200 UT and to decay over several cycles. Figure 11(a) shows one example with a seiche height of ~15 cm. Figure 11(b) presents values of σ_s as a function of time of day showing that most seiche activity occurs around these times.

The radar tide gauge at this location was installed at the end of October 2016 and for about a month such seiches were relatively rare. However, they became more common from November through to May 2017. This winter period coincided with the more frequent use of the port by large cruise vessels. For example, the cruise ship schedule for 2016-17 published by the St. Lucia Air and Sea Ports

Authority (http://www.slaspa.com) shows only one vessel per week during October 2016, increasing to two or three per day in November-April, then declining to one every couple of days after May 2017. The relatively few days of arrivals or departures in October correspond with the fewer days with seiches. Inspection of web sites of ship movements (e.g. http://www.fleetmon.com) confirms that the arrival and departure times of the large cruise vessels coincide with the seiche times.

Cruise ships, such as the *Carnival Fascination* or *Jewel of the Seas*, that use Castries Harbour are typically 80,000 GT (gross tonnage) which corresponds to about 40,000 tonnes displacement (the conversion is not a rigorous one). That is equivalent to ~0.5% of the volume of the harbour. Therefore, two or three ships, which tend to arrive or depart at almost the same times (i.e. within several seiche periods), would displace ~1.5% of harbour volume. One can easily imagine that the displacement of such a large amount of water would induce a seiche in a harbour with a narrow mouth.

3.8 East Coast Guadeloupe and Martinique

As suggested in Section 3.2, more energetic seiches might be expected on the east coasts of the Leeward and Windward Islands than on the west coasts. Unfortunately, there are few east coast stations to investigate this possibility.

The three available are from Guadeloupe and Martinique. Pointe-à-Pitre is the largest town of Guadeloupe, located at the head of Petit Cul-de-Sac Marin bay in the centre of the south-east coast, between the island-halves of Basse-Terre to the west and Grande-Terre to the east. The La Désirade tide gauge is located at the western end of the south coast of La Désirade island, positioned about 20 km off the east coast of Guadeloupe. Le Robert is at the head of a bay on the east coast of Martinique. Pointe-à-Pitre and Le Robert, in particular, have significantly higher seiche amplitudes than those of west coast stations, with seiche heights up to ~20 cm (Table 1). Those at Pointe-à-Pitre have been noted previously and have been associated with Caribbean wave climate (Didenkulova and Zahibo 2007).

Figure 12 shows the time series of σ_n. The peak around 29 September 2016 for Le Robert coincides with Hurricane Matthew. The three time series are correlated weakly (correlation coefficients of 0.311 for Le Robert/La Désirade, 0.391 for Le Robert/Pointe-à-Pitre, and 0.288 for La Désirade/Pointe-à-Pitre). In addition, the autocorrelation of the Le Robert record (the longest of the three) has a width of only ~1 day. This again suggests some common forcing such as tides, meteorology or waves. The Le Robert record also exhibits some seasonality, peaking slightly around October as for the northern group, while seasonal variability is not seen at the other two stations.

3.9 North-Eastern Stations

Saint Martin and Barbuda are located on a wider section of shelf in the NE of the region. The former's tide gauge is located at the eastern end of the Baie de Marigot on the north coast. The tide gauge at Barbuda is on the island's south-west coast. Both records demonstrate evidence for seiches with periods just over an hour (Table 1), with a second peak in the case of Saint Martin, and amplitudes larger than those of the northern group. Each time series of σ_n suggests a near-constant seiche. The two short records do not overlap and so one cannot test for correlation between them. However, they both overlap with that from Basseterre, which provides a correlation coefficient with Saint Martin of 0.457, but no significant correlation with Barbuda.

3.10 UKHO Records

The UKHO provided short (several week) records with 10-minute sampling at five sites in the south of the region (Figure 1b). These included St. George's, the capital of Grenada on the south-west coast,

about 4 km north of the previously-mentioned Prickly Bay on the south coast. The power spectrum has a peak at approximately 1.9 cph, which is mid-way between the double peaks of 1.725/2.025 cph found at Prickly Bay. It is possible that the coarser temporal sampling, and short record, resulted in the double peaks being combined in this record.

Carriacou is a small island to the NE of Grenada and SW of St. Vincent. The power spectrum from Tyrell Bay, on the southwest coast of Carriacou, and one from Owia, on the north coast of St. Vincent, showed no evidence for seiches. However, calculation of their expected seiche frequencies in terms of shelf width (to be discussed for other stations in the next section) suggests that frequencies at these two locations will be above the 3 cph Nyquist frequency for 10-minute sampling. The UKHO record from Calliaqua on the south coast of St. Vincent, obtained from a gauge close to that in the SLSMF set, also showed no evidence for a seiche, but the ~7.7 cph peak reported in Table 1 for Calliaqua would similarly not have been detectable with 10-minute sampling.

The final UKHO record, from a gauge on the west coast of the island of Canuoan, between Grenada and St. Vincent and near to Carriacou, but where the shelf is wider, also demonstrated no seiche peak, whereas calculation suggests that one might exist with a frequency of approximately 1.5 cph.

4. Seiche Frequencies and Shelf Width

Around islands or along island chains there could be a multiplicity of long-shore and cross-shore modes of sea level resonance (e.g. see Munger and Cheung (2008) for discussion of the complicated patterns around Hawaii following the Kuril Islands tsunami in 2006). Nevertheless, inspection of the frequencies in the present data set (Table 1) immediately suggested a relatively simple variation from place to place, with a quarter-wavelength relationship between frequency and shelf parameters:

$$T = 4L/\sqrt{(gh)} \tag{1}$$

where T is the seiche period, L the shelf width (taken as being the 200 m depth contour), g acceleration due to gravity, and h the average depth across the shelf (Rabinovich 2009; Pugh and Woodworth 2014). However, proving such a relationship to an accuracy one would like is difficult, given the lack of detailed bathymetric information in this region. In practice, L and h have been estimated in two ways.

For stations located next to relatively wide shelves, depth information was taken from the GEBCO_2014 data set of the General Bathymetric Chart of the Oceans (GEBCO) (Weatherall et al. 2015). GEBCO_2014 has a 30 arcsecond grid corresponding to ~1 km in this region, and a requirement was made that there were at least 3 grid squares between the coast and the 200m depth contour. Distances were measured in either the W, NW, N etc. directions, whichever seemed the most appropriate direction in each case, as given in Table 3(a). In the case of Caja de Muertos, it was more appropriate to estimate the shelf width and average depth from a point on the mainland to the 200m contour, rather than from the island itself. For stations located next to narrower shelves, the distance and average depth to the 200m contour were estimated from hydrographic charts.

Both of these methods, particularly the latter, are coarse ones. Nevertheless, a relationship between seiche frequency and shelf parameters is obtained (Figure 13), as qualitatively predicted by equation (1). At three of the sites, it became clear that the seiche periods in question were more likely to be associated with either harbour or bay modes, rather than shelf resonances. The resonant periods of idealised harbours and inlets of simple shape can be determined straightforwardly (Wilson 1972; Sorensen 1978; Rabinovich 2009), again yielding periods proportional to the reciprocal of the square root of water depth. In these cases, the seiche periods have been estimated using:

$$T = M\ S\ 4L/\sqrt{(gh)} \tag{2}$$

where L and h are the length and average depth of the harbour or bay. S is a 'shape correction' that depends on the shape of the harbour or bay and its depth profile. M is a 'fractional mouth correction' that accounts for the fact that the seiche node is located outside of the harbour or bay mouth (Neumann 1948; Wilson 1972; Rabinovich 2009). M is defined by:

$$M = \sqrt{1 + 2a} \approx (1 + a)$$

where

$$a = \frac{w}{\pi L}\ (1.5 -\ \gamma - \ln\left(\frac{\pi w}{4L}\right)) \tag{3}$$

and w is the average width of the harbour or bay, and $\gamma = 0.5772$ is Euler's constant. The values assumed for each parameter at each location are given in Table 3(b). This procedure for harbour and bay modes is also imprecise, and given that one is dealing with shorter spatial scales than for most shelf modes, the frequencies involved are higher, and so larger differences between measured and predicted frequencies can be anticipated.

The overall explanation of observed frequencies in terms of simple parameterisations using distances and depths is a satisfactory one, Figure 13 presenting a reasonable correspondence between observed and predicted seiche frequencies.

5. Values of Q

A dimensionless factor Q = f/FWHM is often used to express the extent to which an oscillating system is damped, FWHM being the full width of the peak at half-maximum power (Rabinovich 2009). In principle, Q should be straightforward to calculate for every seiche peak in Table 1. Magueyes Island (Figure 2) provides a good example. In this case, a Gaussian fit to the power spectrum provides a suitable description of the peak, with a standard deviation and central value of 0.088 cph and 1.175 cph respectively, and, therefore, a FWHM of 0.207 cph and a Q of about 6. However, this procedure is not as simple for all the peaks in Table 1. In some cases, they are part of a set of more than one peak on a broad background, in others they may be split, or otherwise not approximately describable by a simple Gaussian.

Table 4 gives a list of values of Q estimated by Gaussian fitting for each of the peaks identified in Table 1, and as shown in the Supplementary Material. Where there is a 'good fit' or 'reasonable fit' (a subjective opinion), then a Gaussian does a reasonable job of parameterising the power spectrum around the peak. These are cases where the signal-to-noise ratio is relatively high. In 'approximate fit' cases then the fit is cruder, usually because the peak shape is narrower or wider than a Gaussian would suggest. In some cases, where the peak is part of a wide band of energy, then it is impossible to use a simple fit; all such cases are mentioned in the Comments column of Table 4. The difficulties of determining Q in some cases may be appreciated from inspection of the spectra themselves in the Supplementary Material.

In most cases of a 'good or reasonable fit', Q has a value of 10-15, which is consistent with peaks with the same frequencies (associated with particular shelf parameters) having similar widths, and therefore similar dissipation. Such values of Q are usually said in engineering studies to represent relatively undamped systems, which could explain why seiches are present at many places on a near-continuous basis. For example, Figure 11 shows examples of seiches from Ganter's Bay, where there is a Q of 17 and, thereby, a time constant $\tau = \frac{Q}{\pi f}$ = 1.47 hours or about 5-6 cycles (τ being the time

for which the envelope of an oscillating system decays to 1/e = 0.37 of its initial value). Even in this example, which is more akin to the 'impulse' situation mentioned above, it is easy to see how, in practice, seiches can be present for much of the time. In other cases, the seiche could be even more frequently re-energised by processes to be discussed in the next section.

Table 4 shows that Q has a smaller value of around 5 for several stations in the Virgin Islands and south coast of Puerto Rico, at Charlotte Amalie, Tortola, Magueyes Island and Mayagüez, but not at Caja de Muertos, Yacuboa Harbor or Vieques, which might be explained partly by more damping on the wider shelf at the former locations (Table 3). It is interesting that similar Q is obtained for nearby stations, and that at Charlotte Amalie, Yabucoa Harbor and Vieques, where there are two main peaks, the Q of the higher frequency peak is the larger. Otherwise, Q does not seem to be related to either frequency or amplitude.

A value of Q of about 5 is more like that obtained for seiches in Monterey Bay (Breaker et al. 2010; Park et al. 2016). Other examples of Q values around the world are given by Rabinovich (2009). However, comparisons between Q obtained at distant locations may not be meaningful, when the background ocean conditions (especially tidal currents), on which seiche motions are superimposed, are so different.

A complicating factor in determining the FWHM of a peak accurately is the possible existence of sidebands. Teixeira and Capella (2000) showed that, when many years of data are used, the Magueyes Island power spectrum can be seen to include secondary peaks, split from the main peak by frequencies of once per fortnight, day or half-day, due to its tidal origin, as described above. In cases when sidebands exist but are not fully resolved, the Q of the main peak may be estimated too low as the sidebands folded in with the peak could have made it appear wider than it really is. The high-amplitude seiche at Le Robert provides an example of sidebands being fully resolved. Its spectrum (Figure 14a) suggests a narrow peak and sidebands split from the main peak by approximately one, or possibly two cycles/day. This Gaussian fit provides one of the largest values of Q in Table 4, suggesting that the seiche at this location is in almost perfect resonance.

6. Reasons for Seiches (or Their Absence)

The power spectrum of any tide gauge record contains peaks due to tides and seiches, together with a continuum that has an overall level that varies from site to site, but which usually decreases roughly exponentially with frequency (i.e. it is approximately 'red'). Therefore, given that any peaks must have greater power than the background continuum (by definition), then one perspective on Table 1 might be that it must be biased in favour of seiches with higher frequencies. This suggestion, which is not supported by the table, is based on an assumption that power in any seiche peak must be independent of the power in the background.

Another perspective is that the important thing is that a continuum exists at all, reflecting sources of energy in physical processes in the ocean across a wide range of frequency. Therefore, given that there are frequencies within the continuum that correspond to natural modes, then it is not surprising that those modes are energised preferentially, compared to frequencies either side, resulting in the observed peaks. In this situation, any genuine modes (seiches) are always likely to be identified, and not buried in the continuum (as long as their Q is large enough), no matter their frequency. An obvious supplementary question is then to ask what processes, in fact, generate the sea level continuum, but we leave that aside for a moment.

Support for this perspective comes from sites where there are two or more peaks in the spectrum. Wavelet analysis can be used to investigate how the variability in sea level at each frequency varies

through the record. It has been found that energy at each seiche frequency fluctuates similarly, suggesting that they are energised in a similar same way by whatever processes are responsible for sea level variability across the spectrum. The different values of Q for seiches in spectra with more than one peak suggest that dissipation occurs differently at different frequencies. However, it is not clear that Q has meaning for multiple modes, or for broadly distributed spectral energy.

Consequently, it is reasonable to argue that, as a general rule, any seiches with high frequencies will have smaller amplitudes than those at lower frequencies, without being able to say precisely what the amplitudes will be. Port St. Charles, Calliaqua, Roseau and St. Croix in Table 1 provide high-frequency/low-amplitude examples. A further issue is then that, if the frequency is too high, it may be higher than the Nyquist frequency of the tide gauge sampling. Le Prêcheur could be an example in the present case, given the 1-minute sampling; from the estimated shelf width and average depth in Table 3, one can estimate that the period of the quarter-wave shelf mode at Le Prêcheur would be about 1.6 minutes.

One further aspect that could be important in determining any seiche amplitude, in the case of shelf resonance, could be whether the gauge is installed on a straight coastline or in a small bay opening onto the shelf, whereby the bay would provide some kind of energy focusing effect. Deshaies and Le Robert might be examples on the west and east coasts respectively.

Therefore, it is possible to see in a general way why seiches might be found at some sites and not at others. We believe that seiches are generally endemic throughout the region. Therefore, at locations without observed seiches, it must be because they have too high a frequency, and too low an amplitude, to be recorded. All the no-seiche sites in our sample are consistent with this picture.

This takes us to consideration of the primary forcings for the seiches that are observed. The only sites for which a clear physical explanation has been suggested so far have been Magueyes Island (internal tides) and Ganter's Bay (ship movements). The latter's man-made seiches raise the question of whether seiches at other sites might also be due partly to marine traffic. Presumably, they would manifest themselves primarily in daylight hours (roughly 1000-2200 UT). However, given that seiches at most of the other 23 sites appear to be associated with variability on the shelf rather than in confined harbours (Figure 13), the large-scale influence of marine traffic appears unlikely.

At other sites, specific explanations for the seiches are much harder to arrive at, primarily owing to them being near-continuous and with large values of Q. Near-continuity could be expected if the analysis method described in Section 3.1 was just providing σ_s values that were standard deviations of noise, and indeed there are sections of some records where the seiche is not discernible by eye and manifests itself only as a peak in the spectrum. Nevertheless, all the peaks in Table 1 show themselves clearly above the background continuum and, as long as the band-pass filtering works correctly, genuine seiche estimates should be obtained. Variants of the code used to determine σ_s were investigated (e.g. the use of harmonic fits to data instead of standard deviations within windows) with no significant modifications to findings.

Explanations for the seiches can be discussed on three timescales: (1) semidiurnal and diurnal, (2) fortnightly, and (3) seasonal and long term.

(1) If the seiches have a semidiurnal or diurnal forcing, such as the tide or local wind, then one might expect there to be a similar time dependence in seiche magnitude. That should produce sidebands at frequencies ±0.04 and ±0.08 cph of the main peak. However, the spectra (Figures SM1.1-43) show the widths of most of the seiche peaks are similar to or larger than this (or one could say that their Q is too low). Therefore, any sidebands will not be fully resolved but combined into the

overall peak. In this situation, it will not be possible to demonstrate the semidiurnal or diurnal variation of seiche magnitude by means of, for example, plots of σ_s as a function of time during the solar, lunar or sidereal days.

One location where sidebands in the spectrum appear to be found is Le Robert (Figure 14a). Figures 14(b,c,d) show the variation of the 50, 70 and 90 percentile values of σ_s for each hour of the solar, lunar and sidereal days, expressed as a percentage departure from the average of each percentile through the day. There can be seen to be ±10% twice-daily variation for each percentile during the lunar day (Figure 14c), suggesting a modulation of σ_s with the M2 lunar tide. This is consistent with Le Robert being located on the east side of Martinique where the tide is predominantly semidiurnal. However, there is less of a modulation during the solar and sidereal days, which suggests that tides are not primarily responsible for the larger diurnal sidebands in Figure 14(a), and so leaves them unexplained.

(2) Daily average values of σ_s can be investigated to test for fortnightly (or other) variation, fortnightly being suggestive of tidal forcing. Tests can include a standard spectral analysis of the σ_s time series. However, such tests failed to show evidence for fortnightly peaks. An alternative approach is the use of Empirical Mode Decomposition (EMD), as developed by Huang and Wu (2008) and employed by Park et al. (2016) in a study of seiches at several locations in the Pacific. (One notes that Chambers (2015) cautioned against making conclusions on low frequency variability in sea level records using EMD).

Figure SM3.1(a) shows the record of σ_n for Le Robert, as in Figure 12, decomposed into 10 intrinsic mode functions (IMFs) and with average periods given in the caption. Figure SM3.1(b) shows the corresponding decomposition for the record of average σ_n for the northern group, as in Figure 8, decomposed into 9 IMFs. The lower-frequency modes in Figure SM3.1(b) describe the seasonal cycle of σ_n with similarities to that in MSL discussed in Section 3.4. In each case, mode 3 could conceivably be claimed to represent a fortnightly mode, with a mean period of 11 and 10 days for (a) and (b) respectively, obtained by counting zero-crossings. The frequency of an IMF varies through the record, and in sections of mode 3 in both (a) and (b) the period is approximately a fortnight. However, the sections do not coincide with the equinoxes or solstices, as one might expect for modulation by the semidiurnal or diurnal tides respectively. Therefore, these two sets of evidence from EMD are not convincing as a demonstration of any tidal influence. Moreover, even if they could be claimed to provide weak evidence, that it is a long way from explaining where most of the seiches come from.

(3) As mentioned in Sections 3.8 and 3.9, the east coast stations and those in the northeast have higher seiche amplitudes than those of the northern group or west coast stations. One oceanographic aspect that distinguishes between stations in this way is wave climate. Figure SM2.1 (a) provides a large-scale map of average significant wave height (SWH) from ERA-Interim, indicating the differences in average values either sides of the islands (data provided on a 0.75° grid and derived from a wave model with a spatial resolution of 110 km, Dee et al. 2011; Aarnes et al. 2015). It also shows how SWH increases in the western part of the Caribbean Basin due to the winds associated with the CLLJ (Appendini et al. 2014). Figure SM2.1 (b) shows examples of time series of SWH at Charlotte Amalie and Le Robert during 2015-16. It can be seen that SWH has roughly the same magnitude through the two years, with largest values at the start and end of the year, and with spikes that are to do with storms and hurricanes such as for Hurricane Matthew at the end of September 2016. On average, SWH at Charlotte Amalie is 72% of that at Le Robert. This approximate constancy in magnitude, similar to that for the seiches, suggests that waves could be one driver of continuous seiches, particularly on the east coasts and at the northeast stations, and especially in large, exposed bays such as at Le Robert, Pointe-à-Pitre and Saint Martin. However, while waves might explain the continuous seiches

of the east coast and north-east stations, they cannot be the whole story for the northern group where there is suggestion of σ_n peaking in October (Figure 8).

Wind speed has a similar seasonal variation to SWH in reducing, rather than increasing, around October. Figure SM2.1c shows the variation in total wind speed at the same locations using ERA-Interim information, and the dominant zonal character of the trade winds results in a similar plot being obtained for zonal wind speed. Vilibić and Šepić (2017) suggested a dependence between the magnitude of high-frequency (< 2 hour) sea level oscillations and the strength of mid-troposphere zonal winds. In turn, that suggests that high-frequency air pressure (or wind) oscillations, which tend to be more intense during high wind conditions, might be a generator of seiches, transferring energy to the sea though resonant or near-resonant forcing. The main focus of Vilibić and Šepić (2017) was on the latitudinal dependence of such processes, instead of variability through the year. However, Figure SM2.1(c) suggests that such a link does not apply in the present case.

The relationship suggested by Vilibić and Šepić (2017) can also be investigated using 6-minute wind and air pressure records from NDBC meteorological stations. Two records from our area (Charlotte Amalie and Barbuda) are almost complete during 2015-16. Figure SM2.1d plots the zonal wind speed at the former, which can be seen to be similar to that obtained from ERA-Interim data in Figure SM2.1(c). (Most station winds have a smaller magnitude than those in ERS-Interim, presumably because of land shelter for the former and the latter being 10-m winds). The standard deviation of 6-minute zonal winds each day (Figure SM2.1e) has a similar magnitude through the year, reflecting the regular diurnal cycle in winds discussed in Section 3.2, with a small seasonal variation superimposed similar to that for the daily winds in Figure SM2.1c. In addition, the standard deviation of zonal wind within 2-hour windows (akin to Vilibić and Šepić 2017) is also roughly constant (Figure SM2.1f). Similar findings are obtained for Barbuda. It seems, therefore, that high-frequency variability in zonal winds (which will include gusts) can be considered as another candidate source of 'constant seiche'.

The seasonal cycles in σ_n and MSL for the northern group are similar, and both exhibit positive trends during 2015-16. This suggests seasonal and interannual changes in hydrographic conditions. (MSL change will also have a contribution from vertical land movements. However, they are likely to be small over two years.) One could also imagine secular changes in the tides inducing changes in σ_n. However, 2015-16 coincides with a point in the lunar nodal cycle of minimum diurnal (K1) and maximum semidiurnal (M2) tidal amplitudes (Pugh and Woodworth 2014). Consequently, amplitudes cannot have been changing rapidly at this time.

In summary, most stations experience near-continuous, low-amplitude seiche activity that suggests a near-constant forcing such as tides, regular diurnal wind variations, high-frequency wind variability, or waves (the latter including wind waves through to infragravity waves). However, deciding between them, on the basis of observational data alone, is extremely difficult owing to the values of Q that pertain at most stations. At sites such as Le Robert, waves provide the most likely candidate for the forcing, there being only a small seasonal variation in SWH. However, there is a need to explain the larger seiches around October (and possibly April) in the northern group, for which the similarity of the seasonal cycle of MSL provides a possible hydrographic clue. For this aspect of the northern group at least, it seems that we are not much further on in understanding the seiches than were Giese et al. (1990). In general, it does seem most likely that there is more than one contribution to the forcing at every site (as concluded by Park et al. 2016 for Pacific locations), with the high Q serving to make them essentially continuous. It is clear that greater understanding of the seiches will require detailed, and localised, observations and ocean modelling.

7. Tidal Ringing

One consequence of shelf resonance is the preferential amplification of higher tidal harmonics when they have frequencies close to those of shelf modes. For example, Cartwright and Young (1974) found an anomalously large M12 component in the spectrum of a record at Balta Sound in the Shetland Islands, and also in nearby offshore pressure recorder data, but not in data from locations to the south. They suggested that the enhancement at M12 (which had an amplitude of only ~4 mm but which was manifested clearly in the spectrum) was due to a form of shelf resonance. They coined the term 'tidal ringing'.

All the power spectra in the Supplementary Material show the presence of tidal lines at 4th-diurnal, 6th-diurnal etc. frequencies (the figures start at 0.1 cph in order to cut off the large main peaks of the diurnal and semidiurnal tides). In most cases, the significant peaks are limited to 6th-diurnals or so. However, for some stations many more lines can be seen. Fort-de-France is an example where the tide is small and predominantly diurnal with M2, S2, K1, O1 amplitudes of only 6, 1, 9 and 7 cm respectively, and the background continuum is also small (in comparison to a higher latitude location such as the Shetland Islands, for example). The spectrum shows well-resolved lines up to M16 (0.644 cph) with peak frequencies that indicate them to be primarily harmonics of M2 rather than K1. There is then a gap in the spectrum, until another peak at around M22 (0.886 cph), that has a tiny amplitude (~1 mm) but is nevertheless clearly evident in the spectrum, at the start of what we have considered to be the broad seiche band around 0.9-1.1 cph (Figure SM1.10). There are no other peaks at higher frequencies.

This is a most peculiar tidal record with many more harmonics than are usual in such spectra. It has to be emphasised that the amplitudes of the harmonics are minute, and one has to be very concerned that they could have an instrumental origin. However, it is hard to see how transmission gaps, for example, which tend to occur at similar times each day, can introduce power at multiples of lunar tidal frequencies. Timing errors, such as clock drifts, can produce false harmonics, but the requirements of satellite data transmission impose a tight timing control on modern tide gauges. The signals have been verified to occur in both halves of the record, so for the moment we conclude that they are real.

These peaks might be explained as follows. Although K1 has the largest amplitude, that of O1 is comparable, a situation which applies for the diurnal tides at all of the Caribbean-facing stations in the northern part of this region. When K1 and O1 have similar magnitude, they can combine into what is effectively an M1 carrier wave within an envelope of a fortnight (see, for example, Woodworth et al. 2005). It is not surprising, therefore, that any higher-order harmonics of the main components have frequencies that are multiples of M1, M2 etc. What is surprising is that there are so many of them at Fort-de-France, up to M16. We assume that the M22 peak is amplified preferentially over the evidently absent M18 or M20 by having a frequency close to that of the seiche band, and so this can be considered as another example of 'tidal ringing'. On the other hand, there is no M24 or M26 that one might have expected to be energised within the band itself.

Another example in our data set is an anomalous peak at M14 in the 1-minute data from Port St. Charles (Figure SM1.3). This is another very small signal, with an amplitude of only 2.1 mm, but is resolved well in the spectrum by the 1-minute sampling, and has been checked to be present in both halves of the record. Port St. Charles is a marina on the NW coast of Barbados, 20km north of Bridgetown. For comparison, Figure SM4.1 shows the corresponding spectrum for Bridgetown using 6 months of hourly data from 1995 obtained from the University of Hawaii Sea Level Center (http://uhslc.soest.hawaii.edu/). Peaks of the main diurnal, and predominantly semidiurnal, tides can be seen in both spectra, together with harmonics to 6th-diurnal. However, the 1-minute sampling and

longer record of Figure SM1.3 enable investigation of the spectrum beyond the 0.5 cph Nyquist frequency of Figure SM4.1. It can be seen that M6 and M8 are resolved (0.242 and 0.322 cph respectively) on the left hand side of the plot, and then there is a gap with only hints of M10 and M12, followed by a larger enhancement at M14 (0.564 cph). One can speculate that the time taken for a shelf wave to propagate around the island circumference (97 km) might be close to the M14 period. Although these possible examples of tidal ringing are of interest, their verification will require further measurements to determine their spatial distribution, by tide gauges with the best possible accuracy and sampling, recording to local loggers that provide continuous records with no gaps and without the complications due to satellite data transmission.

8. Conclusions

Seiches have been shown to exist at almost all tide gauge locations in the eastern Caribbean. In many cases, they have a very small amplitude, but their identification has been possible thanks to the high-quality, high-frequency (1-minute) tide gauge data spanning two years (2015-16).

It has been said that 'all science is either physics or stamp collecting' (Wikiquote 2017). The present investigation has been one of 'seiche collecting', and has had only limited success in determining the physical reasons for them. In several cases, their origin is clear, as at Magueyes Island and Ganter's Bay. In other cases, waves appear to be a possible forcing. At Le Robert, there are hints of diurnal and semidiurnal modulation of seiche amplitudes (perhaps meteorological or tidal) at the 10% level, and at several other stations at the ~5% level (but never more than that). The similarity of seasonal cycles of seiche magnitude and MSL in the northern group suggests some hydrographic dependence.

Overall, it seems most practical to regard the seiches as being simple enhancements at natural mode frequencies of a general continuum of sea level variability that has many forcings, with high values of Q that make them near continuous.

So far as we know, the present study has been a rare (perhaps unique) example of an investigation of seiches across a region, instead of at individual locations. The examination of the frequencies in terms of quarter-wavelength shelf resonance, and the tests for coherence between them, shows that if one can understand them more and, if possible, determine what causes them, then one can learn about processes in the ocean in general. At least, the identification of the main seiches at each location indicates the frequencies at which sea level will oscillate should tsunamis occur, as has been known in the Caribbean region during the recent past (Lander et al. 2002). During those events, the seiches arising from tsunamis and other processes can be mixed together (e.g. Rabinovich et al. 2006; Thomson et al. 2007).

Even though the tides in this region are small, the high-quality and high-frequency sea level data have demonstrated the existence of more lines in the tidal spectrum than is usual in examination of sea level records, and they have pointed to two possible examples of an aspect of shelf resonance called 'tidal ringing', identified by Cartwright and Young (1974).

Finally, even though the seiches of the eastern Caribbean are smaller than those reported in some other parts of the world (and the currents associated with them will also be small), it has been shown that they can be as large as 10s cm in places. Therefore, as Vilibić and Šepić (2017) have remarked in the context of high frequency sea level variability in general, they should be taken into account when extreme levels are calculated for coastal engineers. Even if there is a 'continuous seiche', for which the forcing may not be understood perfectly, then it should be possible to combine the statistics of seiche variability with the extreme levels determined by conventional analysis of hourly data into

better estimates of sea level return probabilities. Therefore, studies of seiches in other regions are to be encouraged together with modelling of the processes that might be responsible for them.

9. Postscript October 2017

This paper was written in early 2017 and was based primarily on tide gauge data spanning 2015-16. There were several major hurricanes in those two years such as Matthew, as mentioned above. However, 2015-16 was a relatively calm period compared to the past few months. As of October 2017, there have been two Category 4 and two Category 5 hurricanes during this season, the latter causing tremendous damage. These were Harvey (Cat 4, ~20 August), Irma (Cat 5, ~5 September), Jose (Cat 4, ~9 September) and Maria (Cat 5, ~19 September) (Wikipedia 2017b).

An obvious question is whether these violent events produced rapid and large-amplitude oscillations in sea level (which includes seiches), as a guide to those which might occur during hurricanes in the future, or might follow the impact of tsunamis on these coasts. In fact, the two Category 4 events had little effect (as can be seen from the displays on the SLSMF web site). Harvey passed directly over Babados and St. Vincent in the southern Leeward Islands, and yet the gauges at Port St. Charles (Barbados), Prickly Bay (Grenada), Calliaqua (St. Vincent) and Ganter's Bay (St. Lucia) showed no unusual activity. Jose passed to the NE of the Virgin Islands, but the gauges nearby that were operational (Lameshur Bay, Barbuda, Basseterre), and had not been destroyed by Irma, showed nothing remarkable.

The Category 5 events were more notable. Irma did tremendous damage on land in the northern Leeward Islands, especially in Barbuda and Saint Martin. The Barbuda gauge measured a storm surge of over 2 m on 6 September, with rapid oscillations of ~0.1 m. The Barbuda gauge continued to function, unlike those at Charlotte Amalie, Saint Martin and other locations, which also indicated decimetric oscillations until a break in their records. Hurricane Maria caused considerable damage to Dominica and Puerto Rico. The Roseau tide gauge went out of action. There were storm surges recorded of over 1.5 m at Yabucoa Harbor, ~1 m at Limetree Bay, over 0.5 m at Pointe-à-Pitre, La Desirade, St. Croix, Caja de Muertos and Vieques, and ~0.3 m at Basseterre. Some of these surges (e.g. Pointe-à-Pitre or St. Croix) had almost no accompanying rapid oscillations, while others had decimetric ones with the largest (~0.4 m peak-to-peak) at Basseterre. Therefore, it appears that rapid oscillations in sea level are limited at the several decimetre level, even during the most violent hurricanes.

To test whether the seiches of Table 1 were present as part of the rapid oscillations during these events, power spectra were computed for Yabucoa Harbor and Basseterre during Hurricane Maria for the period spanning 19-21 September. The Yabucoa Harbor spectrum contained broad features at around ~3 and 5.5 cph, similar to those in Figure SM1.40, suggesting that the seiches identified in Table 1 were present to some extent during the hurricane. On the other hand, the spectrum for Basseterre contained no obvious enhancements. One can conclude that, because the seiches we have been interested in form only a small part of the overall high-frequency variability, they may not always stand out in spectra during violent events. Instead, they may be more readily identified during calmer periods even though, as we discussed above, their forcing mechanisms at those times may be uncertain.

Acknowledgements

This investigation started with trying to understand the seiches observed in data from a new tide gauge at Castries, St. Lucia that had been installed by Govinda Augustin and colleagues in the St. Lucia Meteorological Department, and by Jeff Pugh, Dave Jones and Angela Hibbert from the National Oceanography Centre in Liverpool. I am grateful to the IOC Sea Level Station Monitoring Facility and

its data providers for the 1-min sea level data used in this study. Chris Jones is thanked for access to records from UKHO tide gauges. Joe Park, Edwin Alfonso-Sosa, Alexander Rabinovich, Thorkild Aarup and Richard Ray are thanked for comments on a draft of this paper. Part of this work was funded by UK Natural Environment Research Council National Capability funding. Some figures were generated using the Generic Mapping Tools (Wessel and Smith 1998).

References

Aarnes, O.J., Abdalla, S., Bidlot, J-R. & Breivik, Ø. (2015). Marine wind and wave height trends at different ERA-Interim forecast ranges. Journal of Climate, 28, 819-837, doi:10.1175/JCLI-D-14-00470.1.

Alfonso-Sosa, E. (2015). Seiches costeros de Puerto Rico. 65pp. Available from https://www.researchgate.net/publication/309673699. (Last access 27 February 2017).

Ansong, J.K., Arbic, B.K., Alford, M.H., Buijsman, M.C., Shriver, J.F., Zhao, Z., Richman, J.G., Simmons, H.L., Timko, P.G., Wallcraft, A.J. & Zamudio, L. (2017). Semidiurnal internal tide energy fluxes and their variability in a global ocean model and moored observations. Journal of Geophysical Research Oceans, 122, doi:10.1002/2016JC012184.

Appendini, C.M., Torres-Freyermuth, A., Salles, P., López-González, J. & Mendoza, E.T. (2014). Wave climate and trends for the Gulf of Mexico: a 30-yr wave hindcast. Journal of Climate, 27, 1619-1632, doi:10.1175/JCLI-D-13-00206.1.

Breaker, L.C., Tseng, Y. & Wang, X. (2010). On the natural oscillations of Monterey Bay: Observations, modeling, and origins. Progress in Oceanography, 86, 380–395, doi:10.1016/j.pocean.2010.06.001.

Cambers, G. (2005). Caribbean Islands, coastal ecology and geomorphology, pp. 221-226 in Encyclopedia of Coastal Science (ed. M.L. Schwartz). ISBN: 978-1-4020-1903-6. Dordrecht: Springer. 1213pp.

Cartwright, D.E. & Young, C.M. (1974). Seiches and tidal ringing in the sea near Shetland. Proceedings of the Royal Society of London, A, 338, 111-128, doi:10.1098/rspa.1974.0077.

Chambers, D.P. (2015). Evaluation of empirical mode decomposition for quantifying multi-decadal variations and acceleration in sea level records. Nonlinear Processes in Geophysics, 22, 157–166, doi:10.5194/npg-22-157-2015.

Chapman, D.C. & Giese, G.S. (1990). A model for the generation of coastal seiches by deep sea internal waves. Journal of Physical Oceanography, 20, 1459–1467, doi:10.1175/1520-0485(1990)020<1459:AMFTGO>2.0.CO;2.

Chérubin, L.M. & Richardson, P.L. (2007). Caribbean current variability and the influence of the Amazon and Orinoco freshwater plumes. Deep-Sea Research I, 54, 1451–1473, doi:10.1016/j.dsr.2007.04.021.

Cook, K.H. & Vizy, E.K. (2010). Hydrodynamics of the Caribbean low-level jet and its relationship to precipitation. Journal of Climate, 23, 1477–1494, doi:10.1175/2009JCLI3210.1.

Daniel, P. (1996). A real-time system for forecasting hurricane storm surges over the French Antilles. Small Islands: Marine Science and Sustainable Development. Chapter 9 (pp.146-156) in, Volume 51 of Coastal and Estuarine Studies (ed. G.A. Maul). Washington, D.C.: American Geophysical Union, doi:10.1029/CE051.

Dee, D.P. and 35 others. (2011). The ERA-Interim reanalysis: configuration and performance of the data assimilation system. Quarterly Journal of the Royal Meteorological Society, 137, 553–597, doi:10.1002/qj.828.

Didenkulova, I. & Zahibo, N. (2007). Spectrum of the tide-gauge surface waves in Pointe-a-Pitre bay, Guadeloupe. Geophysical Research Abstracts, 9, 11258, SRef-ID: 1607-7962/gra/EGU2007-A-11258.

Donn, W.L. & Wolf, D.M. (1972). Seiche and water level fluctuations in Grindavik Harbor, Iceland. Limnology and Oceanography, 17, 639–643.

Giese, G.S., Hollander, R.B., Fancher. J.E. & Giese, B.S. (1982). Evidence of coastal seiche excitation by tide-generated internal solitary waves. Geophysical Research Letters, 9(12), 1305-1308, doi:10.1029/GL009i012p01305.

Giese, G.S., Chapman, D.C., Black, P.G. & Fornshell, J.A. (1990). Causation of large-amplitude coastal seiches on the Caribbean coast of Puerto Rico. Journal of Physical Oceanography, 20, 1449-1458, doi:10.1175/1520-0485(1990)020<1449:COLACS>2.0.CO;2.

Gille, S.T., Llewellyn Smith, S.G. & Statom, N.M. (2005). Global observations of the land breeze. Geophysical Research Letters, 32, L05605, doi:10.1029/2004GL022139.

Golmen, L.G., Molvaer, J. & Magnusson, J. (1994). Sea level oscillations with super-tidal frequency in a coastal embayment of western Norway. Continental Shelf Research, 14, 1439–1454, doi:10.1016/0278-4343(94)90084-1.

Harris, R.A. (1907). Manual of Tides. Part V. Report of the US Coast and Geodetic Survey, 472-482.

Heaps, N. S., Mortimer, C. H. & Fee, E. J. (1982). Numerical models and observations of water motion in Green Bay, Lake Michigan. Philosophical Transactions of the Royal Society of London, A, 306, 371–398. doi:10.1098/rsta.1982.0091.

Huang, N.E., Shih, H.H., Shen Z., Long, S.R. & Fan, K.L. (2000). The ages of large amplitude coastal seiches on the Caribbean Coast of Puerto Rico. Journal of Physical Oceanography, 30, 2001-2012, doi:10.1175/1520-0485(2000)030<2001:TAOLAC>2.0.CO;2.

Huang, N.E. & Wu, Z. (2008). A review on Hilbert–Huang transform: method and its applications to geophysical studies. Reviews of Geophysics, 46, RG2006, doi:10.1029/2007RG000228.

IDL (2017). Interactive Data Language. http://www.harrisgeospatial.com/SoftwareandTechnology/IDL.aspx.

IOC (2012). The Global Sea Level Observing System (GLOSS) Implementation Plan - 2012. UNESCO/Intergovernmental Oceanographic Commission. 37pp. (IOC Technical Series No. 100). Available from http://unesdoc.unesco.org/images/0021/002178/217832e.pdf.

IOC (2016). Manual on Sea-level Measurements and Interpretation, Volume V: Radar Gauges. Paris, Intergovernmental Oceanographic Commission of UNESCO. 104pp. (IOC Manuals and Guides No.14, vol. V; JCOMM Technical Report No. 89) (English). Available from http://unesdoc.unesco.org/images/0024/002469/246981E.pdf which include a Supplement: Practical Experiences.

Johns, E.M., Muhling, B.A., Perez, R.C., Müller-Karger, F.E., Melo, N., Smith, R.H., Lamkin, J.T., Gerard, T.L. & Malca, E. (2014). Amazon River water in the northeastern Caribbean Sea and its effect on larval reef fish assemblages during April 2009. Fisheries Oceanography, 23, 472–494, doi:10.1111/fog.12082.

Jury, M.R. (2011). Environmental influences on Caribbean fish catch. International Journal of Oceanography, Volume 2011, Article ID 174729, 11 pages, doi:10.1155/2011/174729.

Krien, Y., Dudon, B., Roger, J. & Zahibo, N. (2015). Probabilistic hurricane-induced storm surge hazard assessment in Guadeloupe, Lesser Antilles. Natural Hazards and Earth System Sciences, 15, 1711–1720, doi:10.5194/nhess-15-1711-2015.

Kulikov, E.A., Rabinovich, A.B., Thomson, R.E. & Bornhold, B.D. (1996). The landslide tsunami of November 3, 1994, Skagway Harbor, Alaska. Journal of Geophysical Research, 101, C3, doi:10.1029/95JC03562.

Lander, J.F., Whiteside, L.S. & Lockridge, P.A. (2002). A brief history of tsunamis in the Caribbean Sea. Science of Tsunami Hazards, 20(2), 57-94.

Martin, E.R. & Schumacher, C. (2011). The Caribbean Low-Level Jet and its relationship with precipitation in IPCC AR4 models. Journal of Climate, 24, 5935-5950, doi:10.1175/JCLI-D-11-00134.1.

Miller, S.T.K., Keim, B.D., Talbot, R.W. & Mao, H. (2003). Sea breeze: structure, forecasting, and impacts. Reviews of Geophysics, 41 (3), 1011, doi:10.1029/2003RG000124.

Munger, S. & Cheung, K.F. (2008). Resonance in Hawaii waters from the 2006 Kuril Islands tsunami. Geophysical Research Letters, 35, L07605, doi:10.1029/2007GL032843.

Neumann, G. (1948). On resonance oscillations of bights and the mouth correction for seiches. Deutsche Hydrographische Zeitschrift, 1, 79-101.

Okihiro, M., Guza, R. T. & Seymour, R. J. (1993). Excitation of seiche observed in a small harbor. Journal of Geophysical Research, 98, C10, doi:10.1029/93JC01760.

Park, J., MacMahan, J., Sweet, W.V. & Kotun, K. (2016). Continuous seiche in bays and harbors. Ocean Science, 12, 355-368, doi:10.5194/os-12-355-2016.

Pugh, D. & Woodworth, P. (2014). Sea-level science: Understanding tides, surges, tsunamis and mean sea-level changes. Cambridge: Cambridge University Press. ISBN 978-1-107-02819-7. 395pp.

Rabinovich, A.B. (2009). Seiches and harbor oscillations. In, Handbook of Coastal Engineering (ed. Y.C. Kim), pp. 193–236. Hackensack, New Jersey: World Scientific Publishing.

Rabinovich, A.B., Thomson, R.E. & Stephenson, F.E. (2006). The Sumatra tsunami of 26 December 2004 as observed in the North Pacific and North Atlantic oceans. Surveys in Geophysics, 27, 647-677, doi:10.1007/s10712-006-9000-9.

Ray, R.D. & Egbert, G.D. (2017). Tides and satellite altimetry. In, Satellite Altimetry Over Oceans and Land Surfaces (D. Stammer and A. Cazenave, eds.), *CRC* Taylor and Francis, in press.

Saunders, M.A., Klotzbach, P.J. & Lea, A.S.R. (2017). Replicating annual North Atlantic hurricane activity 1878–2012 from environmental variables. Journal of Geophysical Research Atmospheres, 122, 6284–6297, doi:10.1002/2017JD026492.

Sibley, A., Cox, D., Long, D., Tappin, D. & Horsburgh, K. (2016). Meteorologically generated tsunami-like waves in the North Sea on 1/2 July 2015 and 28 May 2008. Weather, 71, 68-74, doi:10.1002/wea.2696.

Sorensen, R.M. (1978). Basic coastal engineering. Hoboken, New Jersey: John Wiley.

Teixeira, M. & Capella, J. (2000). A long-lead forecast model for the prediction of shelf water oscillations along the Caribbean Coast of the island of Puerto Rico. Proceedings of the OCEANS 2000 MTS/IEEE Conference and Exhibition, doi:10.1109/OCEANS.2000.881296.

Thomson, R.E., Rabinovich, A.B. & Krassovski, M.V. (2007). Double jeopardy: concurrent arrival of the 2004 Sumatra tsunami and storm-generated waves on the Atlantic coast of the United States and Canada. Geophysical Research Letters, 34, L15607, doi:10.1029/2007GL030685.

Torres, R.R. & Tsimplis, M.N. (2012). Seasonal sea level cycle in the Caribbean Sea. Journal of Geophysical Research, 117, C7, doi:10.1029/2012JC008159.

Vilibić, I. & Šepić, J. (2017). Global mapping of nonseismic sea level oscillations at tsunami timescales. Scientific Reports, 7, 40818, doi:10.1038/srep40818.

VIPO (1997). Marine environments of the Virgin Islands. Technical Supplement No.1. Virgin Islands Planning Office. 120pp.

Walter, R.K., Reid, E.C., Davis, K.A., Armenta, K.J., Merhoff, K. & Nidzieko, N.J. (2017). Local diurnal wind-driven variability and upwelling in a small coastal embayment. Journal of Geophysical Research Oceans, 122, 955–972, doi:10.1002/2016JC012466.

Weatherall P., Marks, K.M., Jakobsson, M., Schmitt, T., Tani, S., Arndt, J.E., Rovere, M., Chayes, D., Ferrini, V. & Wigley, R. (2015). A new digital bathymetric model of the world's oceans, Earth and Space Science, 2, 331-345, doi: 10.1002/2015EA000107.

Wessel, P. & Smith, W.H.F. (1998). New, improved version of Generic Mapping Tools released. EOS, Trans. AGU 79, 579.

Whyte, F.S., Taylor, M.A., Stephenson, T.S. & Campbell, J.D. 2008. Features of the Caribbean low level jet. International Journal of Climatology, 28, 119-128, doi:10.1002/joc.1510.

Wijeratne, E.M.S., Woodworth, P.L. & Pugh, D.T. (2010). Meteorological and internal wave forcing of seiches along the Sri Lanka coast. Journal of Geophysical Research, 115, C03014, doi:10.1029/2009JC005673.

Wikipedia (2015). https://en.wikipedia.org/wiki/2015_Atlantic_hurricane_season. (Last access 31 October 2017).

Wikipedia (2016). https://en.wikipedia.org/wiki/2016_Atlantic_hurricane_season. (Last access 31 October 2017).

Wikipedia (2017a). https://en.wikipedia.org/wiki/Atlantic_hurricane_season. (Last access 31 October 2017).

Wikipedia (2017b). https://en.wikipedia.org/wiki/2017_Atlantic_hurricane_season. (Last access 31 October 2017).

Wikiquote (2017). https://en.wikiquote.org/wiki/Ernest_Rutherford. (Last access 1 April 2017).

Wilson, B. W. (1972). Seiches. Advances in Hydroscience, 8, 1–94.

Woodworth, P.L., Blackman, D.L., Pugh, D.T. & Vassie, J.M. (2005). On the role of diurnal tides in contributing to asymmetries in tidal probability distribution functions in areas of predominantly semi-diurnal tide. Estuarine, Coastal and Shelf Science, 64, 235-240, doi:10.1016/j.ecss.2005.02.014.

Zahibo, N., Pelinovsky, E., Talipova, T., Rabinovich, A., Kurkin, A. & Nikolkina, I. (2007). Statistical analysis of cyclone hazard for Guadeloupe, Lesser Antilles. Atmospheric Research, 84, 13–29, doi:10.1016/j.atmosres.2006.03.008.

Figure Captions

1. (a) Map of the eastern Caribbean showing the locations of the 24 tide gauges with 1-minute sea level data. Also shown are the 500m (blue) and 2000m (red) depth contours, with greater depths contoured every 1000m (black annotated). The relatively shallow area in the middle of the map bounded by the red contours marks the Aves Ridge, which separates the deep Venezuelan Basin to the west from the Grenada Basin to the east. (b) Locations of five short records provided by the UKHO between Grenada and St. Vincent: Tyrell Bay, Grenada (TB), St. Georges, Grenada (SG), Calliaqua, St. Vincent (CA), Owia, St. Vincent (OW) and Canuoan (CN). Depth contours as in (a).
2. Power spectral density (PSD) of 1-minute sea levels from Magueyes Island during 2015-16. The figure starts at 0.1 cph in order to cut off the large peaks of the diurnal and semidiurnal tides: the line spectrum of other tidal components can be seen on the left of the plot.
3. (a) Sea levels recorded at Magueyes Island on 6 September 2015 showing a seiche on that day with a magnitude comparable to that of the diurnal tide. (b) The band-passed filtered signal, which is taken to represent the seiche itself, is shown in blue while σ_s, calculated as described in the text, is shown in red.
4. An example of the semidiurnal cycles in air pressures (solid lines) and diurnal cycles in wind speeds (triangles) from the Magueyes Island tide gauge (red) and a buoy anchored in 17 m of water near to the shelf edge, SE of the city of Ponce and to the south of Caja de Muertos Island (blue). Data are for 2015-16.
5. Daily values of MSL at each site in Table 1 (apart from the short record from Ganter's Bay, St. Lucia) with each record adjusted to have zero mean. All records are shown in black except for Port St. Charles (red) and Le Prêcheur (blue).
6. A histogram of the intervals after syzygy for which σ_s values at Magueyes Island are larger than 1.5 times the average σ_s during the whole record.
7. Daily average values of σ_n at the six stations in the northern group and those at Magueyes Island. Stations are shown east to west from bottom to top: Tortola (T), Lameshur (L), Charlotte Amalie (C), Vieques (V), Yacuboa (Y), Caja de Muertos (CM) and Magueyes Island (MA). By definition, σ_n has an average value of 1.0, as indicated in each case by the dashed line.
8. An overall average of the daily average values of σ_n at the six stations in the northern group.
9. Daily average values of σ_n at Lime Tree Bay, St. Croix Island.
10. Daily average values of σ_n at three west coast stations: Fort-de-France (FF), Deshaies (DE) and Basseterre (BA).
11. (a) Sea level during 22-23 November 2016 at Ganter's Bay, Castries Harbour, St. Lucia showing the 16-minute period seiche. (b) A scatter plot of 1-minute values of σ_s versus time of day for the band-pass filtered record (October 2016-May 2017).
12. Daily average values of σ_n at three east coast stations: Le Robert (LR), La Désirade (LD) and Pointe-à-Pitre (PP).
13. Measured and predicted seiche frequencies. For the red and black dots, the predicted seiche frequencies were estimated using equation (1) and shelf parameters were derived from GEBCO bathymetric data, or from inspection of hydrographic charts, respectively. A green dot indicates Caja de Muertos for which a point on the nearby mainland was used to estimate shelf parameters instead of the island location itself. For the blue dots, the predicted seiche frequencies were estimated using equation (2) and harbour or bay parameters in Table 3. Points outside the plotted ranges are Port St. Charles with (observed, predicted) frequencies of (6.4, 10.2), Calliaqua (7.7, 14.4), Roseau (17.4, 22.1) and St. Croix (11.0, 6.5) cph.
14. (a) Power spectrum of 1-minute sea levels from Le Robert, Martinique showing diurnal and semidiurnal sidebands (±0.04 and ±0.08 cph) and a Gaussian fit to the central peak. In this

case, power is shown on a linear scale so as to easily identify half-power. The Gaussian fit is made to the range of frequency shown by the red line. (b,c,d) Variation of the 50, 70 and 90 percentile values of σ_s for each hour of the solar, lunar and sidereal days respectively, expressed as a percentage departure from the average of each percentile through the day. An 'hour' represents $1/24^{th}$ of the solar, lunar and sidereal days respectively. An arbitrary time zero has been used for (c) and (d).

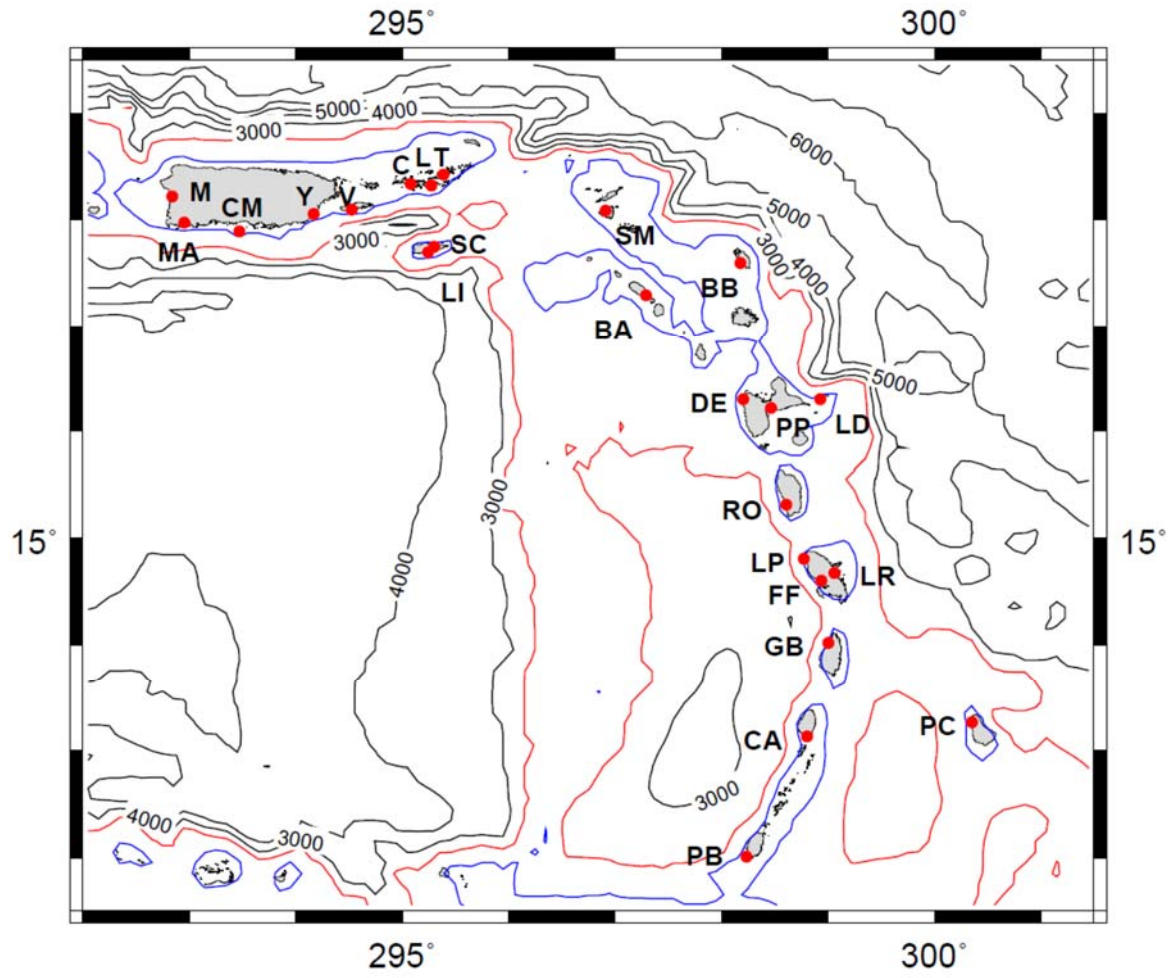
295°
300°
15°
5000
4000
3000
6000
M
CM
Y
V
C
LT
MA
SC
LI
SM
BB
BA
DE
PP
LD
RO
LP
FF
LR
GB
CA
PC
PB

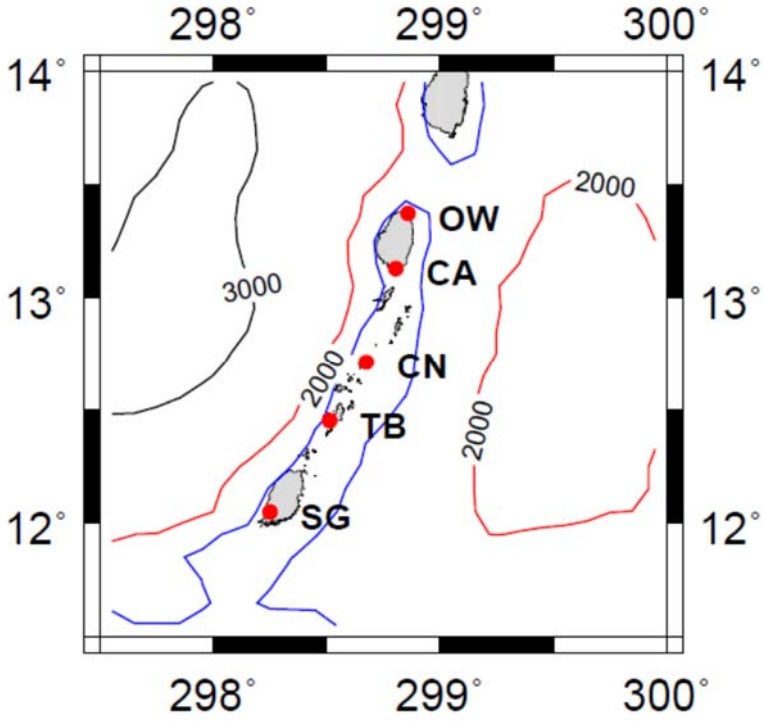
298°
299°
300°
14°
13°
12°
3000
2000
OW
CA
CN
TB
SG

Figure 1(a,b)

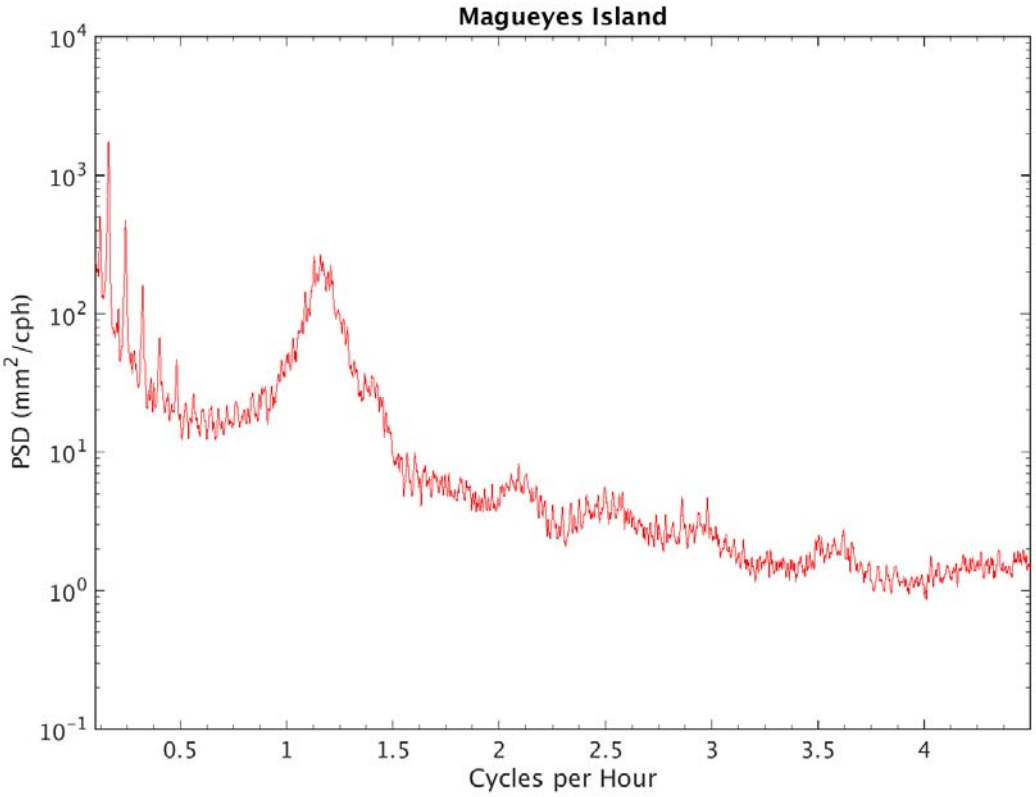
Magueyes Island
PSD (mm²/cph)
Cycles per Hour
10⁴
10³
10²
10¹
10⁰
10⁻¹
0.5
1
1.5
2
2.5
3
3.5
4

Figure 2

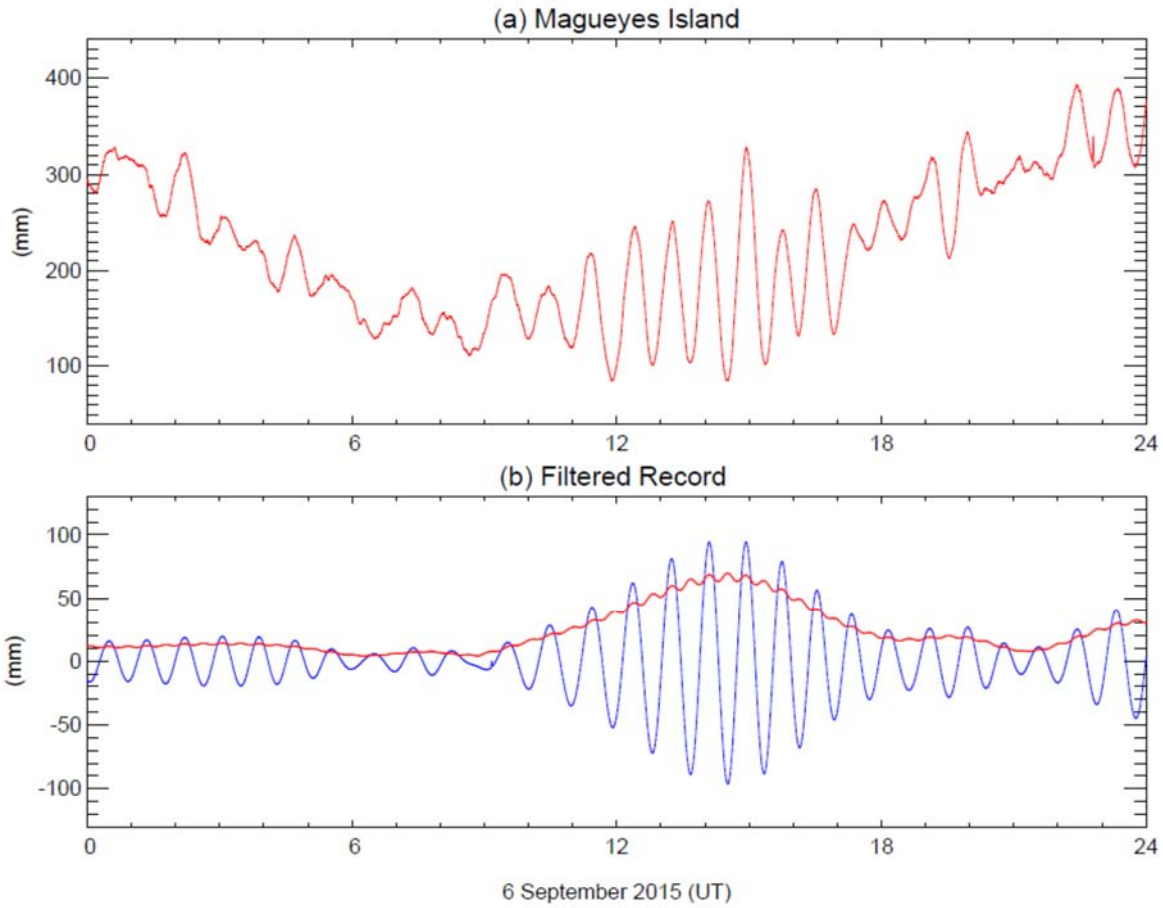
(a) Magueyes Island
400
300
200
100
(mm)
0
6
12
18
24
(b) Filtered Record
100
50
0
-50
-100
(mm)
0
6
12
18
24
6 September 2015 (UT)

Figure 3

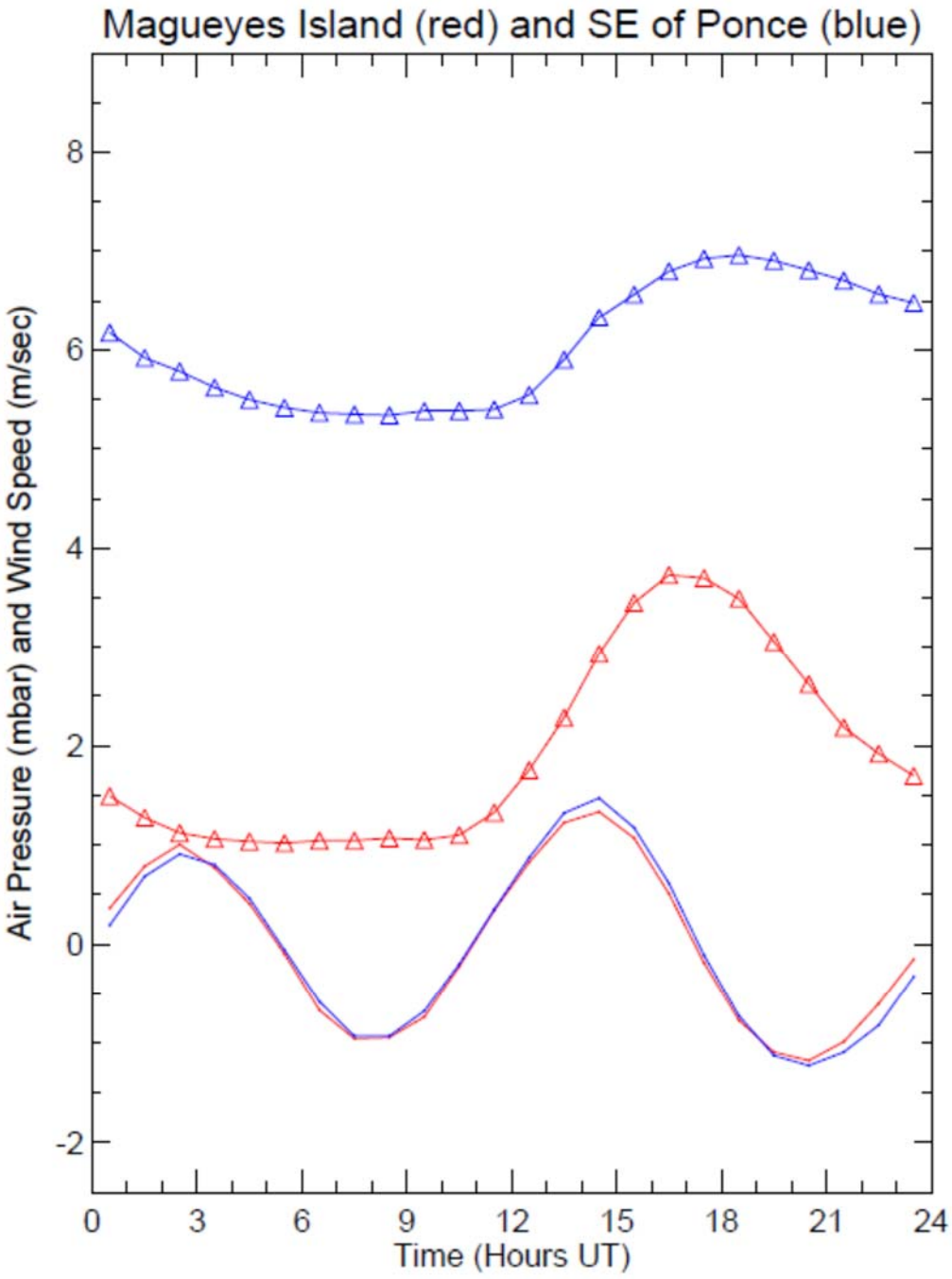
Magueyes Island (red) and SE of Ponce (blue)
Air Pressure (mbar) and Wind Speed (m/sec)
8
6
4
2
0
-2
0
3
6
9
12
15
18
21
24
Time (Hours UT)

Figure 4

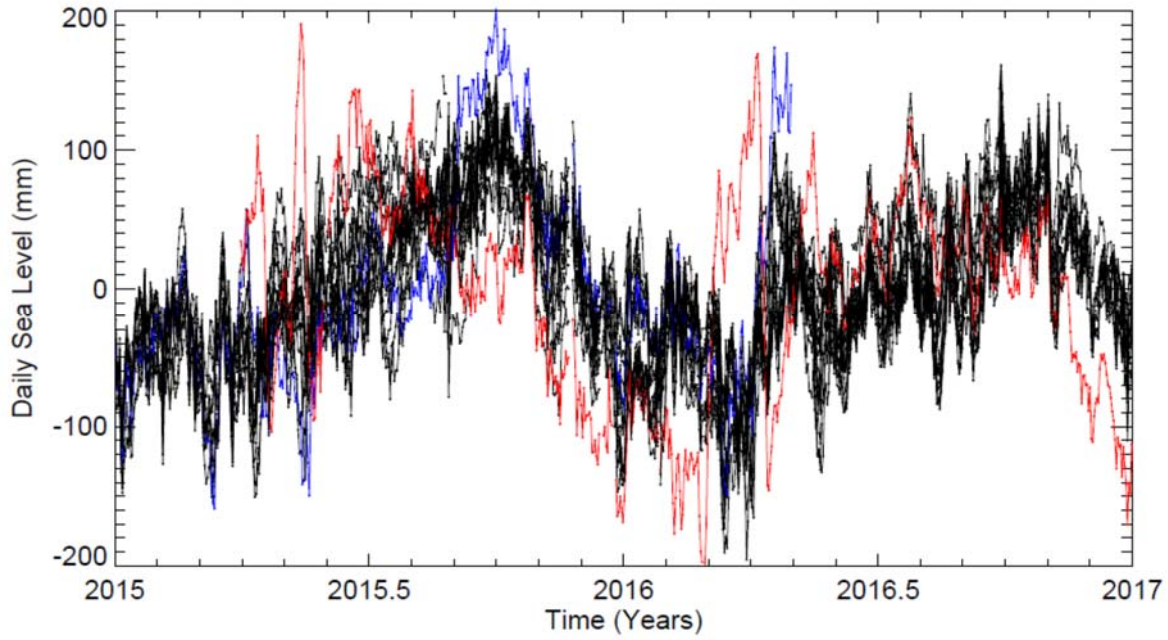

Figure 5

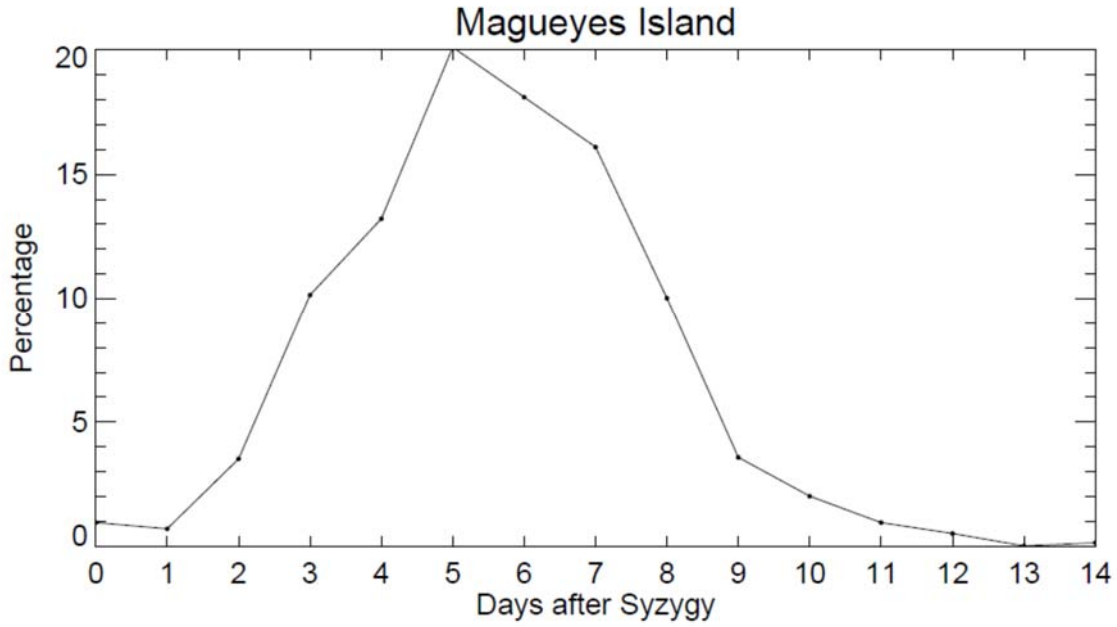

Figure 6

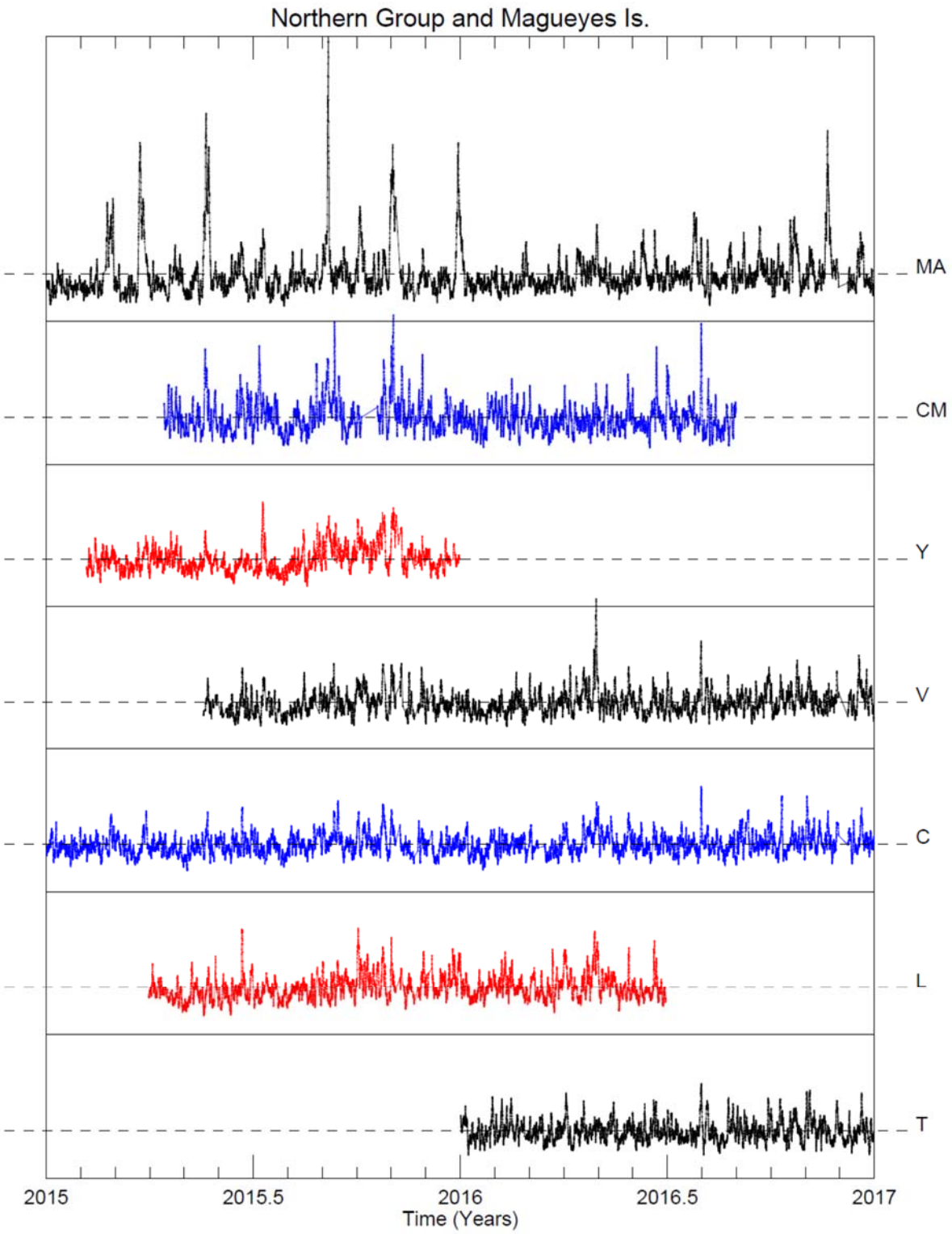
Northern Group and Magueyes Is.
MA
CM
Y
V
C
L
T
2015
2015.5
2016
2016.5
2017
Time (Years)

Figure 7

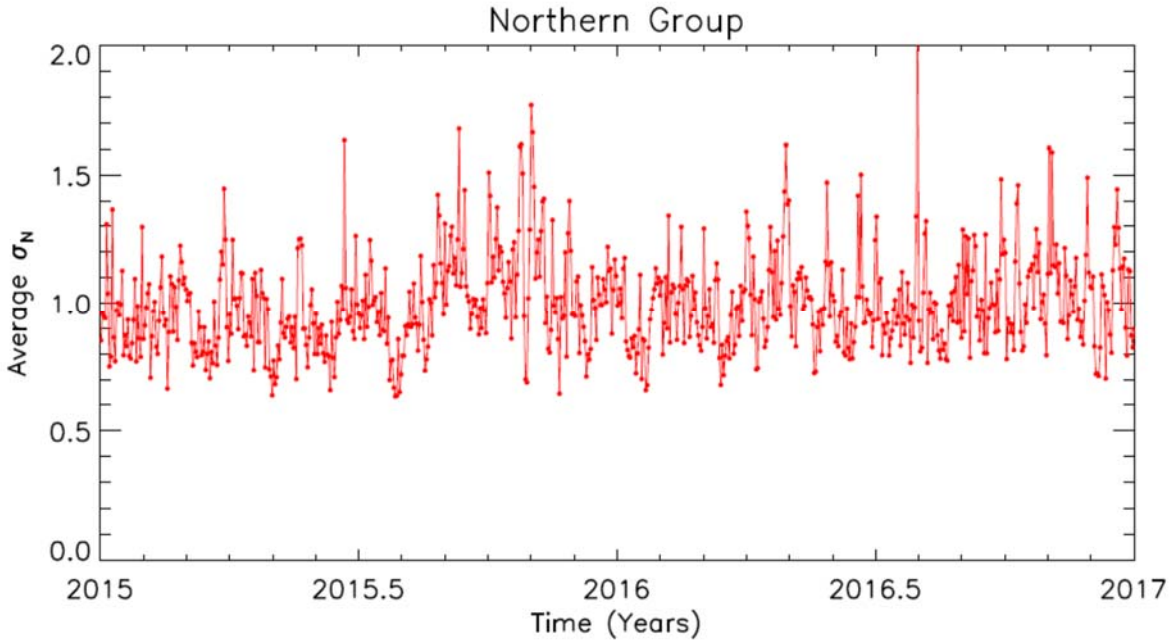

Figure 8

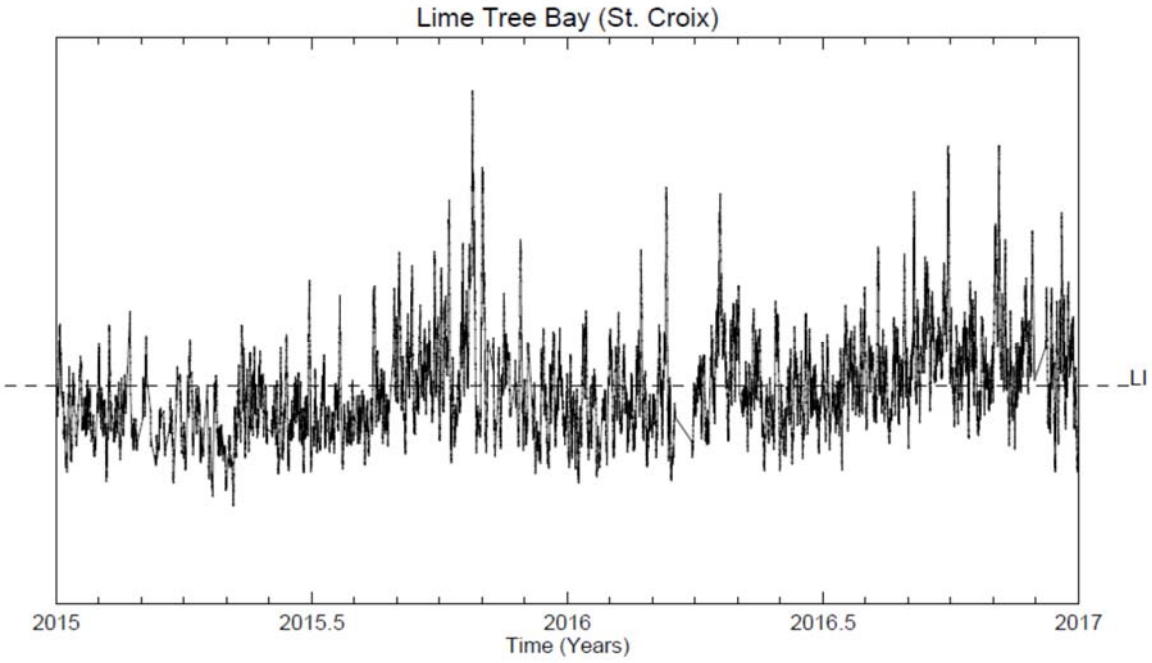

Figure 9

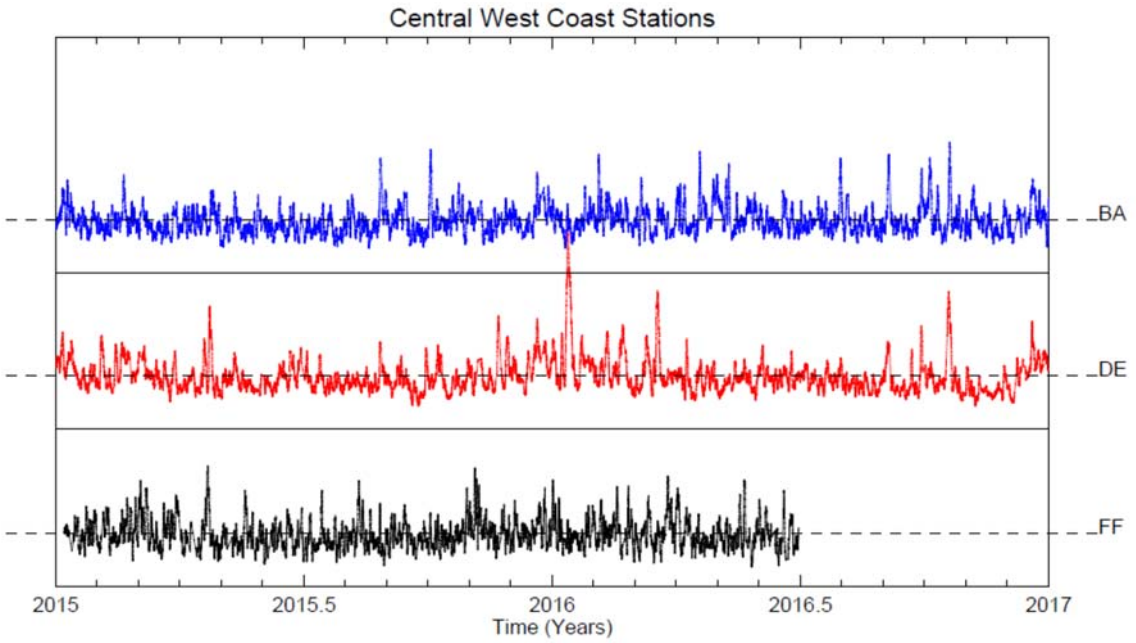

Figure 10

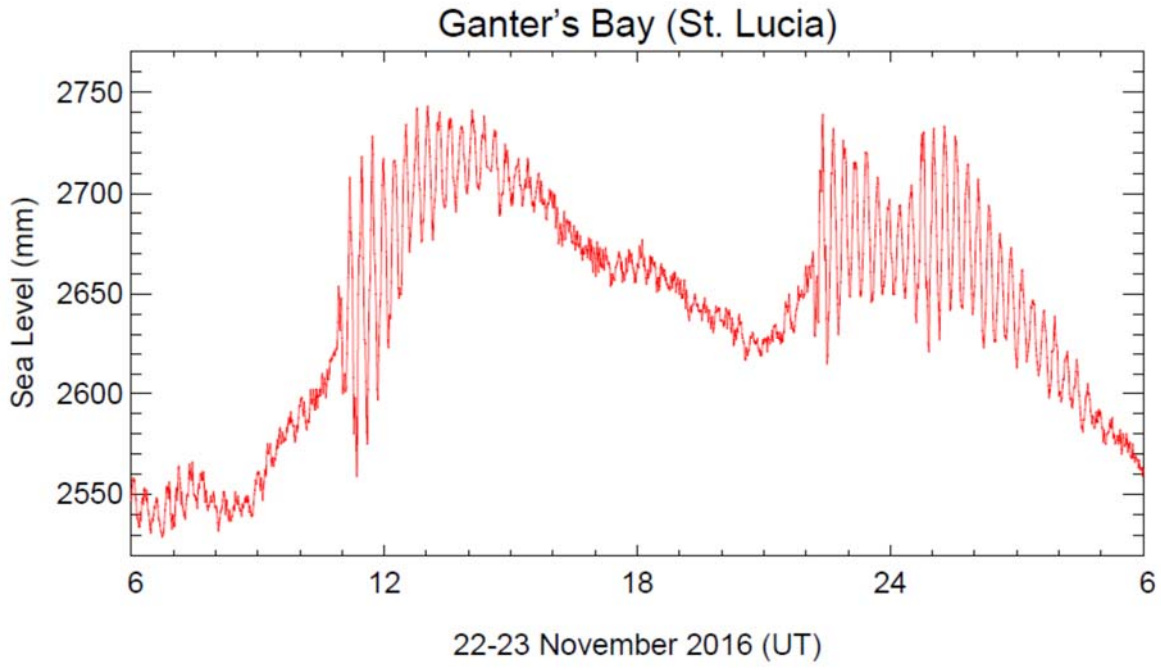

Figure 11(a)

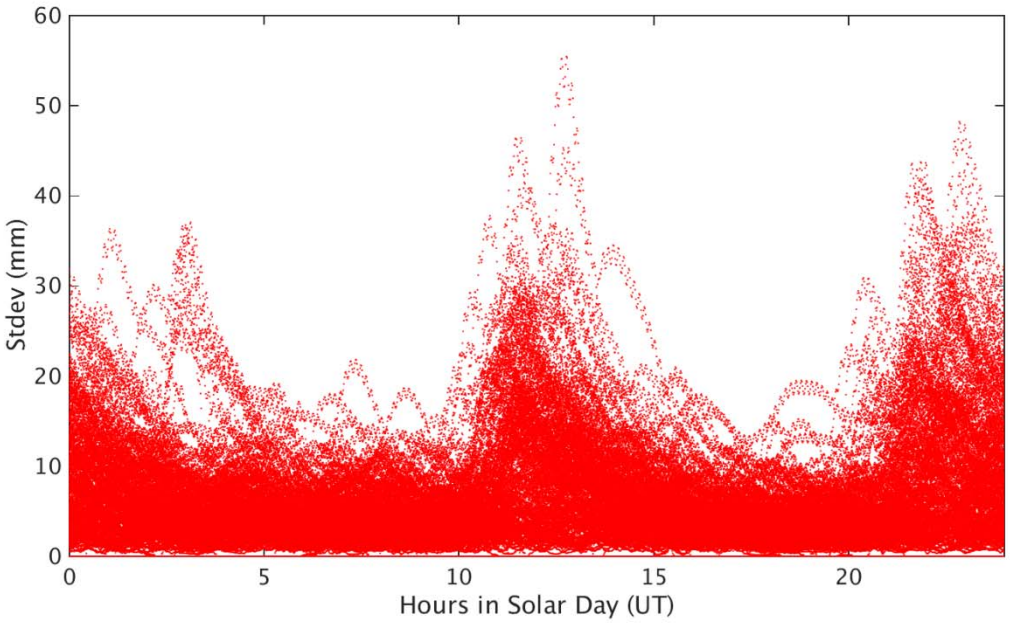

Figure 11(b)

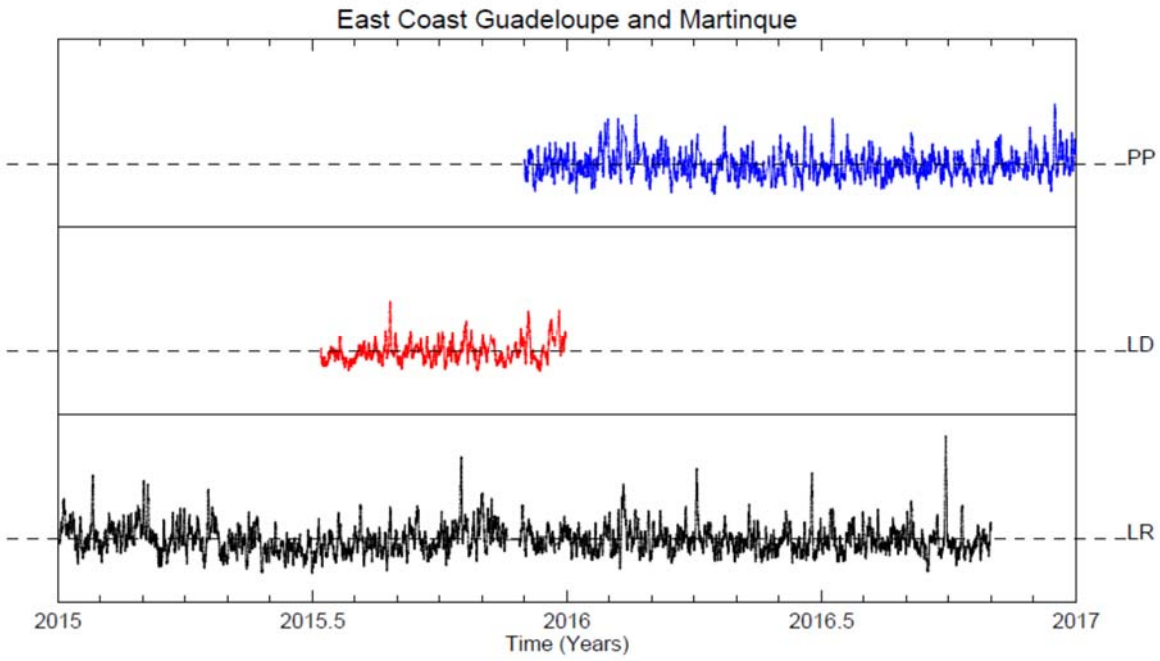

Figure 12

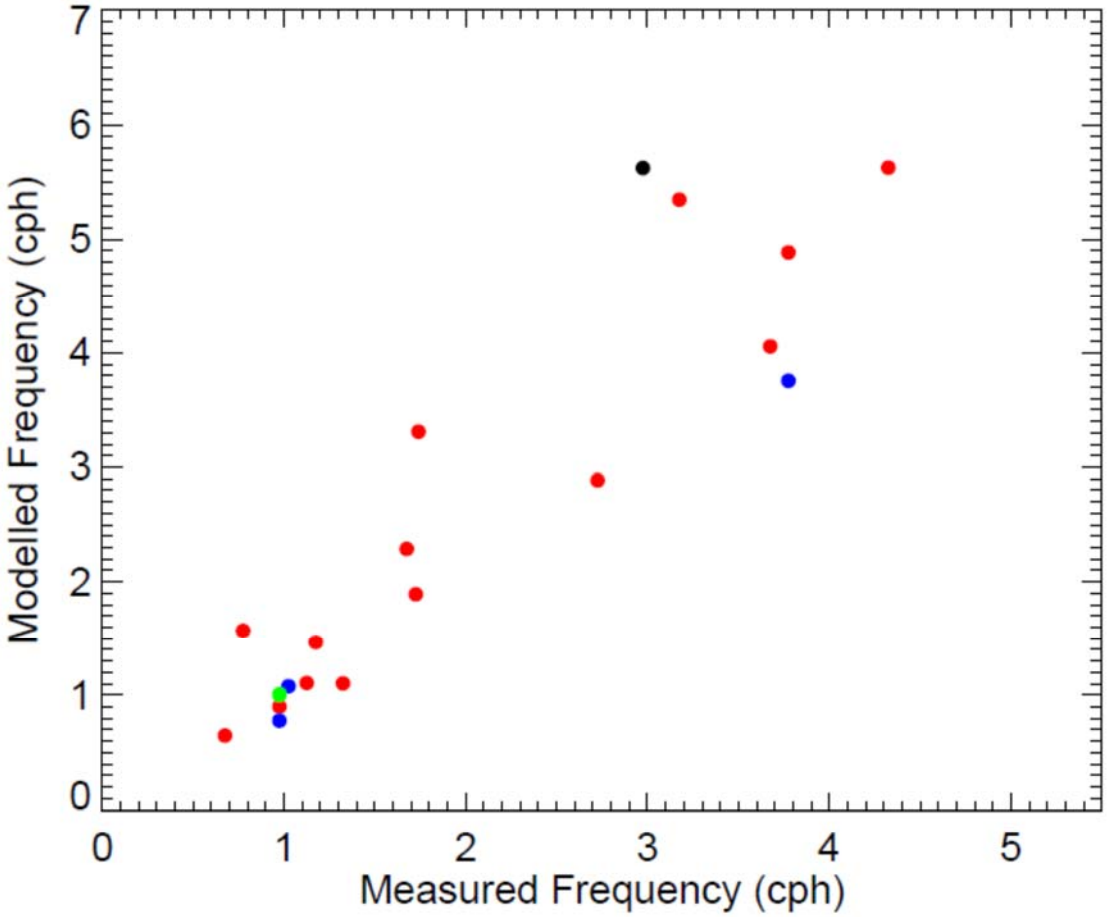

Figure 13

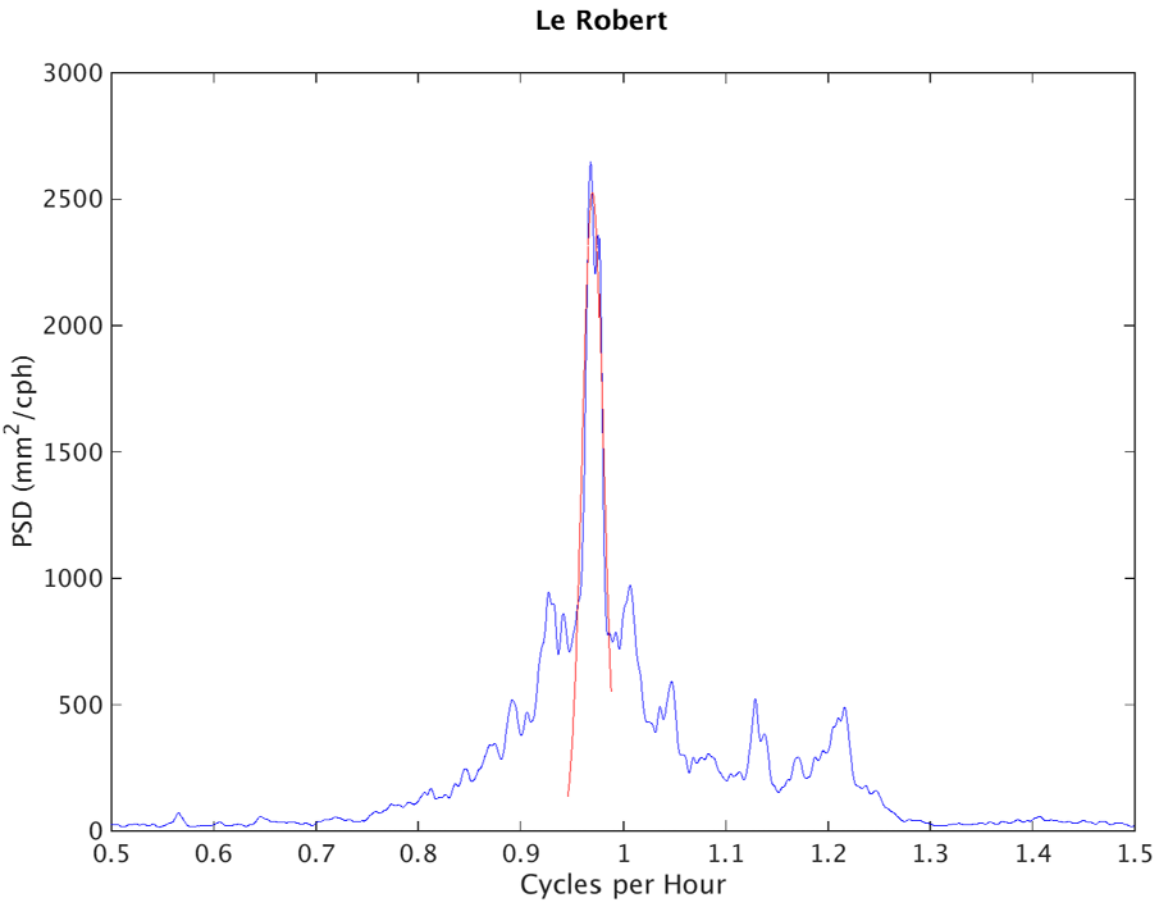
Le Robert
3000
2500
2000
1500
1000
500
0
PSD (mm^2/cph)
0.5
0.6
0.7
0.8
0.9
1
1.1
1.2
1.3
1.4
1.5
Cycles per Hour

Figure 14(a)

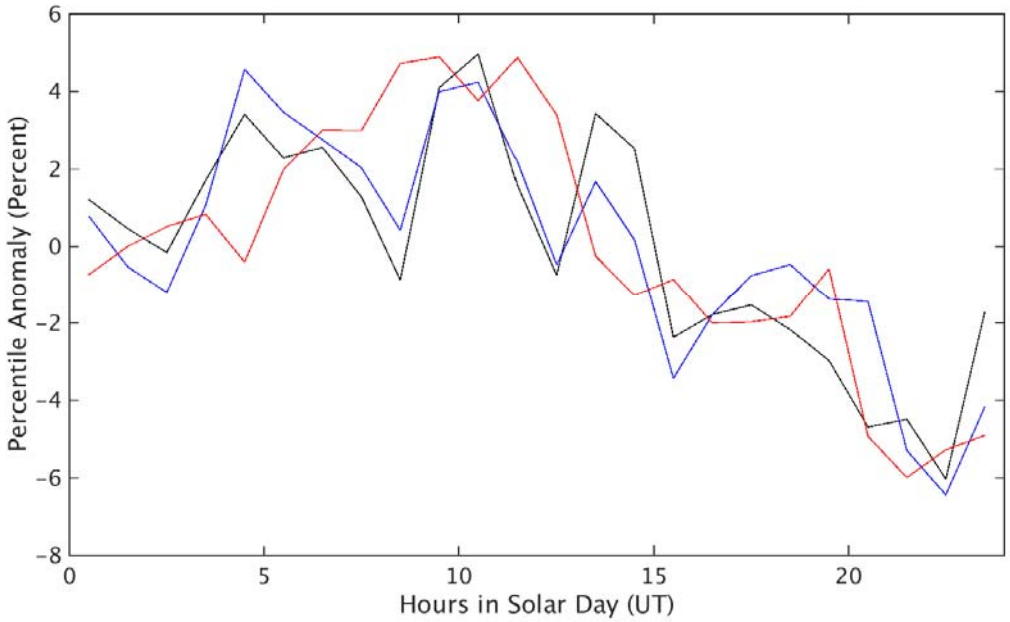
6
4
2
0
-2
-4
-6
-8
Percentile Anomaly (Percent)
0
5
10
15
20
Hours in Solar Day (UT)

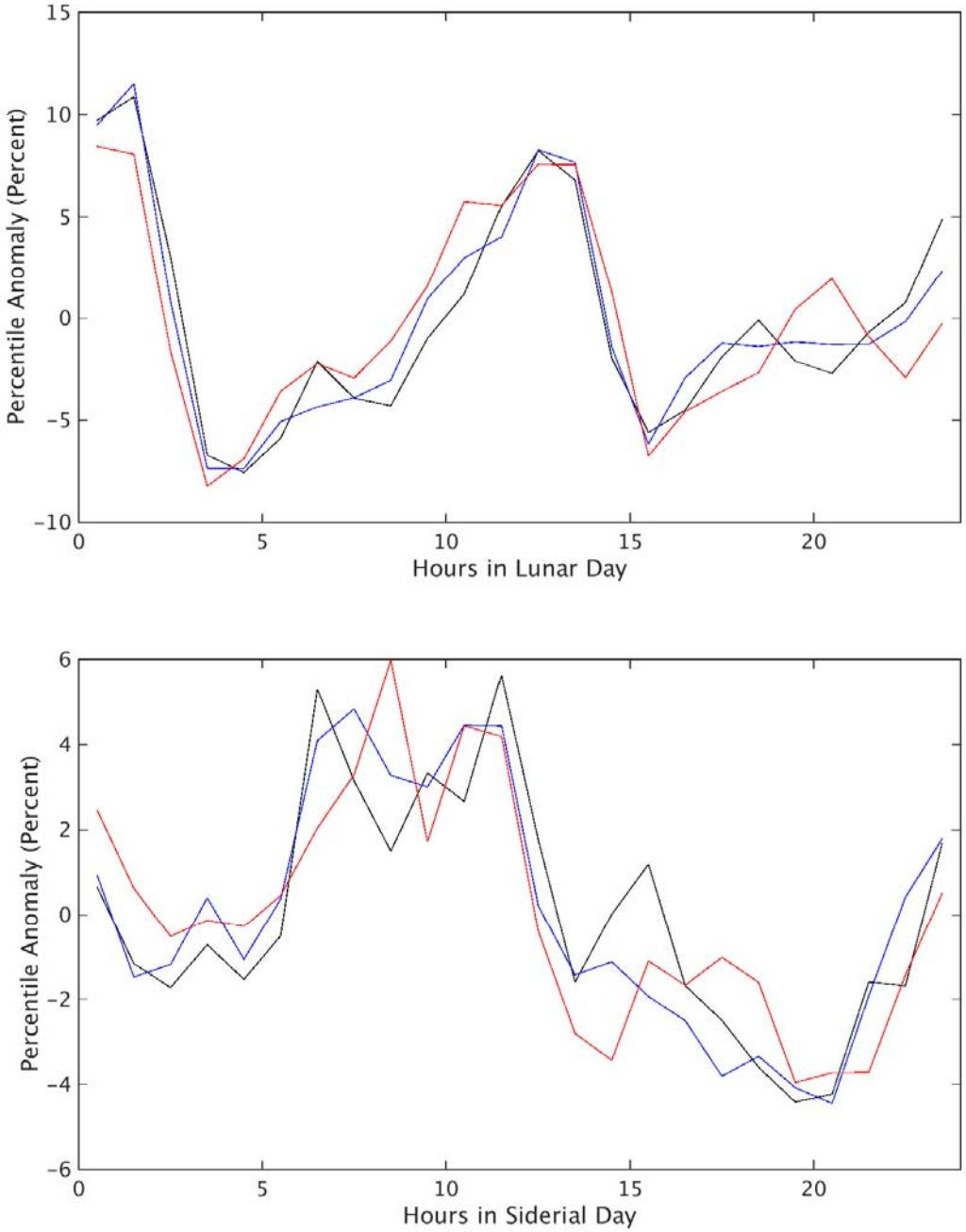

Figure 14(b,c,d)

Table Captions

1. The 24 stations with 1-minute sampling: station name and island, code as shown in Figure 1(a), data span, frequency of the main seiche peak (with period in minutes), the defined 'seiche bands' for filtering, standard deviation of the filtered record, median and maximum range of the seiche calculated on a daily basis. For some stations, the frequency of a second peak is noted.
2. (a) Correlation coefficients (zero lag) between daily average values of σ_n at pairs of the six northern group stations and also Magueyes Island. The Tortola and Yacuboa records do not overlap. (b) Coefficients after values have been high-pass filtered to remove seasonal variability and keep variability on timescales of less than a month.
3. (a) For each station in column 1, columns 2-4 show the direction from each tide gauge to the shelf edge, shelf width and average depth, estimated from GEBCO_2014. Columns 5-6 show shelf width and average depth estimated from hydrographic charts. (b) The length, average depth and average width assumed for three harbours or bays. Shape refers to the surface shape and depth profile as described in Table II of Wilson (1972) or Table 9.2 of Rabinovich (2009).
4. Values of Q obtained for each seiche peak as determined from the Gaussian fits shown in the figures in the Supplementary Material.

Table 1

Station Name/ Island	Code	Data Span	Peak (cph)	Seiche Band (cph)	Stdev (mm)	MedR (mm)	MaxR (mm)
Prickly Bay, Grenada	PB	Jan 15-Sep 16	1.725 (35) 2.025 (30)	1.5-2.2	5.6	30	66
Port St Charles, Barbados	PC	Apr 15-Dec 16	~ 6.4	5.8-7.0	2.5	14	55
Calliaqua, St Vincent	CA	2015-16	~ 7.7	6.8-8.6	2.9	18	44
Ganter's Bay, St Lucia	GB	Oct 15-May 16	3.775 (16)	3.0-5.0	8.4	54	152
Fort de France, Martinique	FF	Jan 15-Jun 16	1.025 (59)	0.9-1.1	0.9	4	11
Le Prêcheur, Martinique	LP	Jan 15-Apr 16	None				
Le Robert, Martinique	LR	Jan 15-Oct 16	0.975 (62)	0.5-1.5	14.9	75	206
Roseau, Dominica	RO	2015-16	~17.4	16.8-18.0	1.3	6	27
Deshaies, Guadeloupe	DE	2015-16	2.975 (20) 4.025 (15)	2.5-4.5	3.3	18	101
Pointe-à-Pitre, Guadeloupe	PP	Dec 15-Dec 16	0.975 (62)	0.5-1.5	16.1	80	153
La Desirade, Guadeloupe	LD	Jul 15-Dec 15	2.725 (22) 2.925 (21)	2.0-4.5	5.7	34	73
Basseterre,	BA	2015-16	4.325 (14)	4.0-4.6	5.0	25	93

St Kitts							
Barbuda, Barbuda	BB	Jan-Sep 2015	0.675 (89)	0.5-1.0	7.4	36	78
Saint Martin, Saint Martin	SM	May-Aug 2016	0.775 (77) 1.075 (56)	0.5-2.5	12.6	68	189
Limetree Bay, St Croix, US VI	LI	2015-16	3.775 (16)	3.5-4.5	2.0	11	33
St Croix, St Croix, US VI	SC	2015-16	~11.0	9.0-13.0	3.0	14	120
Charlotte Amalie, St Thomas, US VI	C	2015-16	1.325 (45) 2.525 (24)	1.0-1.6	5.9	30	94
Lameshur Bay, St John, US VI	L	Apr 15-Jun 16	1.675 (36) 2.475 (24)	1.5-2.0	2.1	10	32
Tortola, British Virgin Is.	T	2016	1.125 (53)	0.8-1.5	5.4	27	63
Magueyes Island, Puerto Rico	MA	2015-16	1.175 (51)	0.95-1.45	6.0	24	191
Mayagüez, Puerto Rico	M	2016	~1.74	1.4-2.1	7.1	37	85
Caja de Muertos, Puerto Rico	CM	Apr 15-Aug 16	0.975 (62)	0.8-1.1	1.5	6	21
Yabucoa Hbr, Puerto Rico	Y	Feb 15-Dec 15	3.175 (19) 5.525 (11)	2.8-3.6	5.3	27	79
Vieques, Puerto Rico	V	May 16-Dec 16	3.675 (16) 5.675 (11)	3.4-4.0	2.6	13	44

Table 2(a)

	L	C	V	Y	CM	MA
T	0.350	0.469	0.311	-	0.345	0.202
L		0.506	0.477	0.415	0.196	0.173
C			0.421	0.414	0.330	0.227
V				0.473	0.306	0.181
Y					0.463	0.390
CM						0.355

Table 2(b)

	L	C	V	Y	CM	MA
T	0.311	0.515	0.308	-	0.373	0.107
L		0.466	0.397	0.248	0.179	0.100
C			0.382	0.188	0.413	0.206
V				0.173	0.329	0.114
Y					0.305	0.351
CM						0.295

Table 3(a)

Station	Direction	Shelf Width (km)	Average Depth (m)	Shelf Width (km)	Average Depth (m)
PB	SE	11.7	61.4		
PC				2.8	100
CA				1.4	50
LP				0.7	80
LR	E	18.0	33.1		
RO				1.0	60
DE				3.2	40
LD	E	7.1	53.3		
BA	SW	3.8	59.0		
BB	W	28.3	42.6		
SM	W	10.6	34.8		
LI	S	4.6	64.6		
SC				1.4	10
C	S	17.6	47.5		
L	SE	12.8	107.8		
T	SE	16.6	42.6		
MA	S	12.1	39.4		
M	W	7.1	68.6		
CM	S	6.5	61.1		
Y	SE	5.1	94.3		
V	S	4.6	44.5		

Point on mainland coast of Puerto Rico north of Caja de Muertos:

	S	16.7	35.6		

Table 3(b)

Station	Harbour/Bay Length (km)	Average Depth (m)	Average Width (km)	Shape
GB (Ganter's Bay)*	2.28	13	0.5	rectangular, rectangular
FF (Fort-de-France)	9.0	30	2.5	rectangular, triangular
PP (Pointe-à-Pitre)	11	20	6.5	semi-circular, semi-paraboloidal

(*) The harbour length has been taken as far as the 20 m depth contour on the shelf.

Table 4

Station	Q	Comments
PB	24	lower frequency peak, approximate fit
	12	upper frequency peak, good fit
PC	9	approximate fit
CA	6	approximate fit
GB	17	good fit
FF	7	good fit
LP	-	no peaks, see Table 1
LR	41	see text
RO	79	approximate fit
DE	13	lower frequency peak, approximate fit
	13	upper frequency peak, good fit
PP	3	approximate fit due to many sub-peaks
LD	-	two close peaks do not lend themselves to a simple fit
BA	23	reasonable fit
BB	3	reasonable fit
SM	-	no fit made as power distributed over a wide band
LI	-	no fit made as power distributed over a wide band
SC	6	good fit
C	5	lower frequency peak, reasonable fit
	16	upper frequency peak, good fit
L	-	no fit made as power distributed over a wide band
T	4	reasonable fit
MA	6	good fit. See text
M	5	approximate fit due to sub-peaks
CM	21	approximate fit
Y	10	lower frequency peak, good fit
	13	upper frequency peak, good fit
V	13	lower frequency peak, good fit
	21	upper frequency peak, good fit

Supplementary Material for 'Seiches in the Eastern Caribbean' by

Philip L. Woodworth, Pure and Applied Geophysics

Figures SM1.1-1.43 (Power Spectra at Each Site)

Figures SM1.1-1.43 show the power spectral density (PSD) of 1-minute sea level values at each site. The spectra were computed by the Matlab® *pwelch* function at most stations (except Barbuda) using windows of 16384 points with 50% overlap.

Spectra are plotted in the order of stations in Table 1. The first plot for each station starts at a frequency of 0.1 cph in order to cut off the large main peaks of the diurnal and semidiurnal tides. The upper frequency of each plot was selected as seemed most suitable (the Nyquist frequency for 1-minute sampling is 30 cph). For some stations, there is a second plot which shows the Gaussian fits to determine values of Q. These plots are shown with a linear scale so as to easily identify half-power. The fit is made to the range of frequency shown by the red line.

Comments for Each Station

Prickly Bay has two main peaks between 1.5 and 2.2 cph and a number of others higher up and a wide band of higher power at about 8 cph.

Port St Charles has no obvious peaks at lower frequencies apart from one at approximately 6.4 cph. The narrow peak at about 0.56 cph is consistent with being an M14 tidal harmonic (see text).

Calliaqua has no peaks apart from very minor ones around 1.7 and 2.9 cph and a stronger and wider one at 7.7 cph.

Ganter's Bay has a main peak around 3.775 cph (see text) and secondary ones around 2.775, 5.275 cph and around 12-16 cph.

Fort de France has a broad but low amplitude peak around 1.025 cph. There are peaks also around 2.775, 3.325, 5.125 cph and a broad and large enhancement around 6.925-7.475 cph.

Le Prêcheur has nothing obvious in its spectrum.

Le Robert has a large seiche peak at 0.975 cph that is possibly split at diurnal and semidiurnal sidebands (see text). Another broad enhancement around 2.625 cph.

Roseau has nothing to mention in its spectrum at lower frequencies. Peak at about 17.4 cph. Note this site has more transmission errors than some others.

The **Roseau** record suffered from many transmission gaps that generated false spikes at 12 and 24 cph which have been excluded by the plot limits used below.

Deshaies has large peaks around 2.975 and 4.025 cph and also a higher frequency peak around 12 cph.

Pointe-à-Pitre has a large peak around 0.975 cph. Also one at about 2.675 cph and others higher.

La Désirade has a broad peak centred around 2.8 cph with a split spectrum (approximately 2.725 and 2.925 cph) and others at around 3.4 and 4 cph, and a broad plateau of energy from 5-10 cph.

Basseterre has a big peak at about 4.325 cph and smaller ones around 2.52 and 5.575 cph.

Barbuda has many data transmission drop outs, especially between 9-12 UT. Peaks around 0.675 and 2.775 cph. The original version of this spectrum was very spiky, possibly due to inaccuracies in filling transmission gaps, and so the spectrum was smoothed by using 1/8 the normal number of points for windowing. That had no effect on the estimated seiche parameters.

Saint Martin has an energetic record. Several peaks between 0.6 and 2.3 cph.

Lime Tree Bay has a low energy record. Many peaks at about 1.875, 2.175, 2.975, 3.775 cph (the latter being the main one), 4.875, 5.875 and 7.025-7.275 cph.

St Croix has no obvious peaks at lower frequencies (perhaps a very small one at just below 1 cph) but an enhancement at around 11.0 cph.

Charlotte Amalie has two main peaks at about 1.325 and 2.525 cph and high frequency ones at about 5 and 10 cph and higher all the way out to 30 cph.

Seiches at **Charlotte Amalie** were mentioned in a draft NOAA report concerned with tsunami forecast modelling (Tolkova, 2016). The report shows a part of the sea level record in 2011 and a power spectrum containing the 1.325 and 2.525 cph peaks also obtained here. However, in Tolkova (2016) the former is suppressed compared to the latter, probably because of the linear power scale used. In the present study, we have selected the former as the shelf seiche on the basis that it was the lowest-frequency peak with significant power. However, its maximum power level is indeed less than that of the 2.525 cph peak which Tolkova (2016) classified as a harbour seiche.

Lameshur is a low energy station. Peaks around 1.675, 2.475 (both split) and 3.875 cph and others at 7.275 and around 11 cph.

Tortola has a peak at about 1.125 cph and smaller ones higher up around 1.875 and 2.6-4 cph.

Magueyes Island has a main peak at about 1.175 cph with several much smaller at 2 cph and above.

Mayagüez has a broad peak centred on 1.74 approximately with two peaks and smaller peaks either side at about 1.25 and 2.3.

Caja de Muertos has a peak at about 0.975 cph and a smaller one at about 6.175 cph.

Yabucoa Harbor has a main peak at about 3.175 cph, also 5.525 and 7.275 cph and higher ones, and a shoulder in the spectrum around 2.7 cph.

Vieques has a main peak at 3.675 cph, also ones at 4.375, 5.675, 7.425 and a shoulder at 3.275 cph.

Figure SM2.1 (SWH and Wind Speed)

Figure SM2.1 shows (a) Average significant wave height (SWH) (metres) from ERA-Interim 6-hourly data during 2015-16. (b) Time series of ERA-Interim SWH at points one degree south of Charlotte Amalie and one degree east of Le Robert. (c) Time series of ERA-Interim 10-m wind speed (m/sec) at the two locations. (d) Daily mean zonal wind speed (m/sec) from the meteorological station at Charlotte Amalie. (e) Standard deviation of 6-minute zonal wind speed at Charlotte Amalie during each day. (f) Standard deviation of 6-minute zonal wind speed within 2-hour windows centred on each hour.

Figure SM3.1 (Empirical Mode Decomposition)

Figure SM3.1 (a) shows the record of σ_n for Le Robert (red), decomposed into intrinsic mode functions (IMFs) with average periods 3, 6, 11, 20, 30, 67, 191, 223 and 669 days shown bottom to top. Each IMF is offset by 1 unit for plotting. (b) The corresponding average record of σ_n for the northern group, decomposed into IMFs with average periods 3, 6, 10, 22, 47, 81, 209 and 487 days shown bottom to top. In each case, there is also a low frequency mode, which is essentially a constant, that is not plotted.

Figure SM4.1 (Bridgetown)

Power spectral density (PSD) from Bridgetown, Barbados obtained from 6 months of hourly data from 1995 provided by the University of Hawaii Sea Level Center.

Data files for Stations in Table 1

There are 24 ASCII data files for the tide gauge stations in Table 1. (Files for the five additional tide gauges from the UKHO cannot be made available this way.) Data were downloaded from the Sea Level Station Monitoring Facility of the Intergovernmental Oceanographic Commission (http://www.ioc-sealevelmonitoring.org), inspected and reformatted. The station corresponding to each file will be evident from the filename which in each case ends in '_task'. Each one has a header of 20 blank lines followed by lines of data in 10 columns: (1) a counter, (2) a flag which if non-zero indicates bad data, (3) year, (4) day (1 Jan = day 1), (5) time (hours UT), (6) sea level (mm), (7-10) empty. Data outside the data spans shown in Table 1 should not be used as they will not have been inspected in any detail (see text).

References for the Supplementary Material

Tolkova, E. 2016. A tsunami forecast model for Charlotte Amalie, VI. (Undated and 2016 assumed). Available from http://nctr.pmel.noaa.gov/forecast_reports/draft_reports/CharlotteAmeliaSIM_rev2appC.pdf.

Figure SM1.1 Prickly Bay

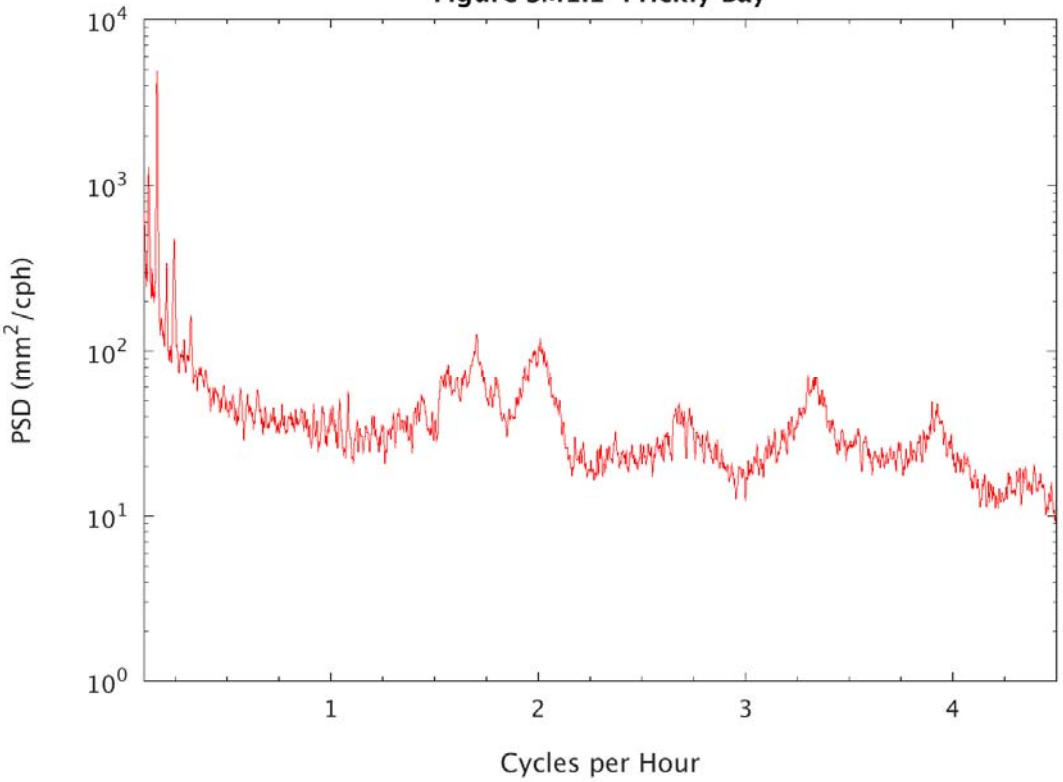

Figure SM1.2 Prickly Bay

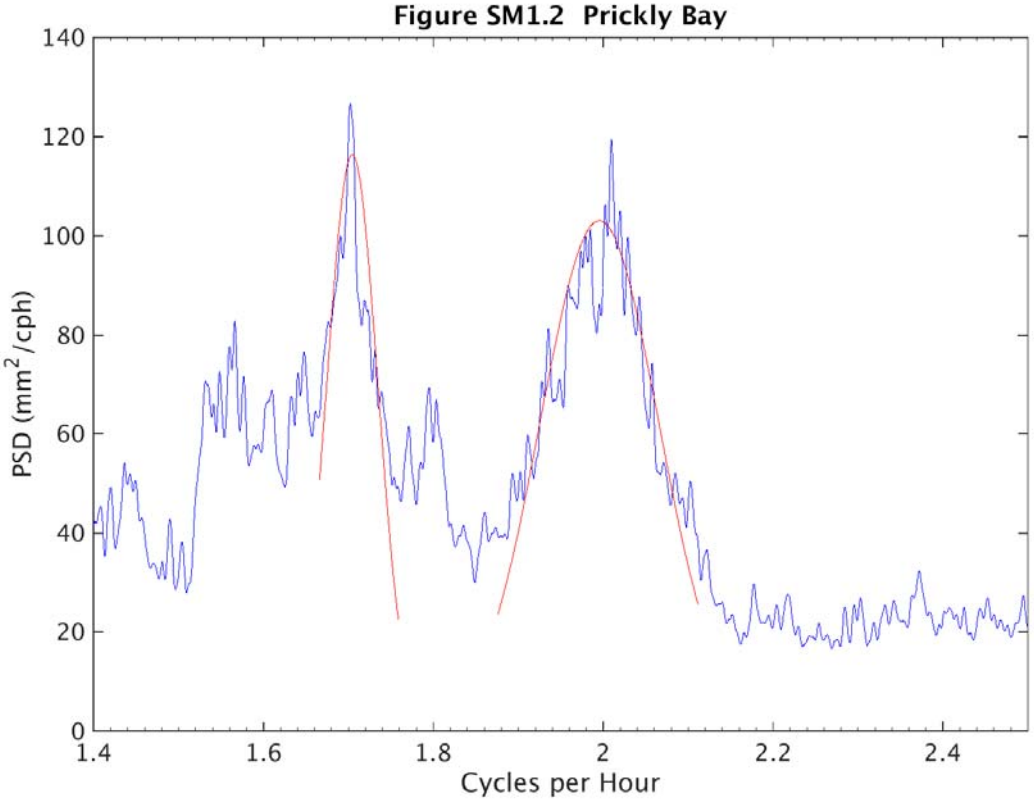

Figure SM1.3 Port St. Charles

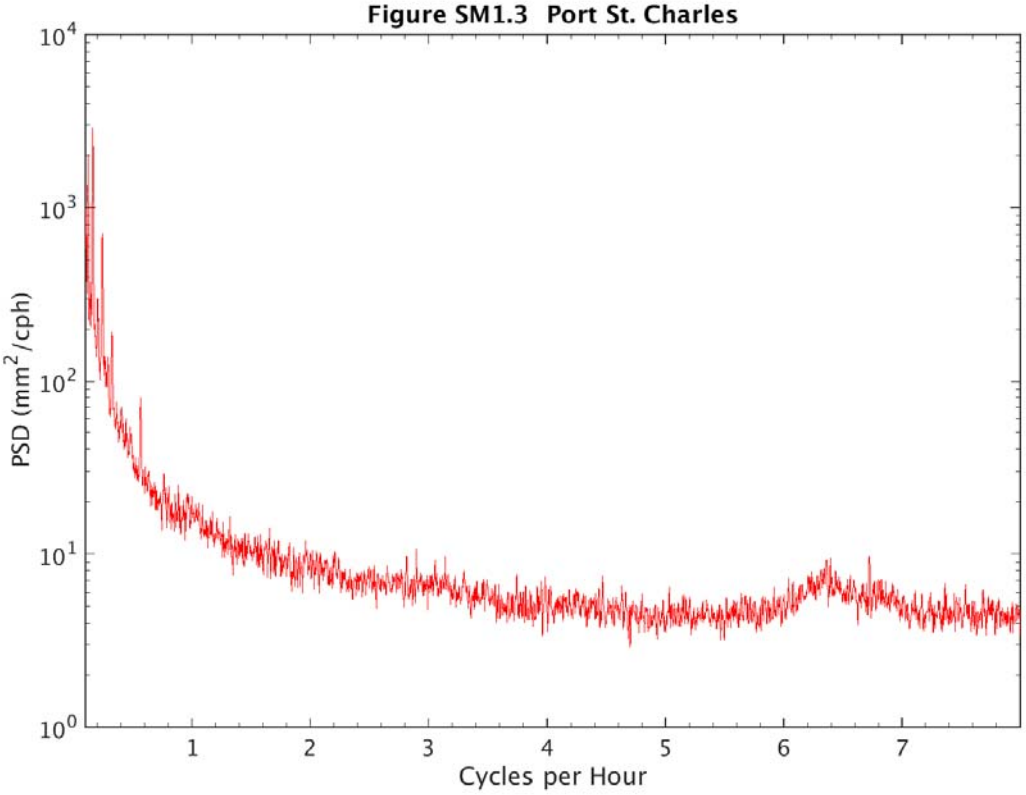

Figure SM1.4 Port St. Charles

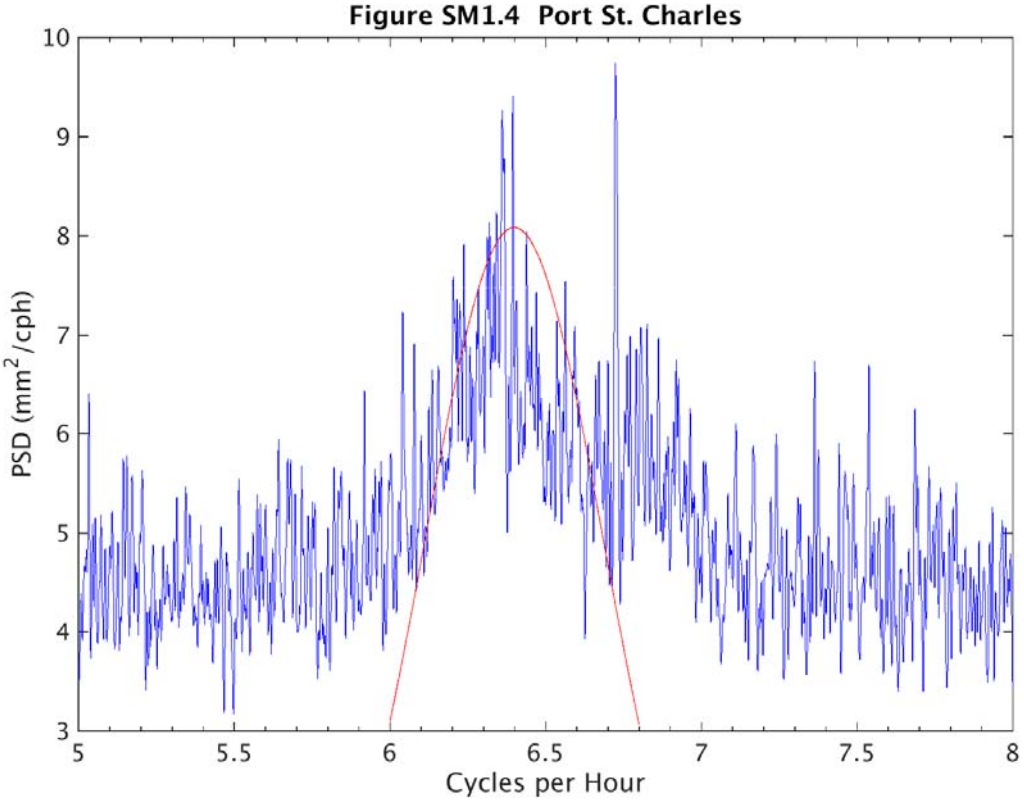

Figure SM1.5 Calliaqua

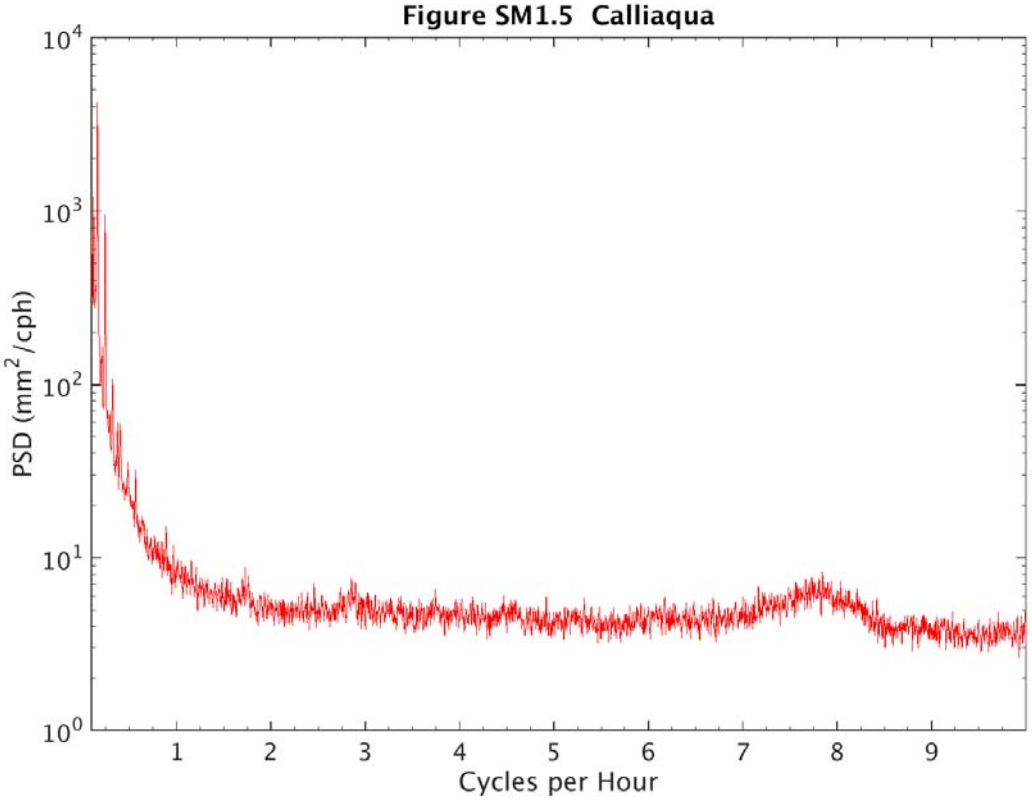

Figure SM1.6 Calliaqua

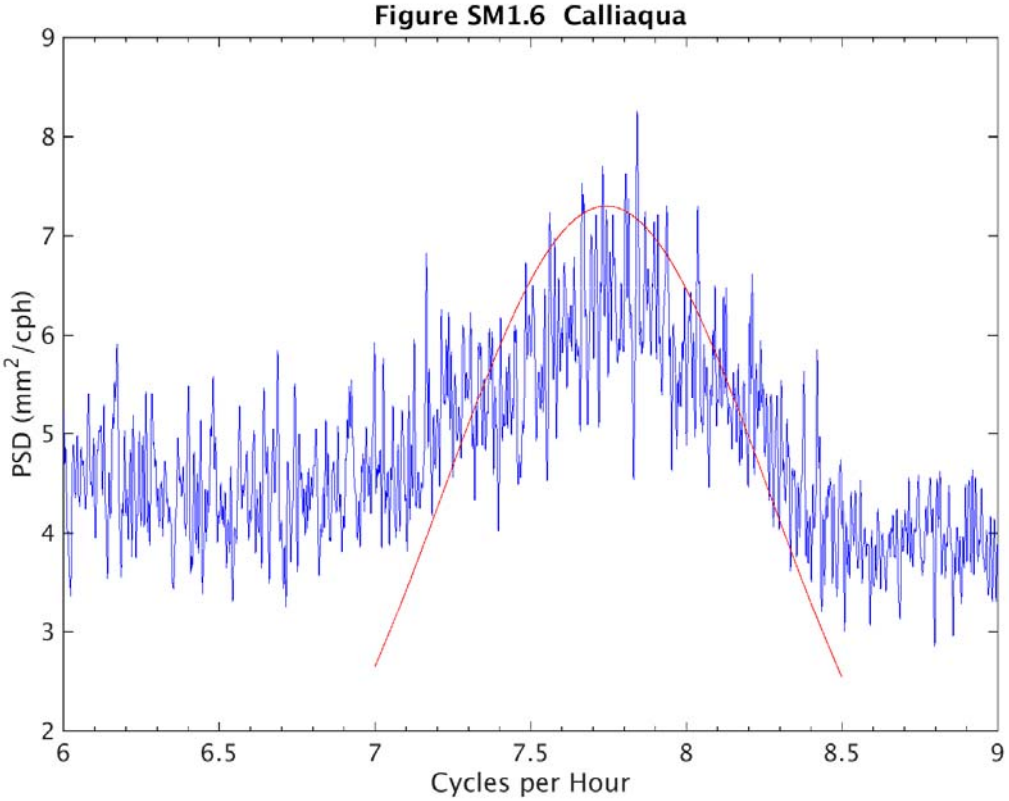

Figure SM1.7 Ganter's Bay

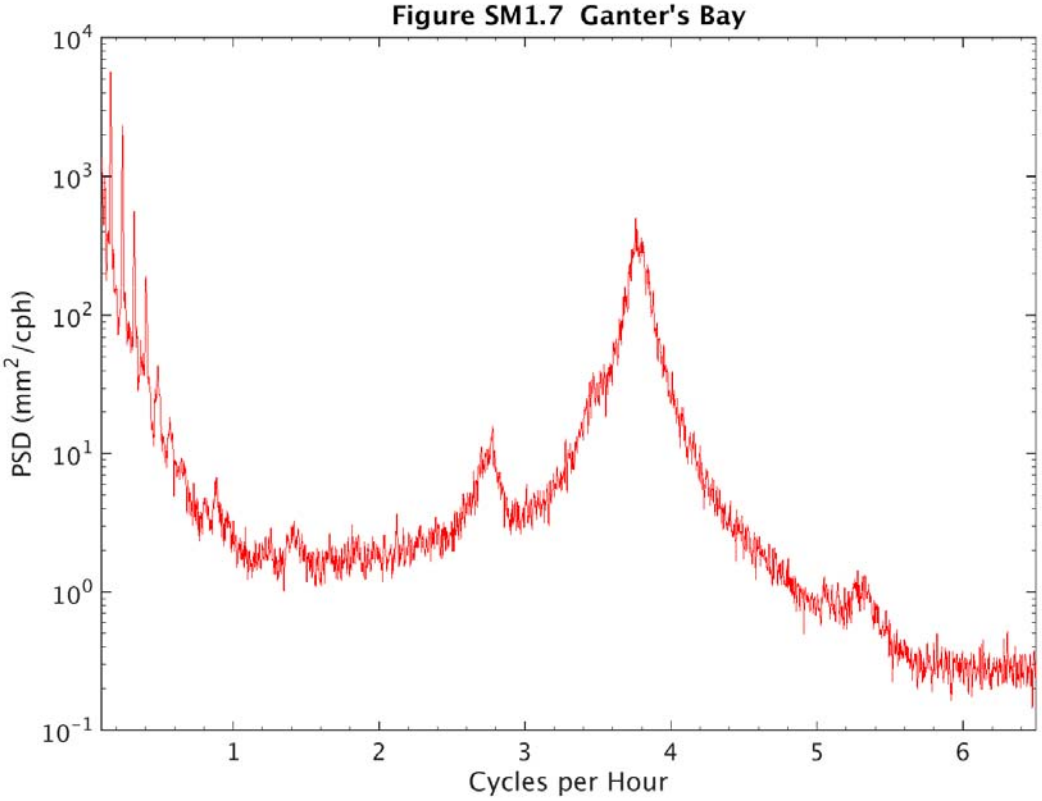

Figure SM1.8 Ganter's Bay

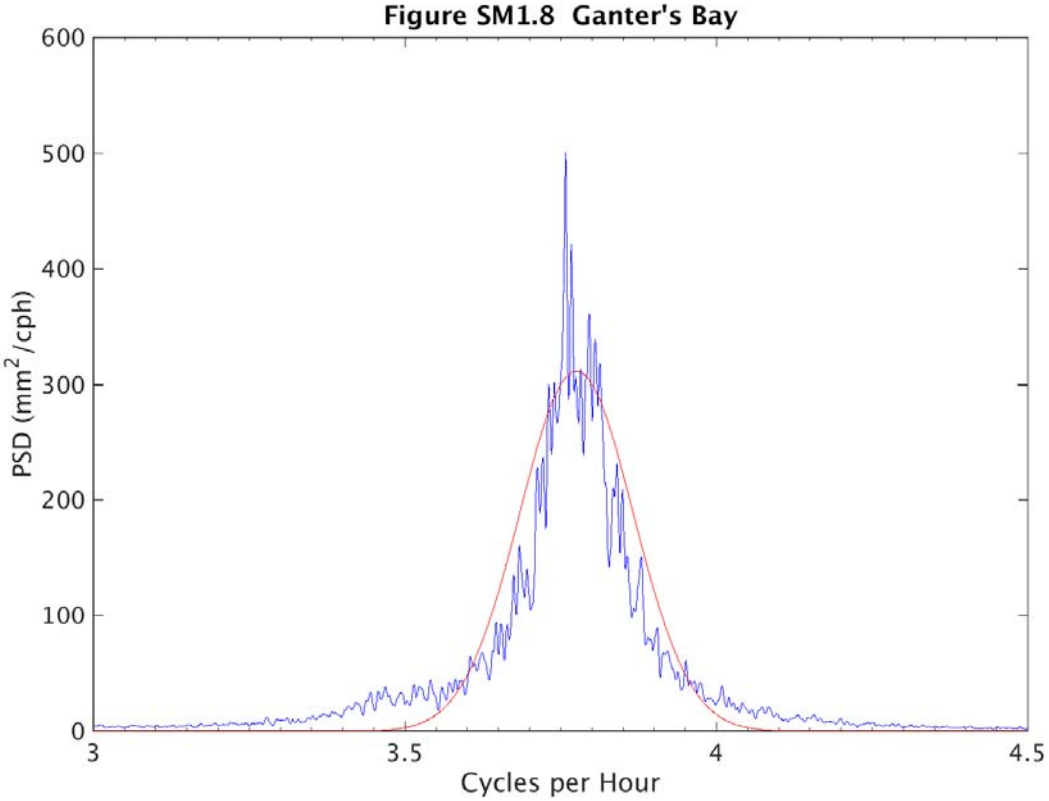

Figure SM1.9 Fort-de-France

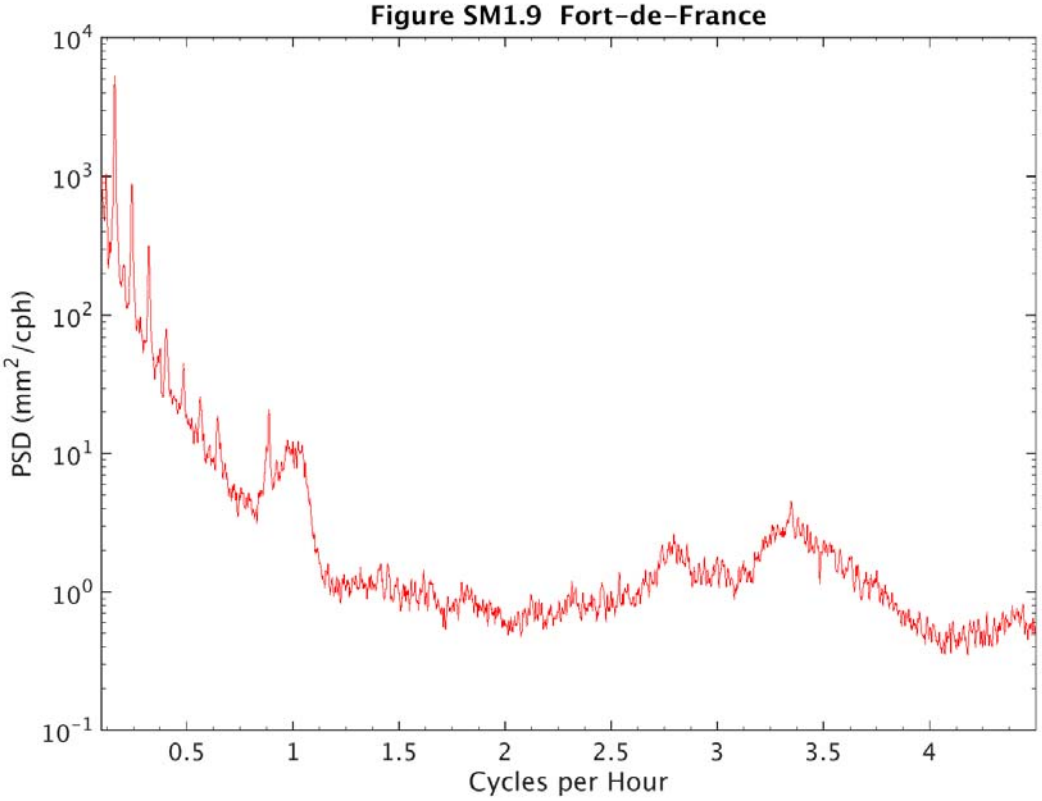

Figure SM1.10 Fort-de-France

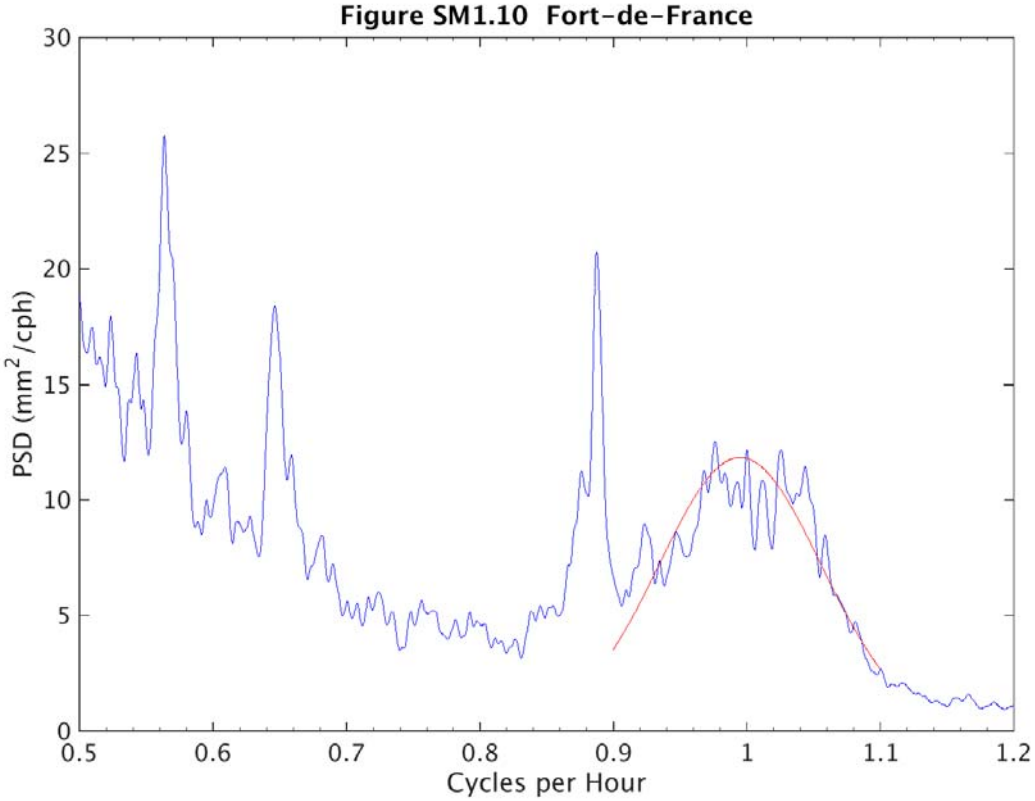

Figure SM1.11 Le Precheur

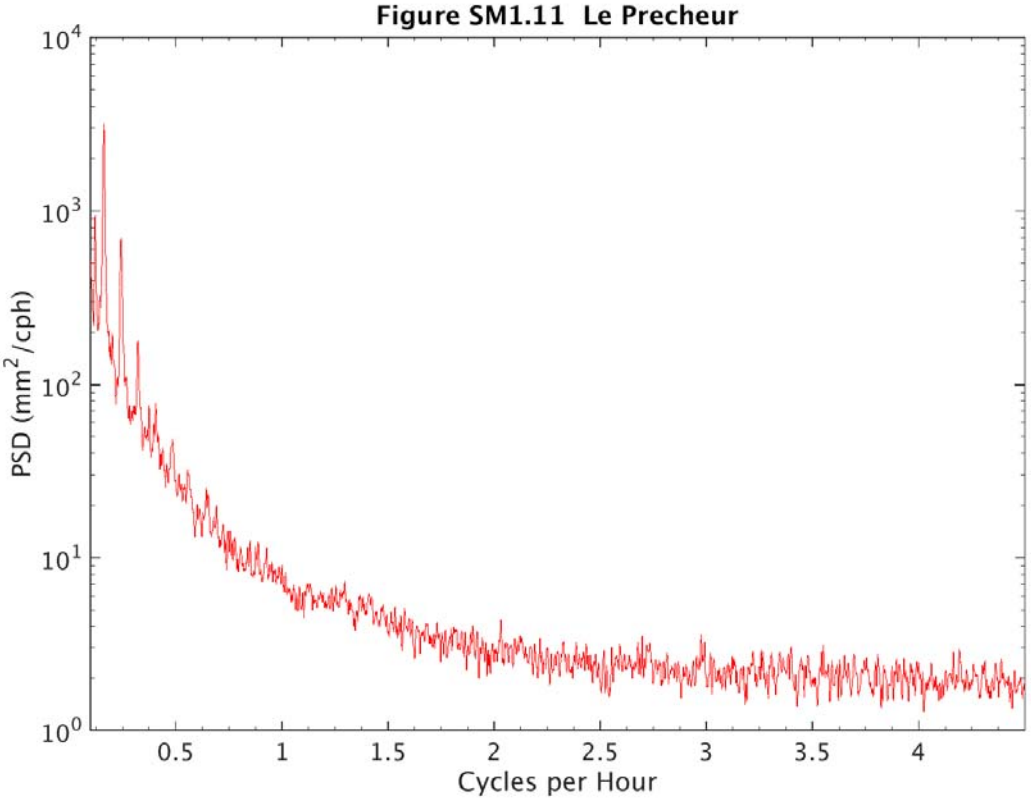

Figure SM1.12 Le Robert

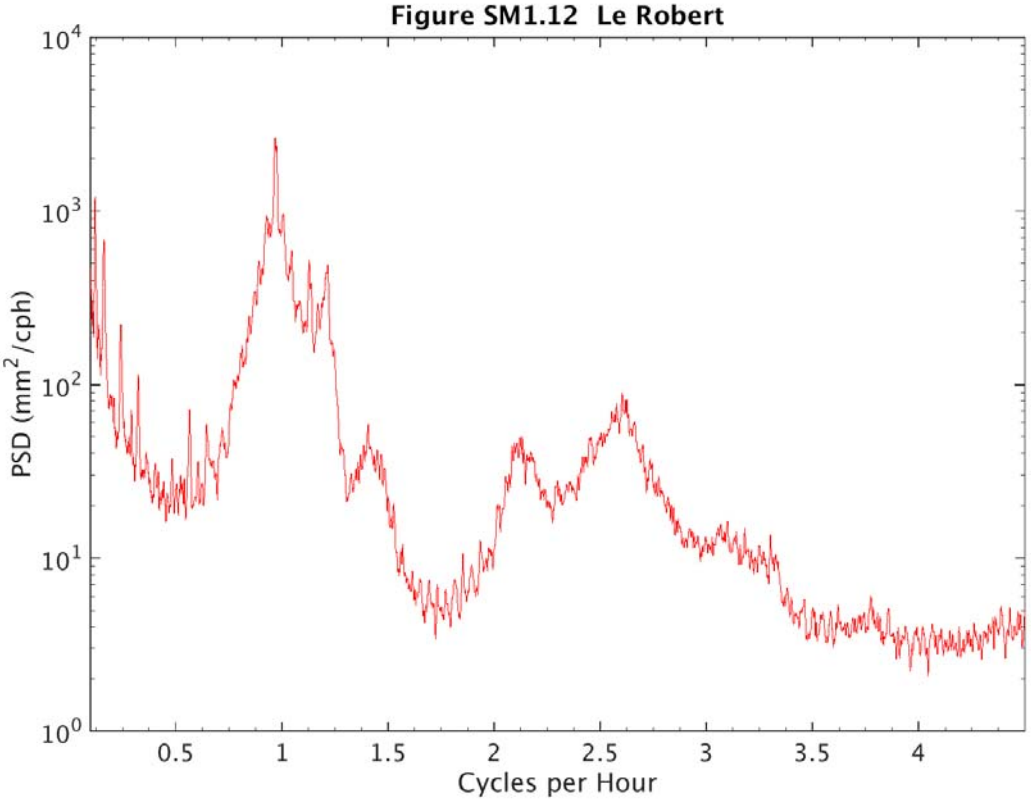

Figure SM1.13 Le Robert

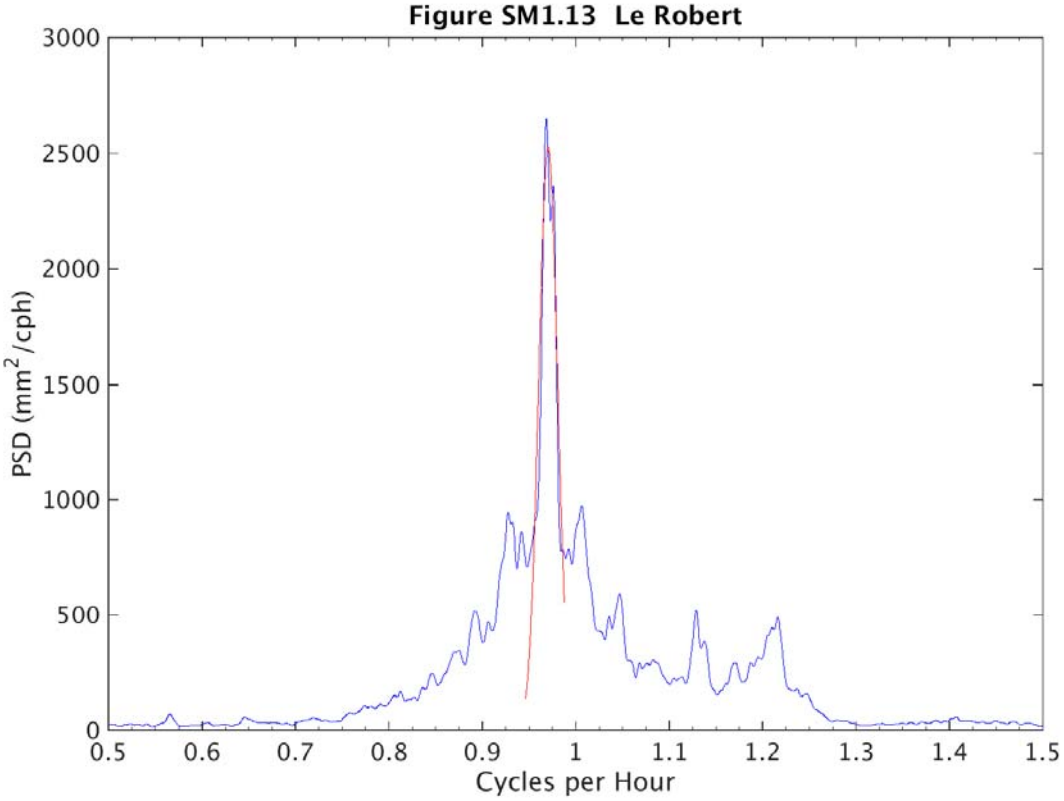

Figure SM1.14 Roseau

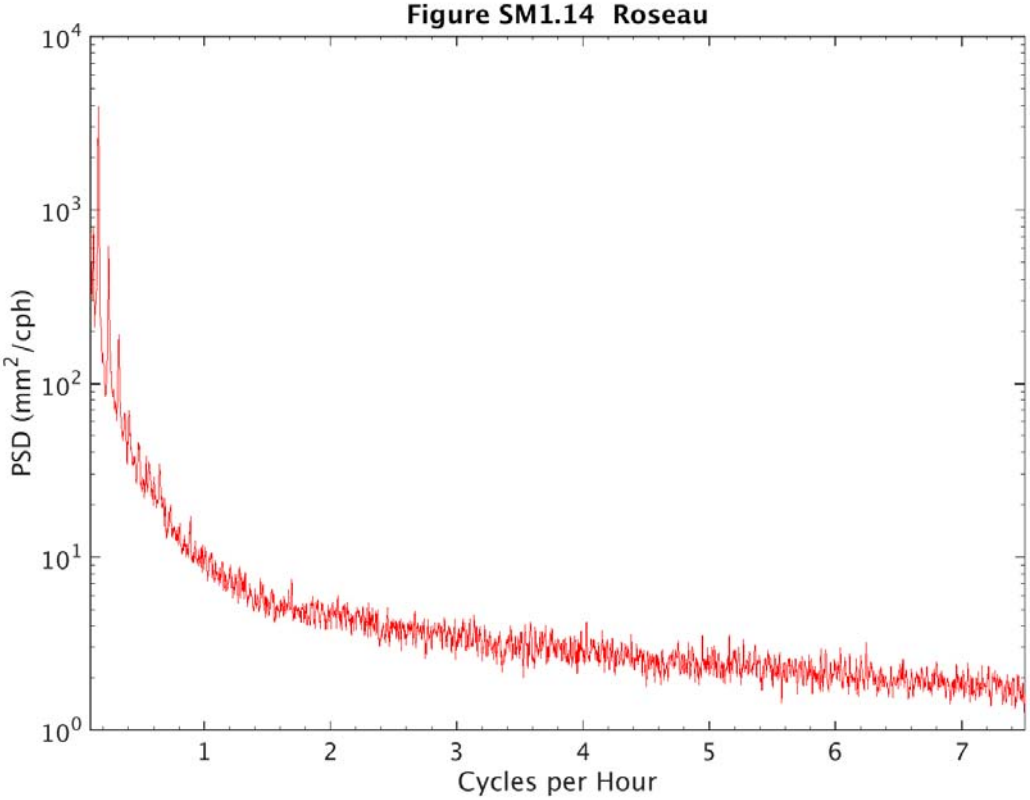

Figure SM1.15 Roseau

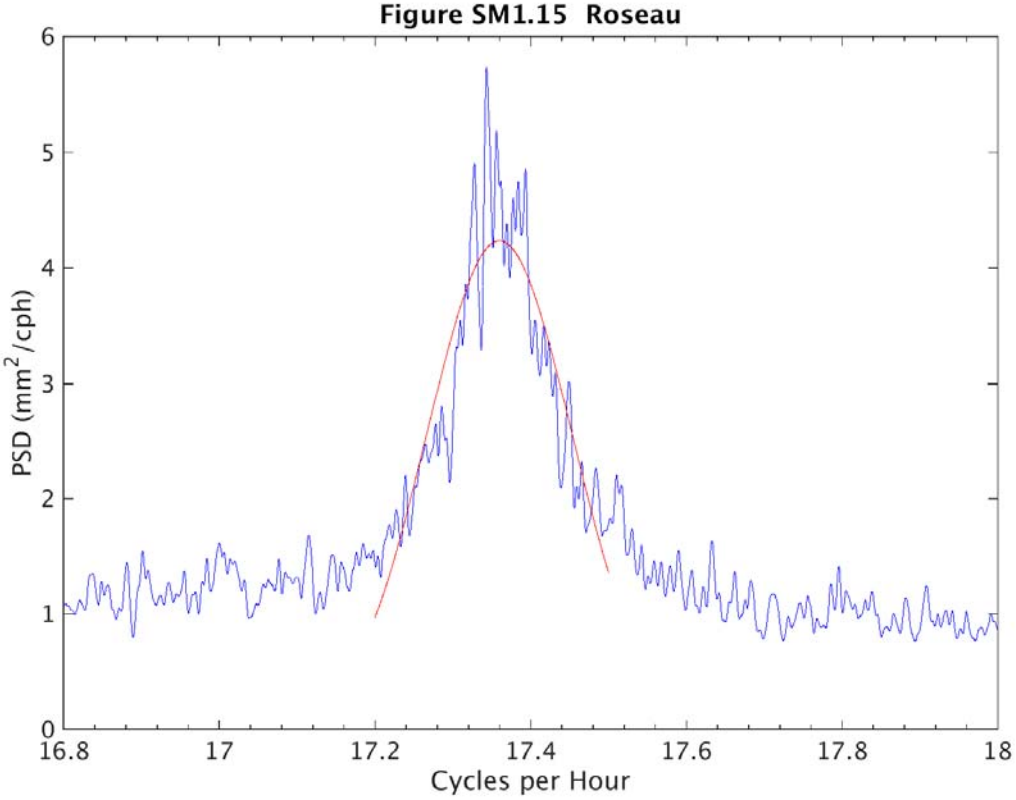

Figure SM1.16 Deshaies

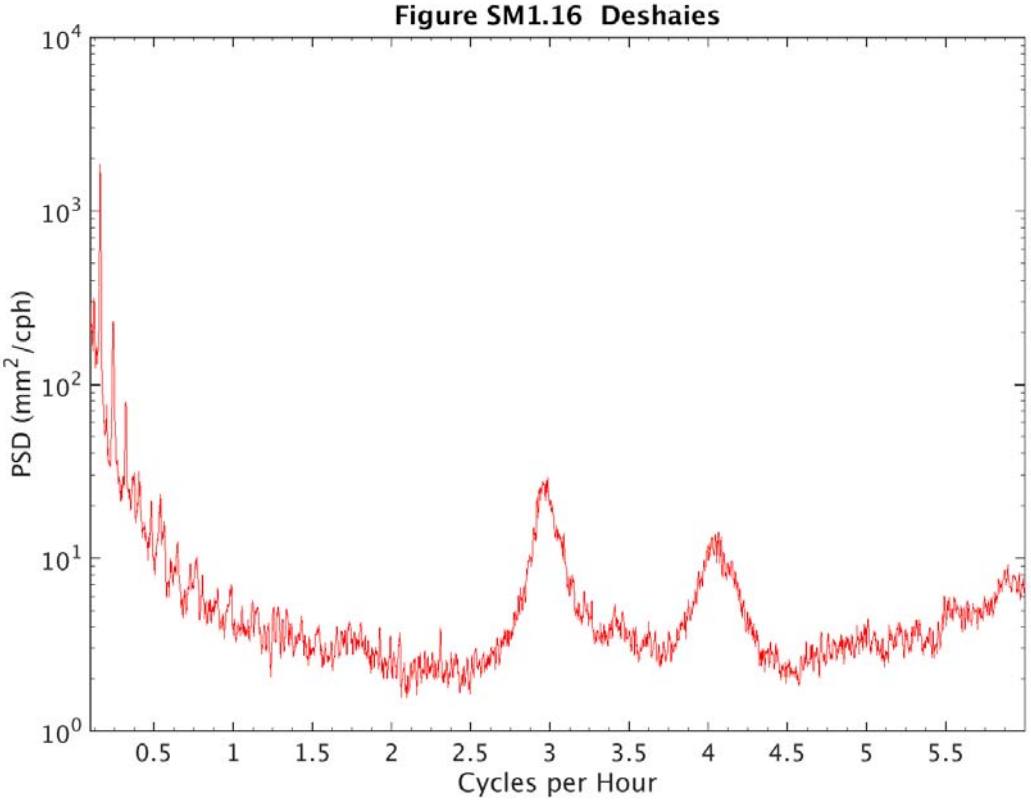

Figure SM1.17 Deshaies

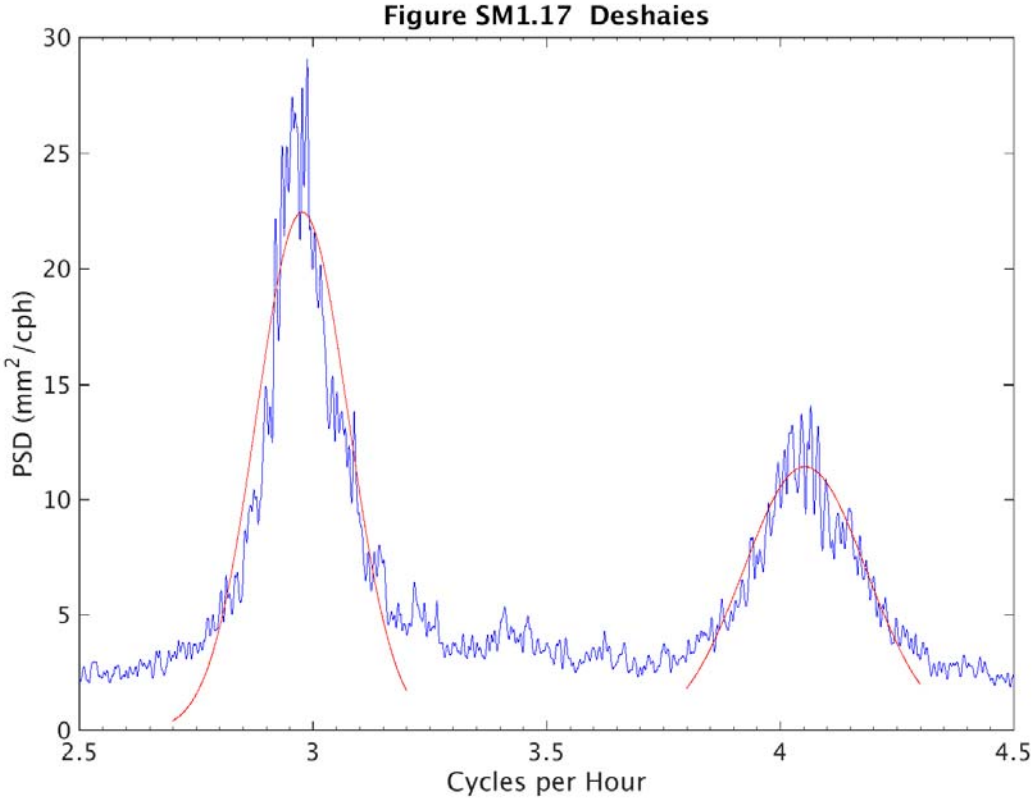

Figure SM1.18 Pointe-a-Pitre

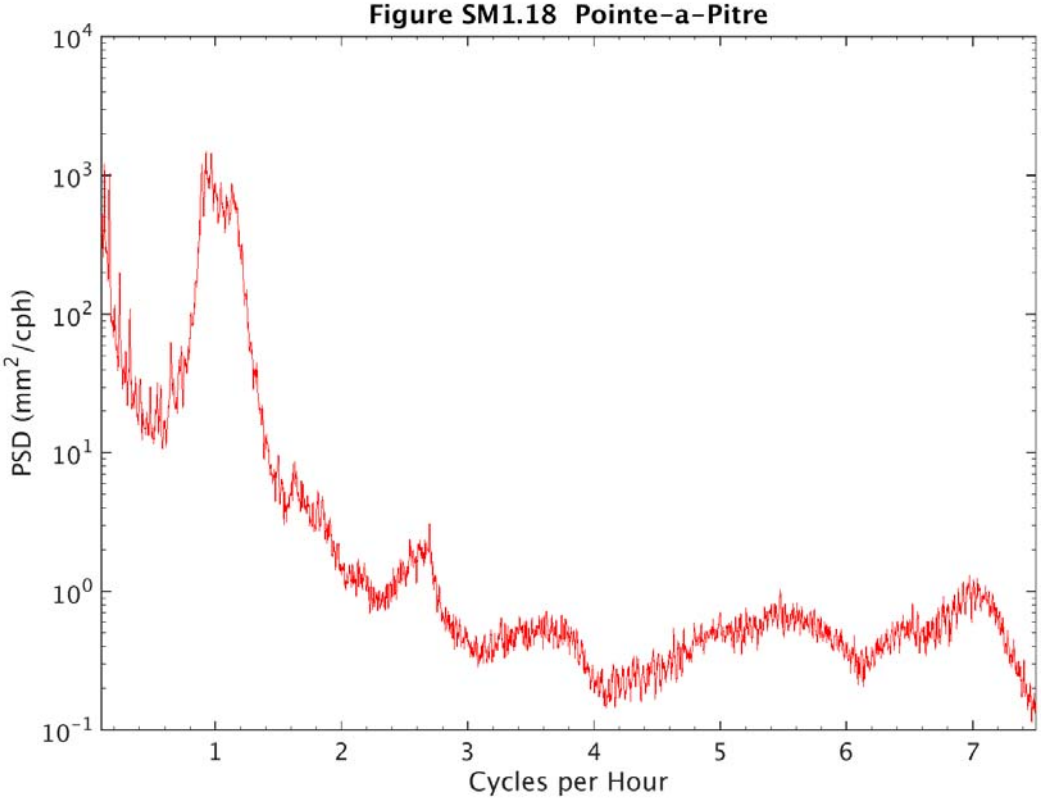

Figure SM1.19 Pointe-a-Pitre

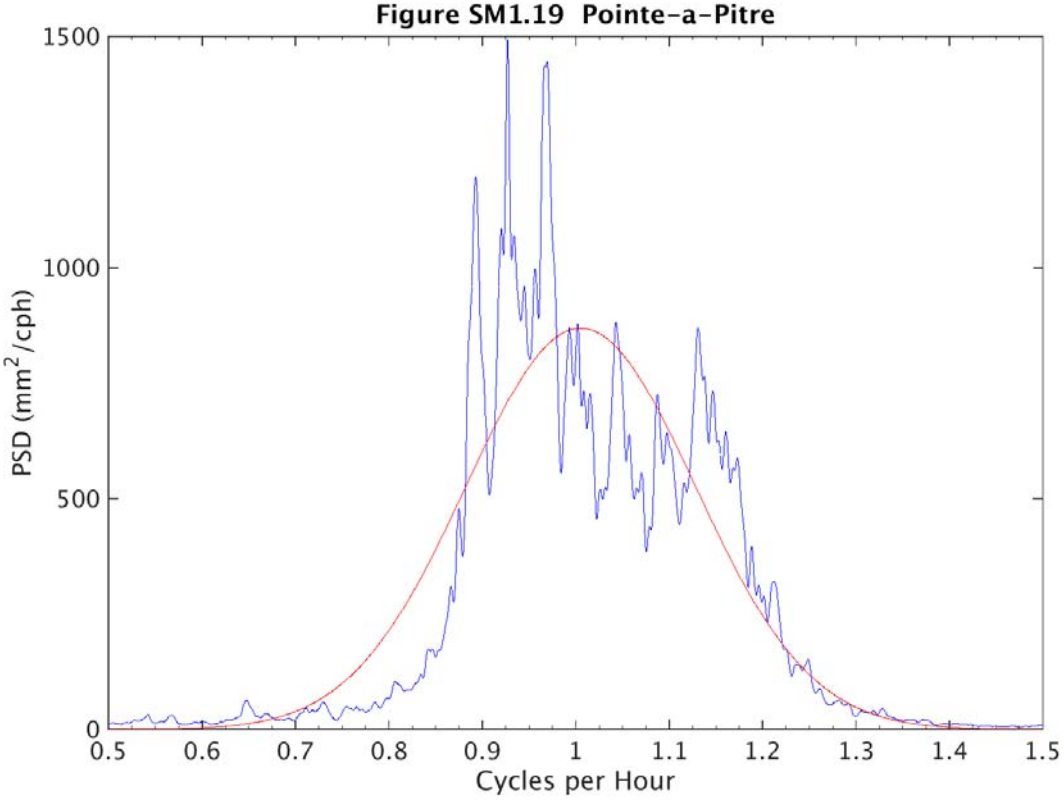

Figure SM1.20 La Desirade

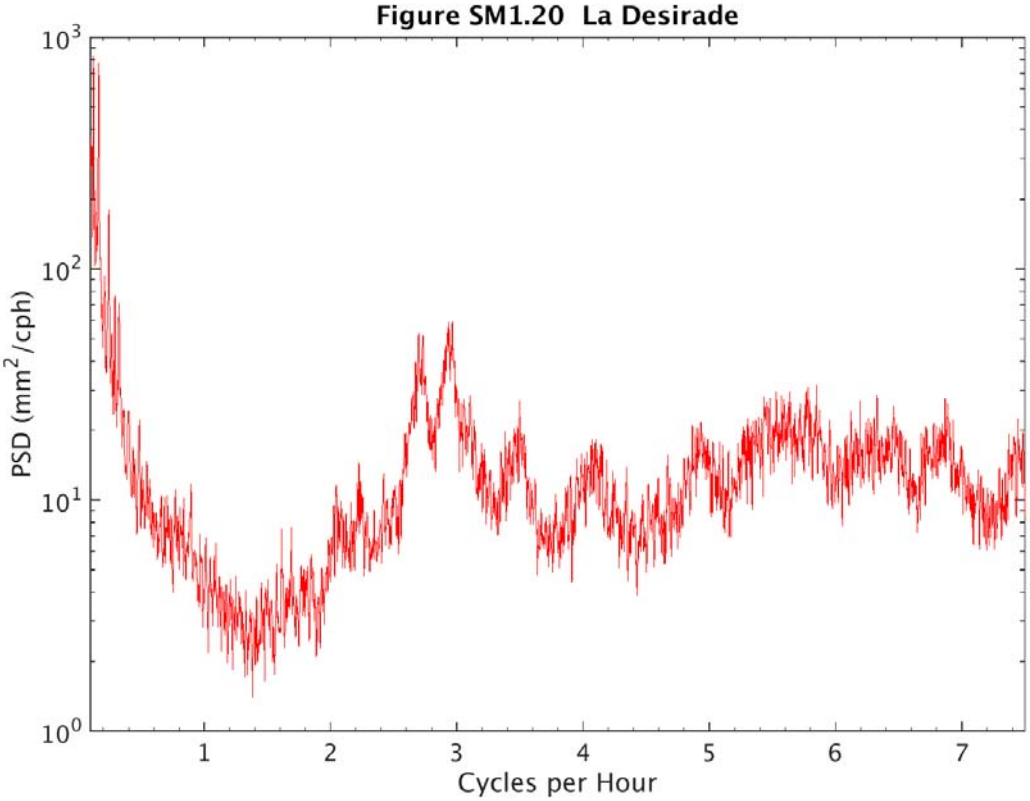

Figure SM1.21 Basseterre

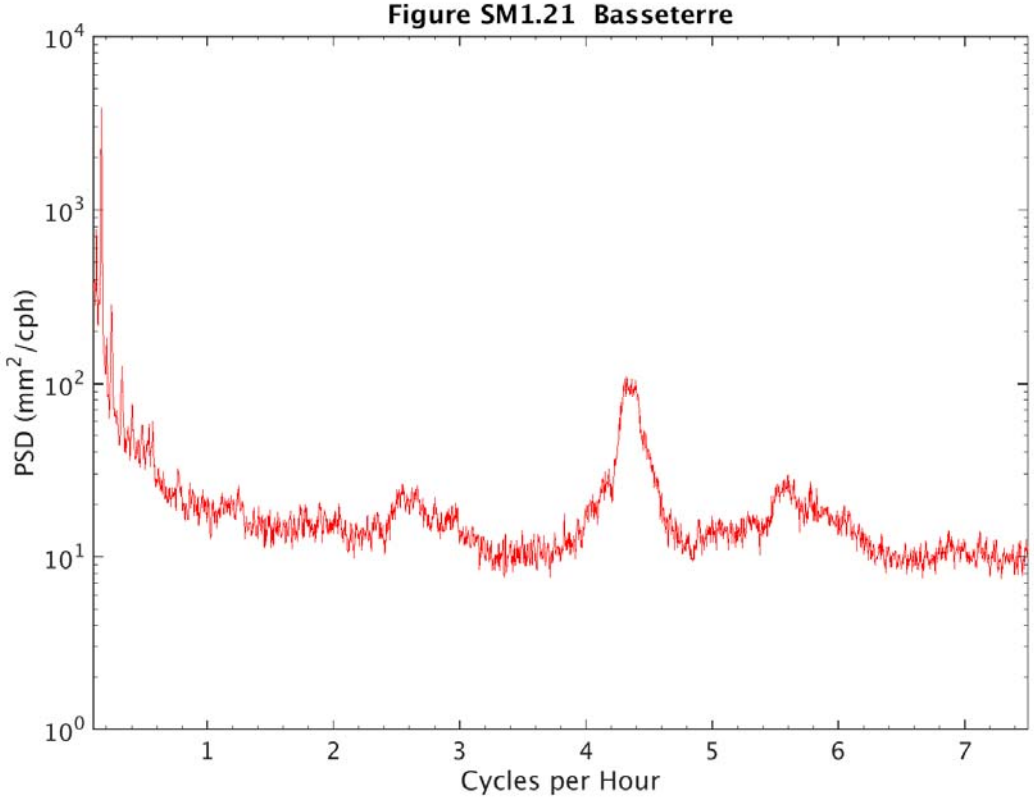

Figure SM1.22 Basseterre

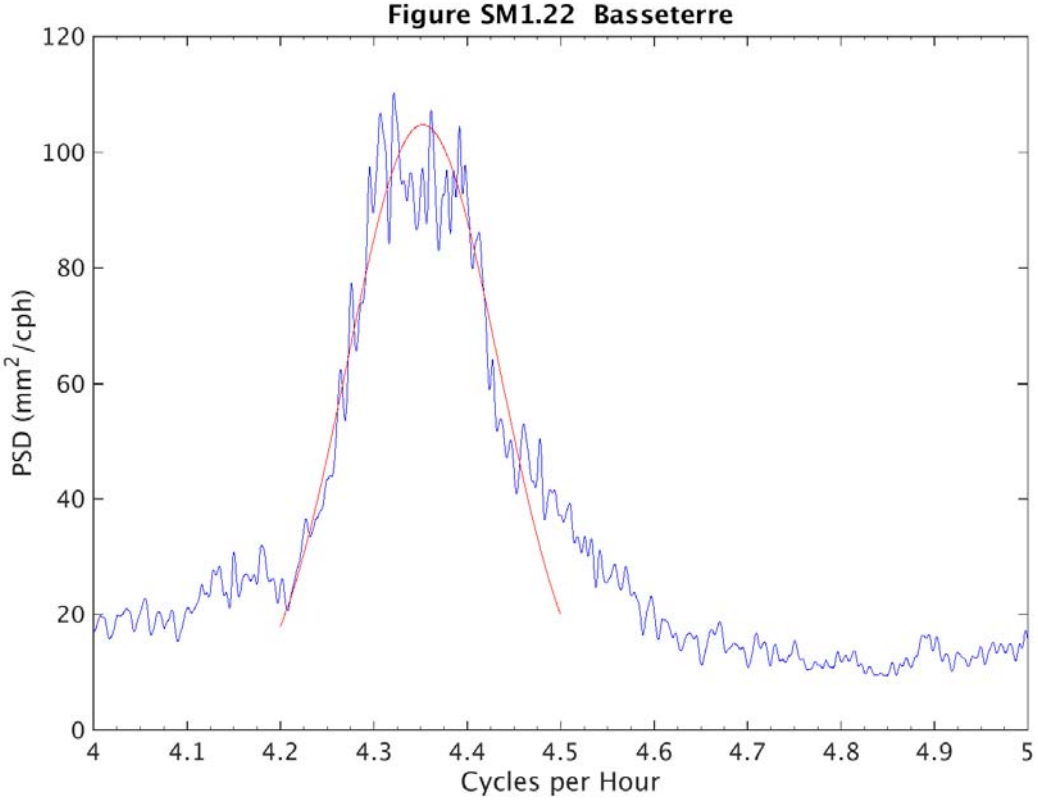

Figure SM1.23 Barbuda

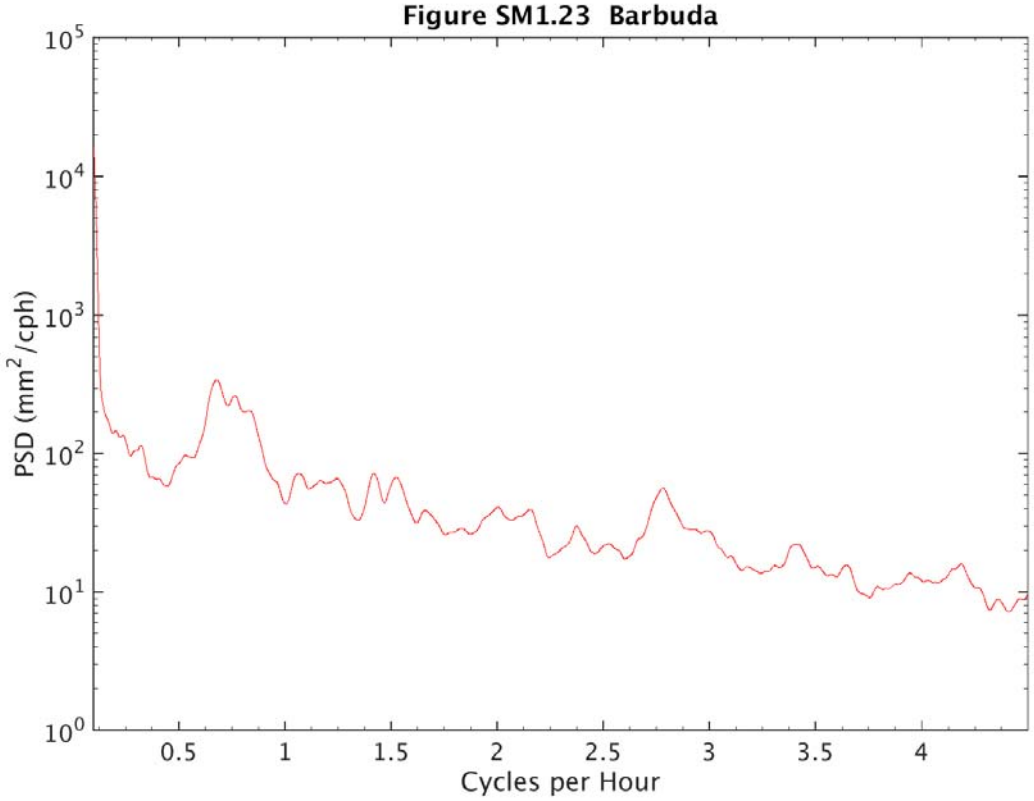

Figure SM1.24 Barbuda

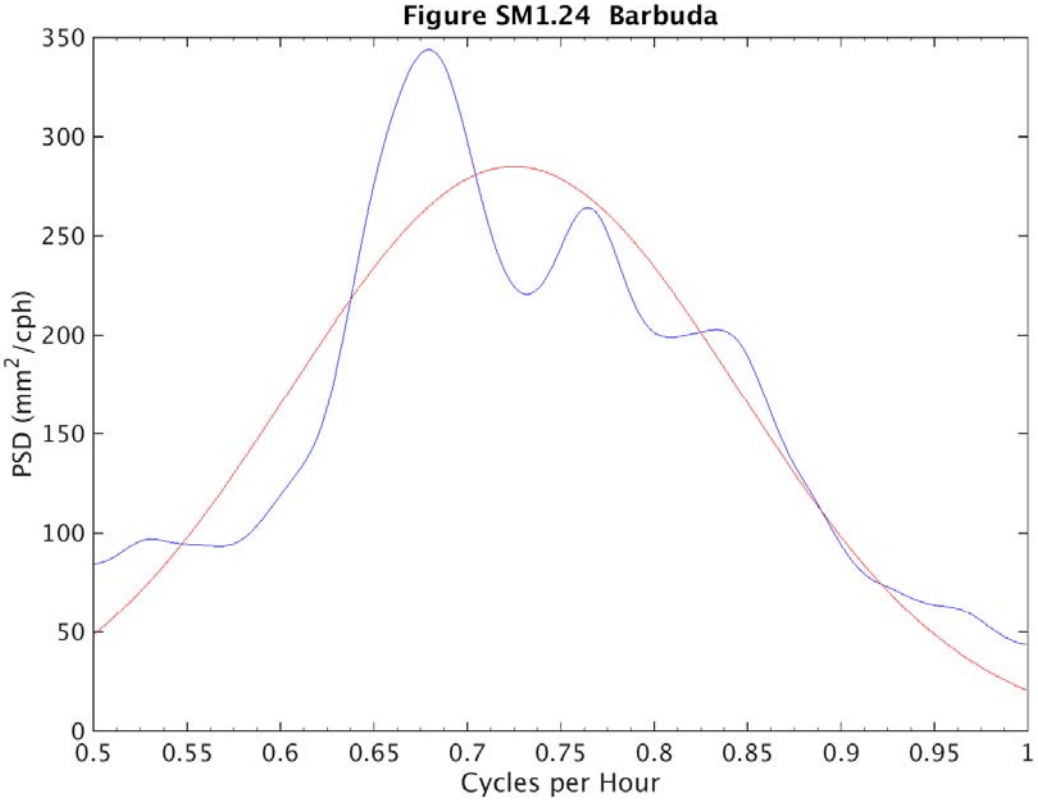

Figure SM1.25 Saint Martin

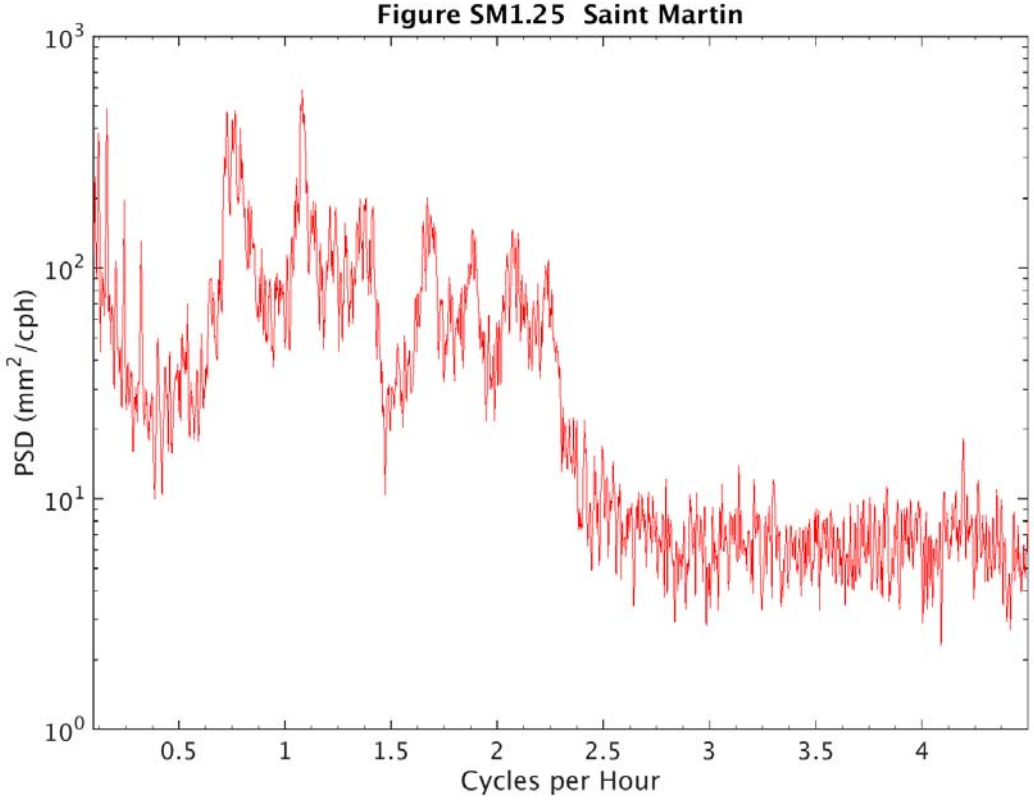

Figure SM1.26 Lime Tree Bay

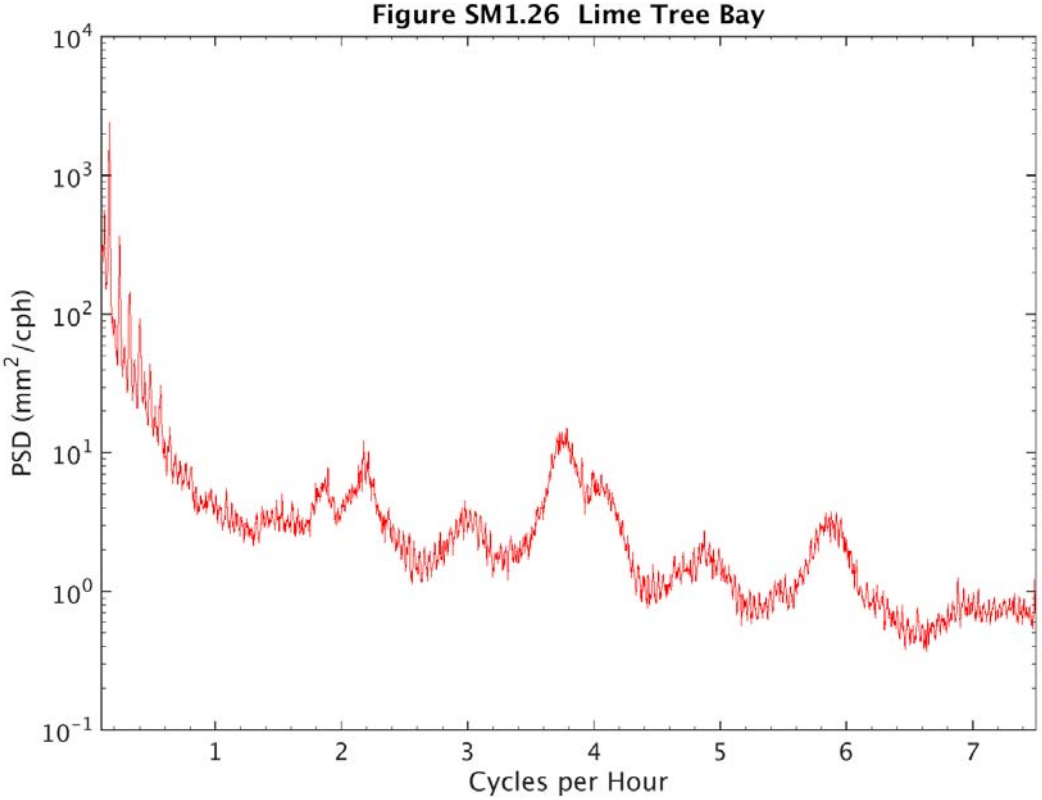

Figure SM1.27 St. Croix

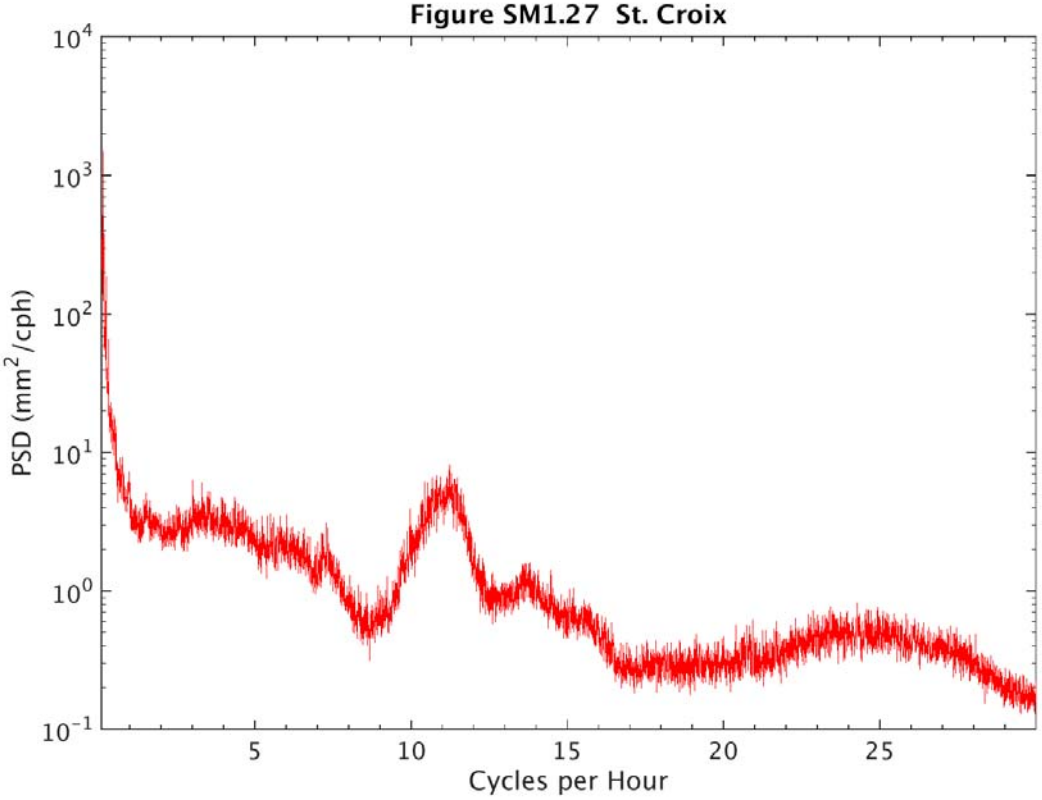

Figure SM1.28 St. Croix

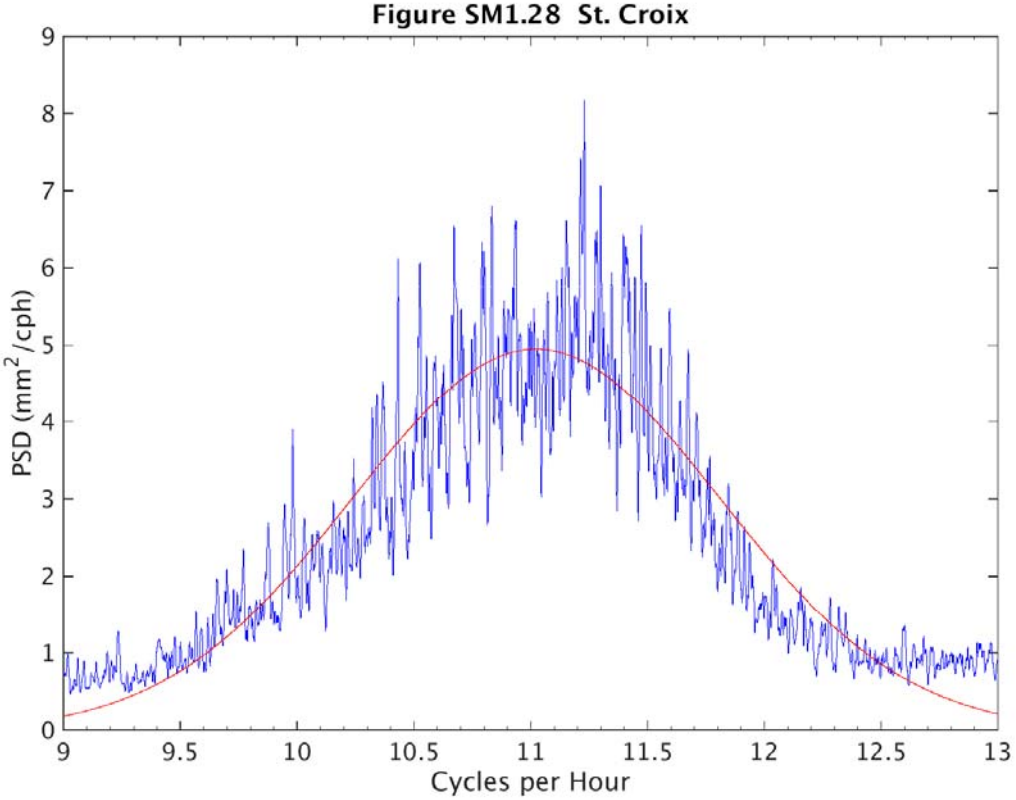

Figure SM1.29 Charlotte Amalie

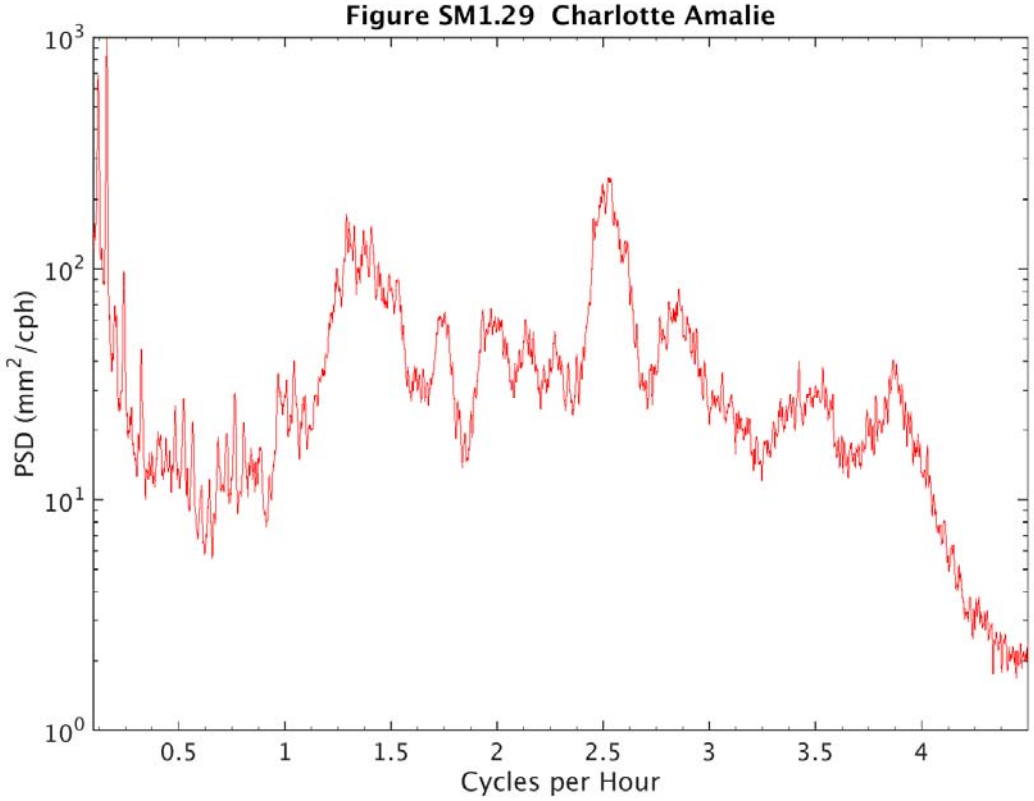

Figure SM1.30 Charlotte Amalie

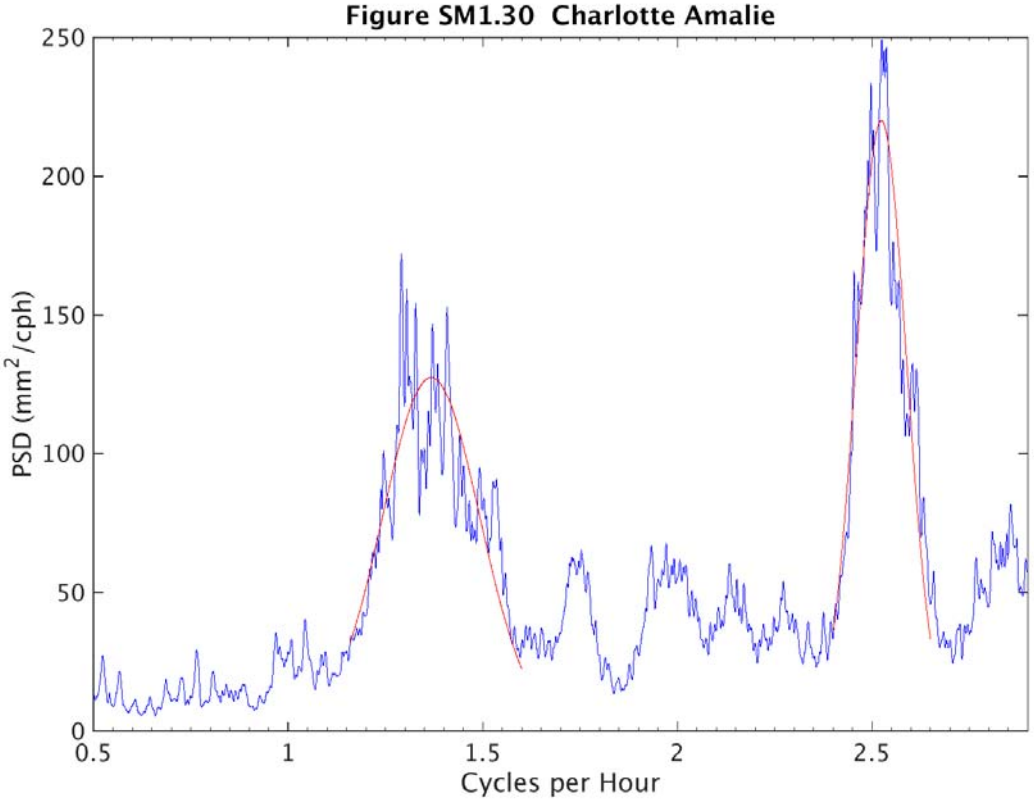

Figure SM1.31 Lameshur Bay

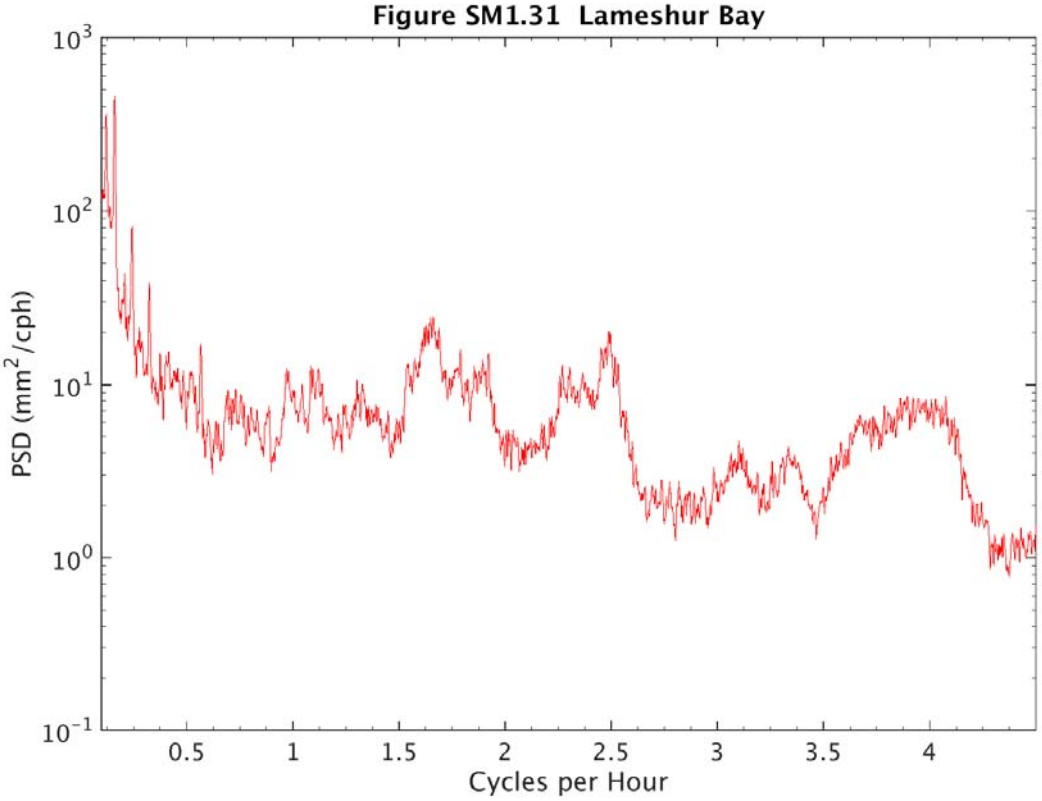

Figure SM1.32 Tortola

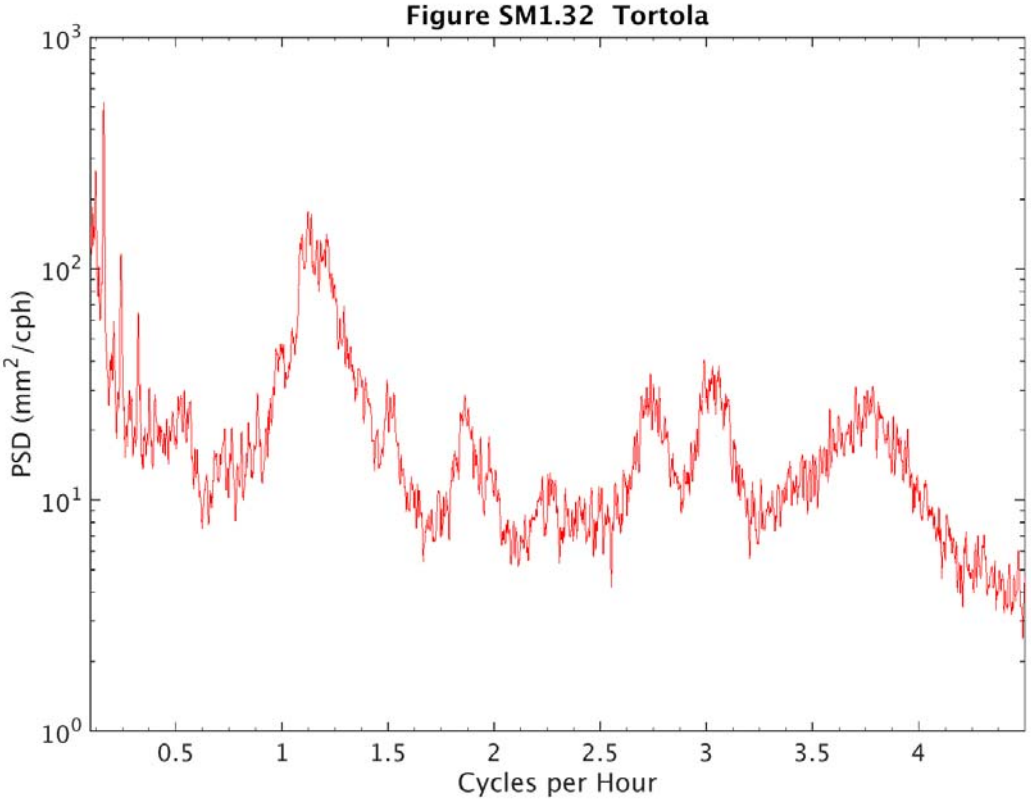

Figure SM1.33 Tortola

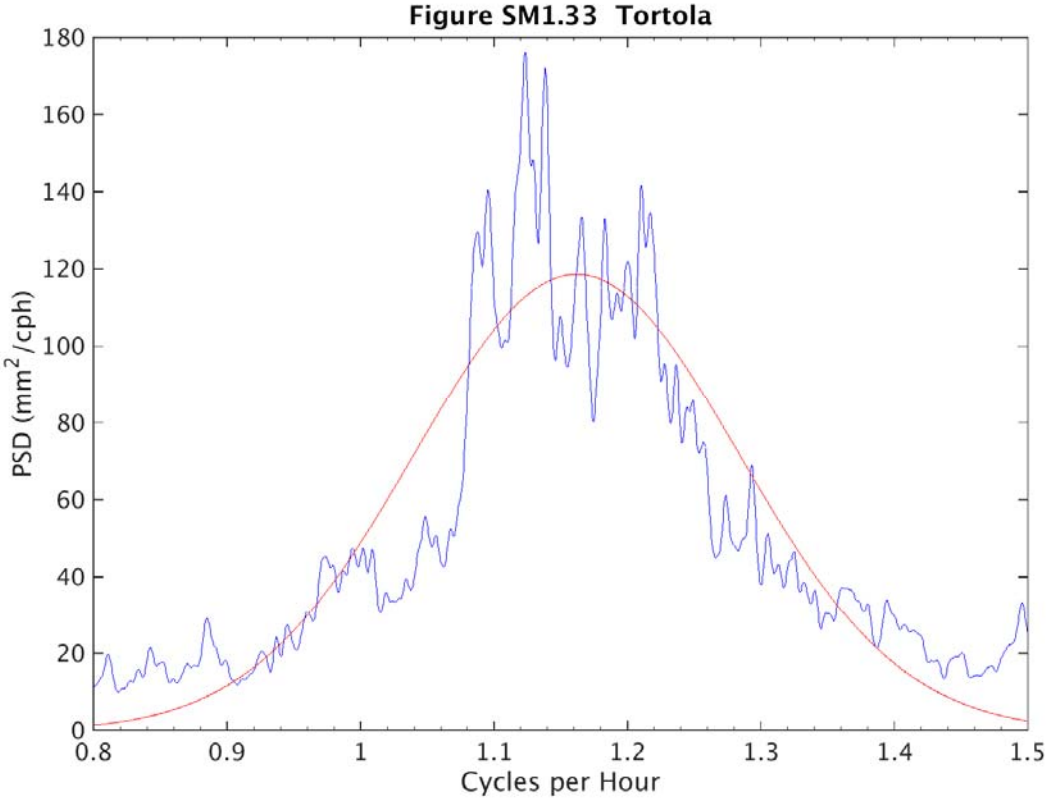

Figure SM1.34 Magueyes Island

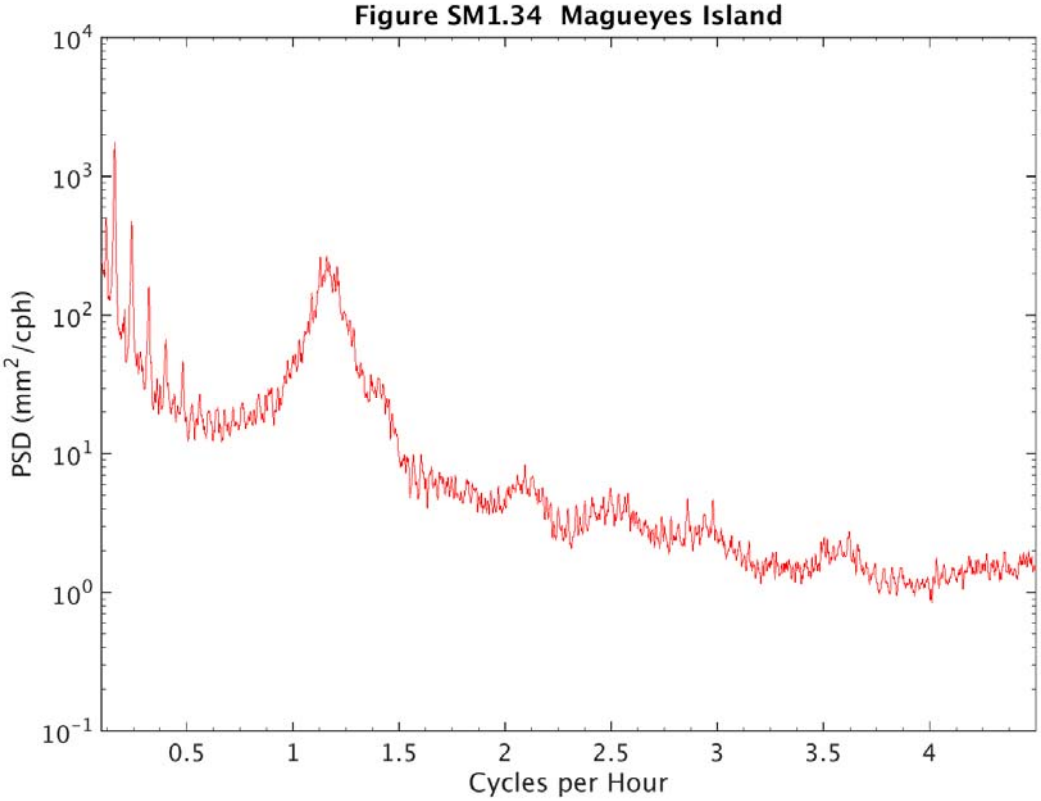

Figure SM1.35 Magueyes Island

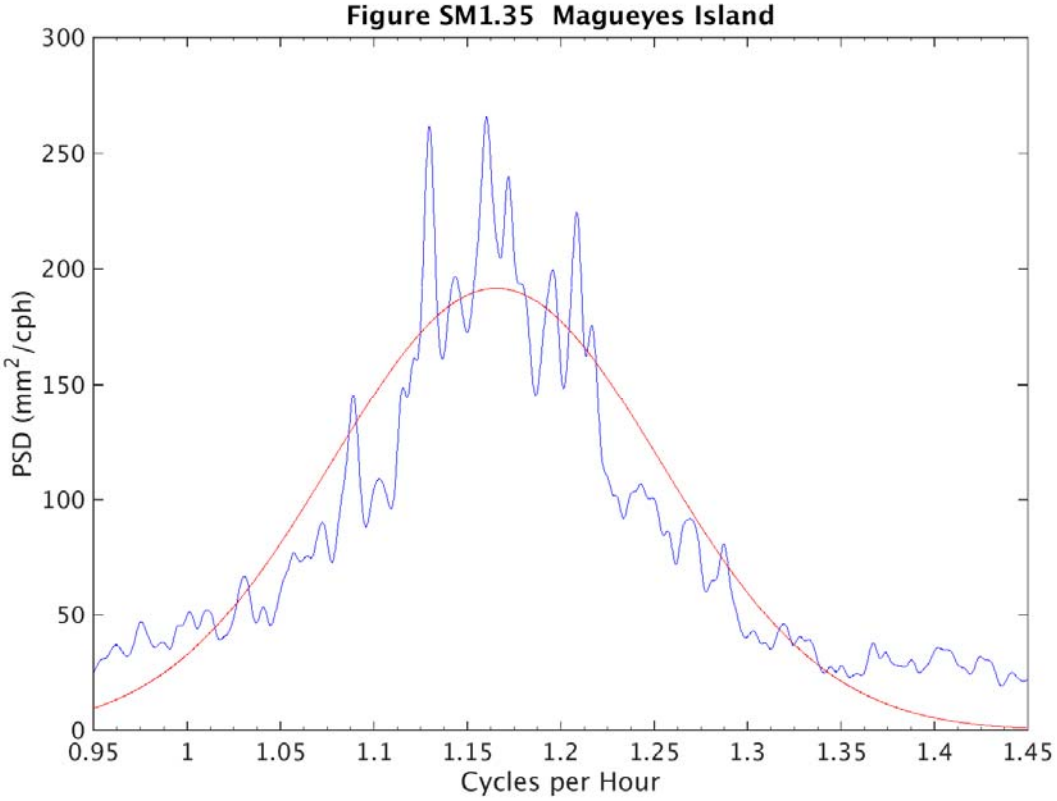

Figure SM1.36 Mayaguez

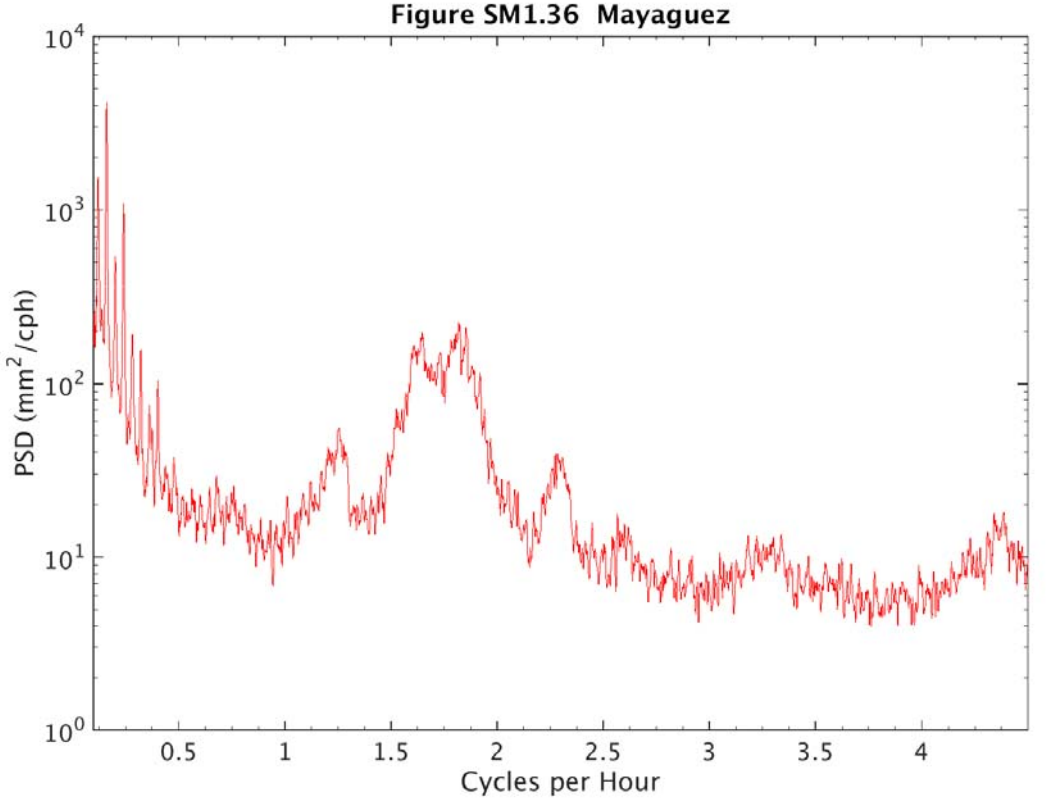

Figure SM1.37 Mayaguez

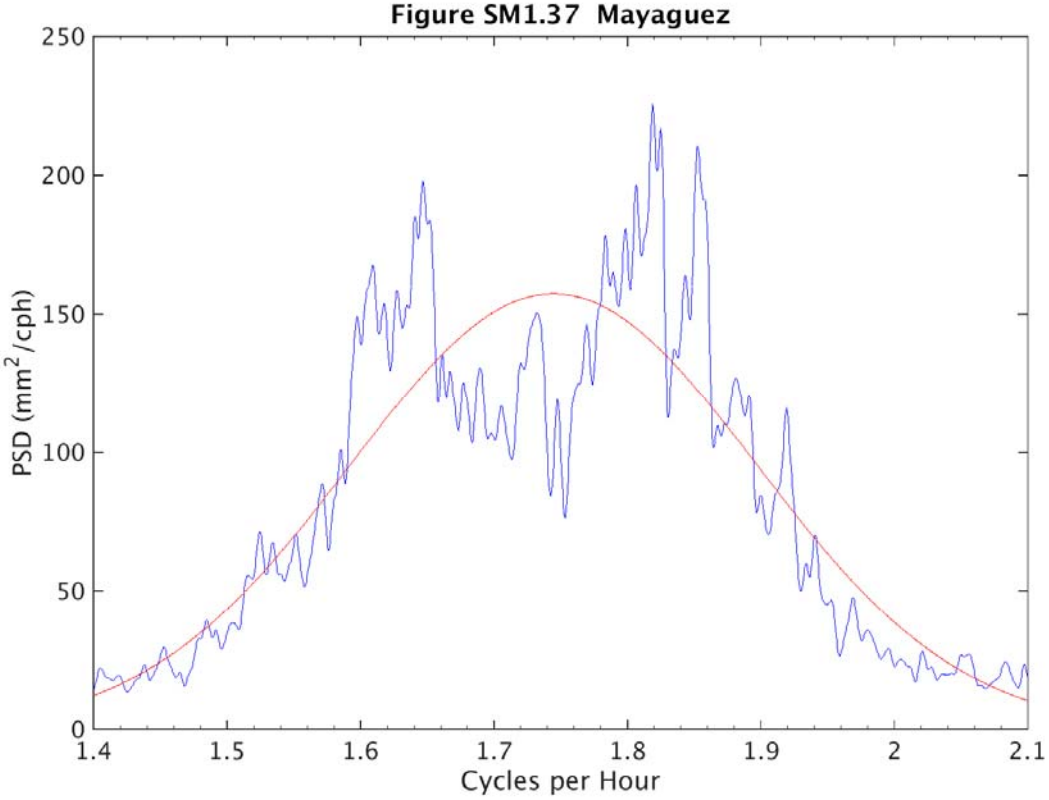

Figure SM1.38 Caja de Muertos

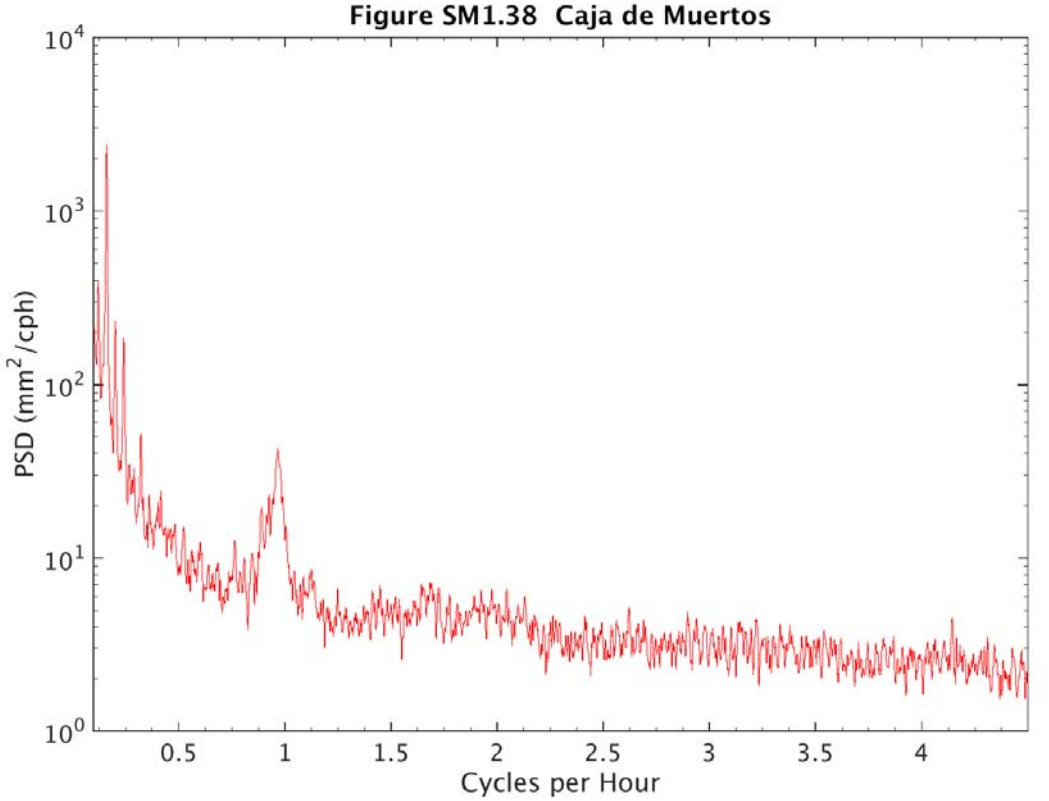

Figure SM1.39 Caja de Muertos

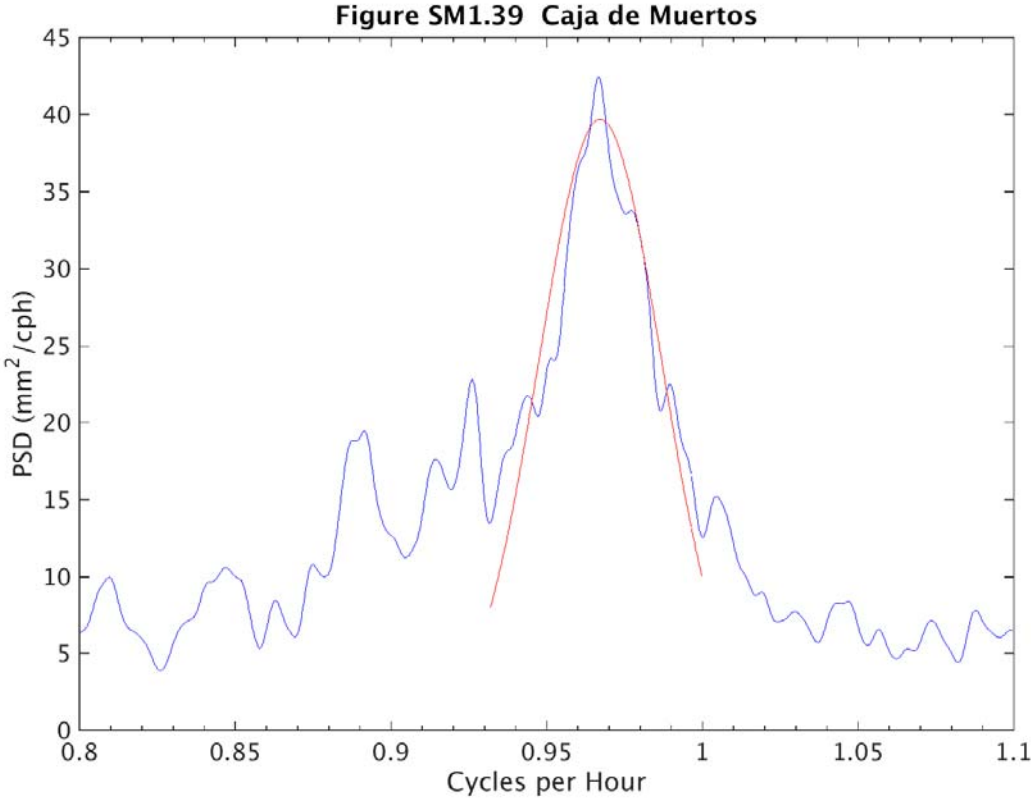

Figure SM1.40 Yabucoa Harbor

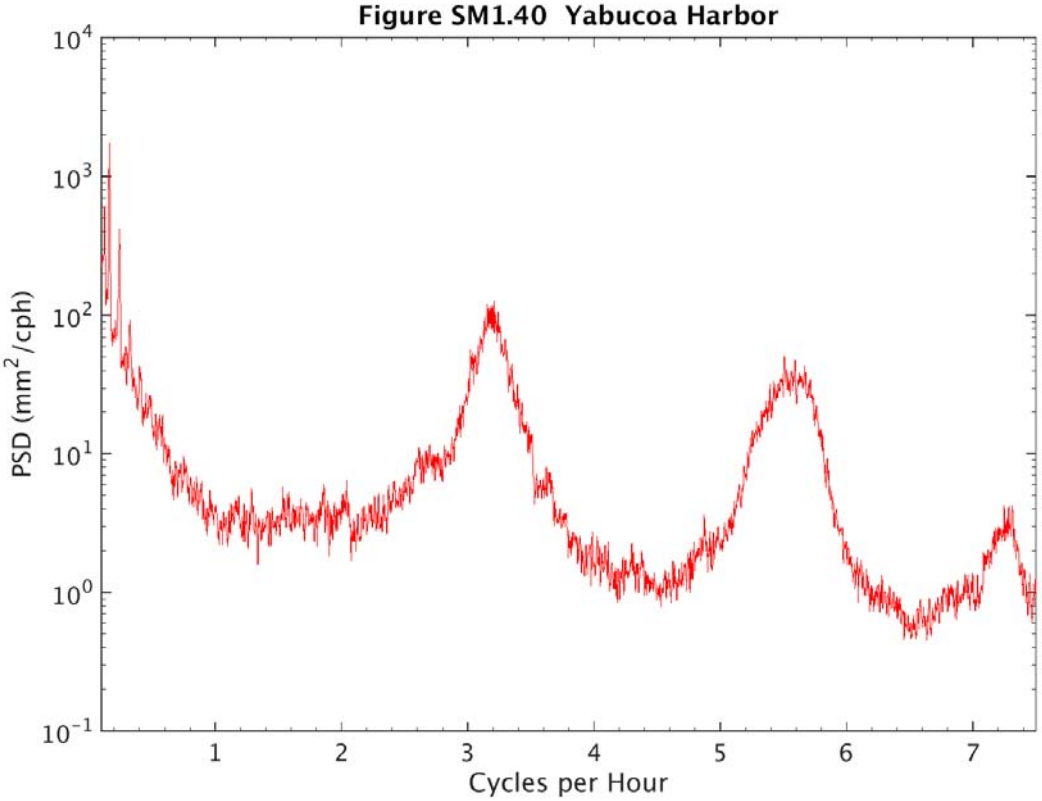

Figure SM1.41 Yabucoa Harbor

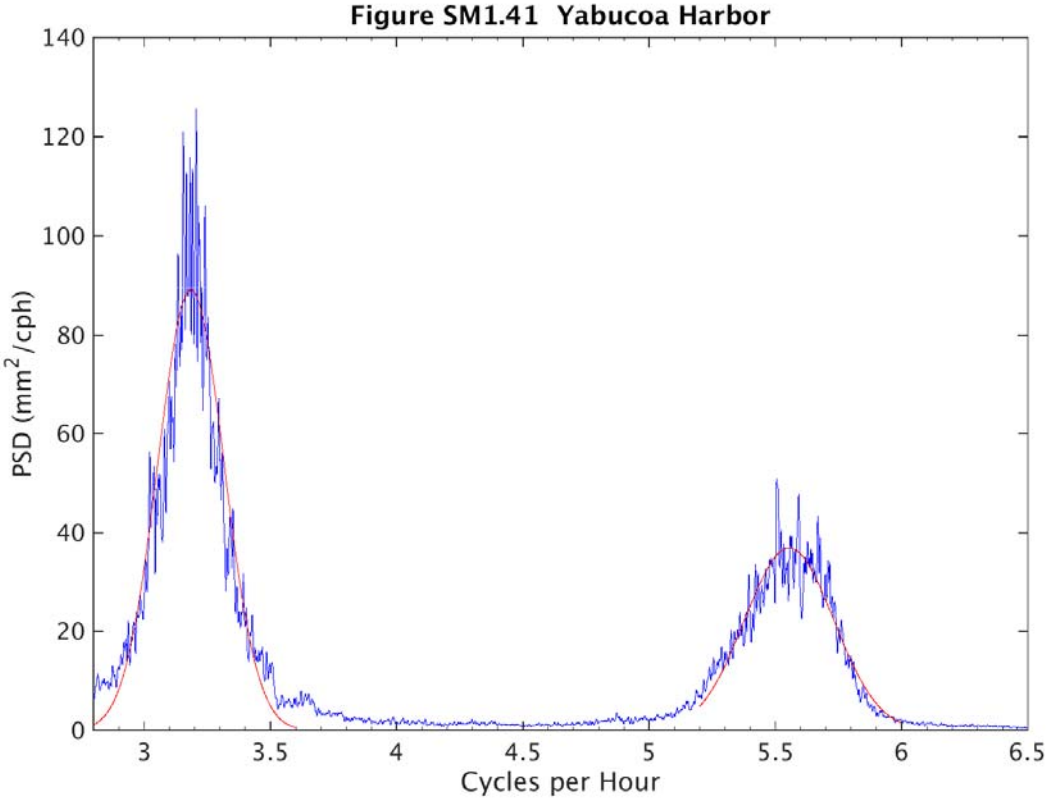

Figure SM1.42 Vieques

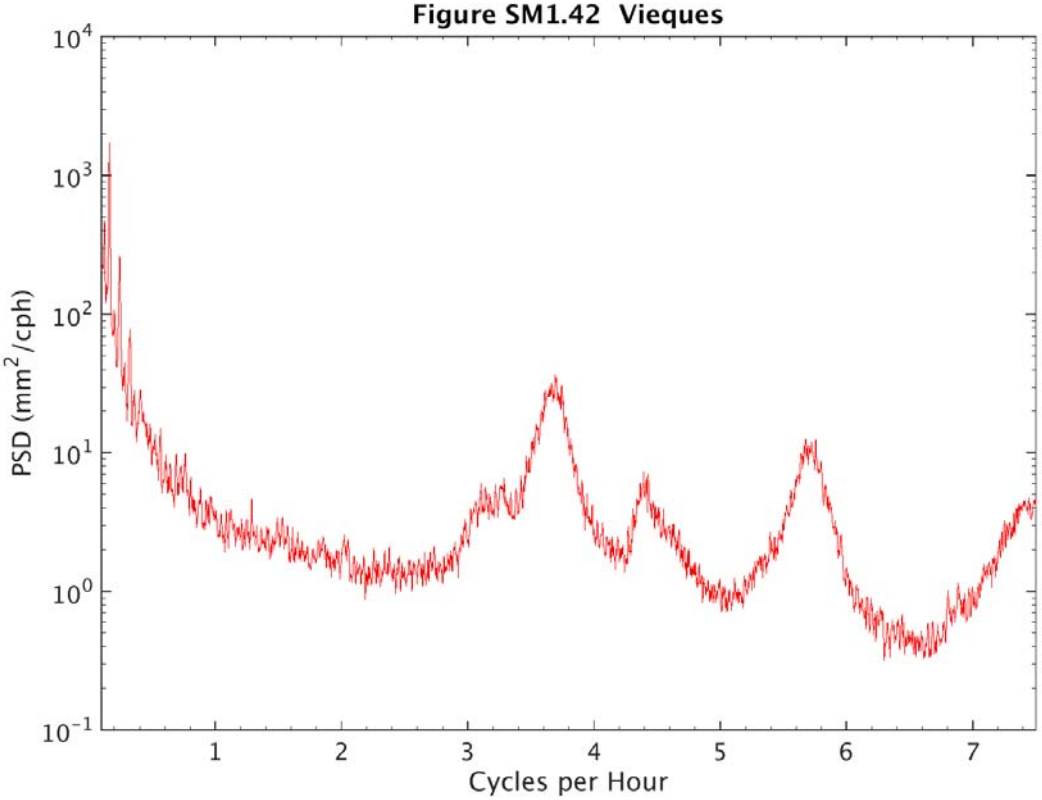

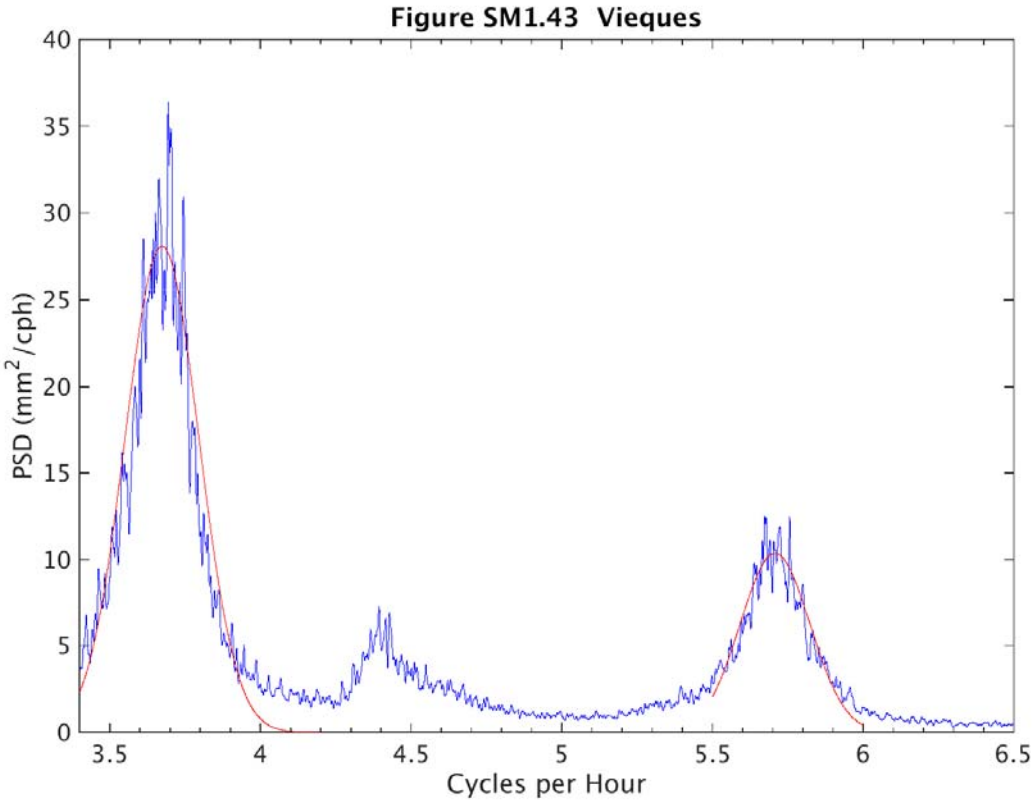

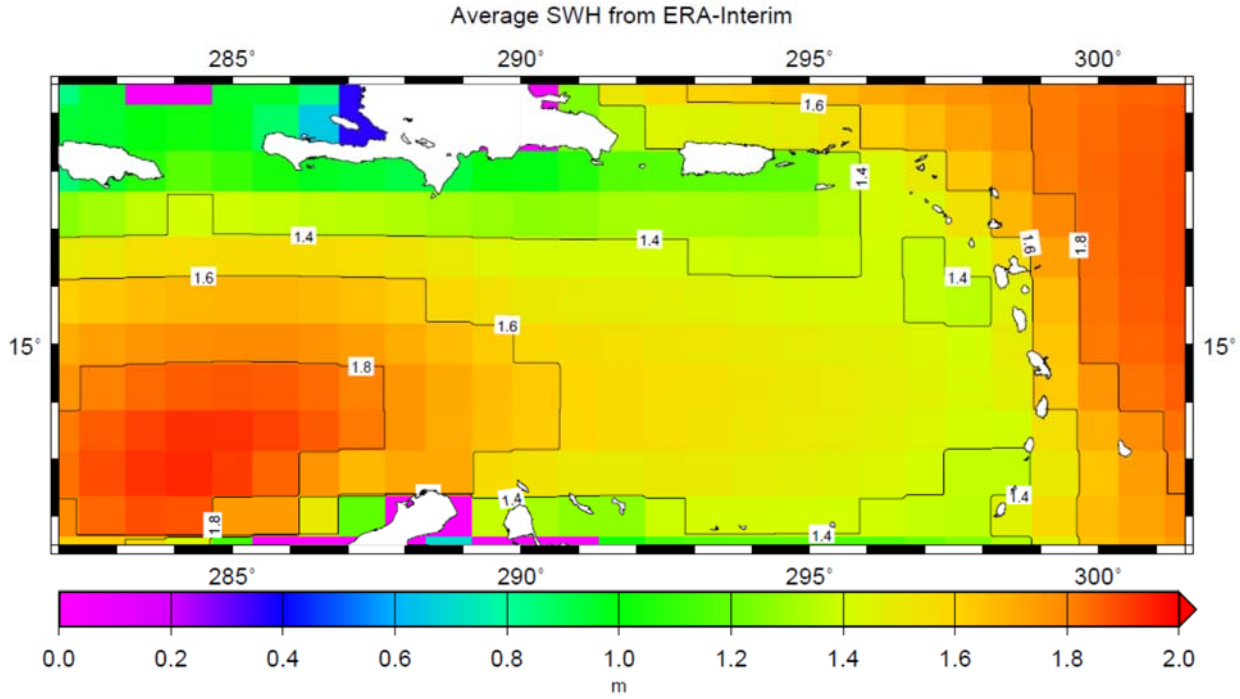

Figure SM2.1 (a) Average significant wave height (SWH) in metres from ERA-Interim during 2015-16.

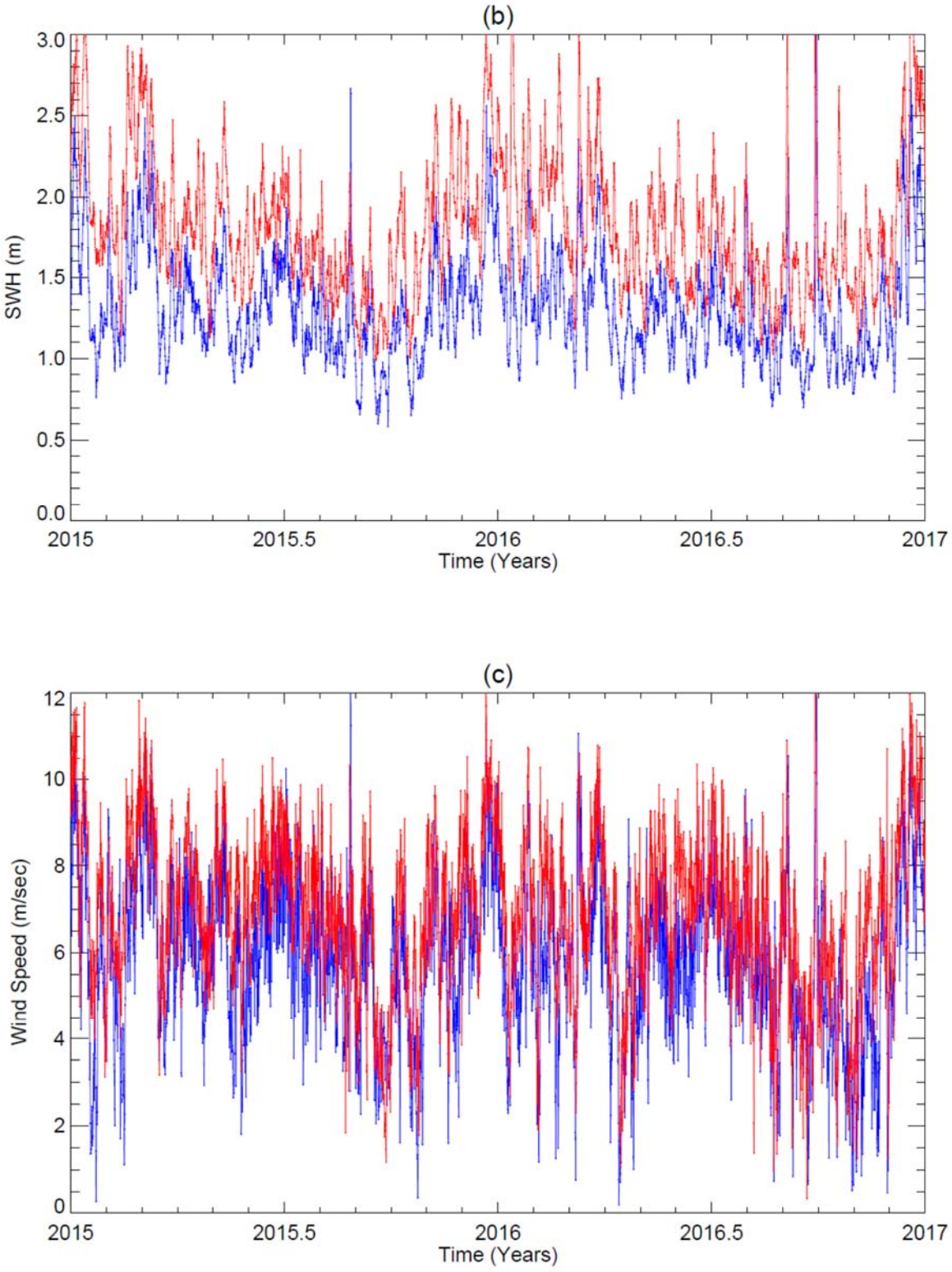

Figure SM2.1 (b,c) Time series of ERA-Interim SWH and 10-m wind speed respectively at points one degree south of Charlotte Amalie (blue) and one degree east of Le Robert (red).

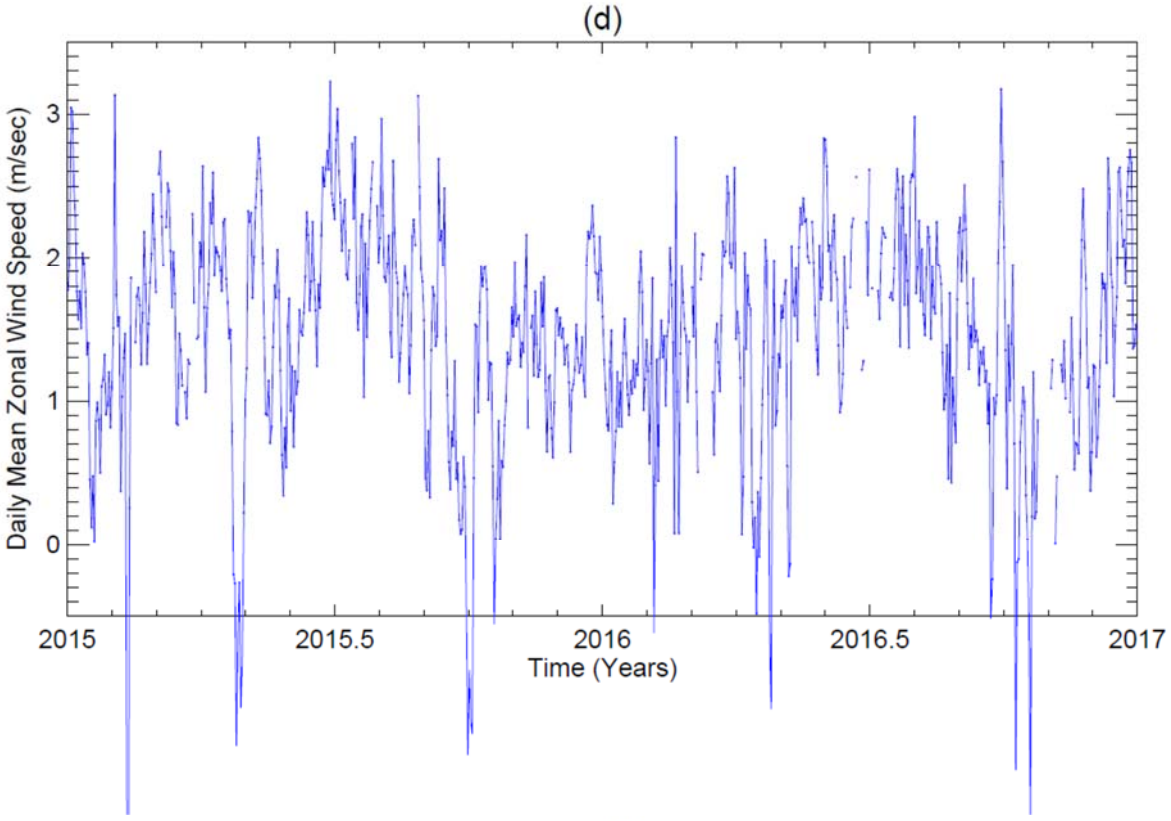
(d)
Daily Mean Zonal Wind Speed (m/sec)
3
2
1
0
2015
2015.5
2016
2016.5
2017
Time (Years)

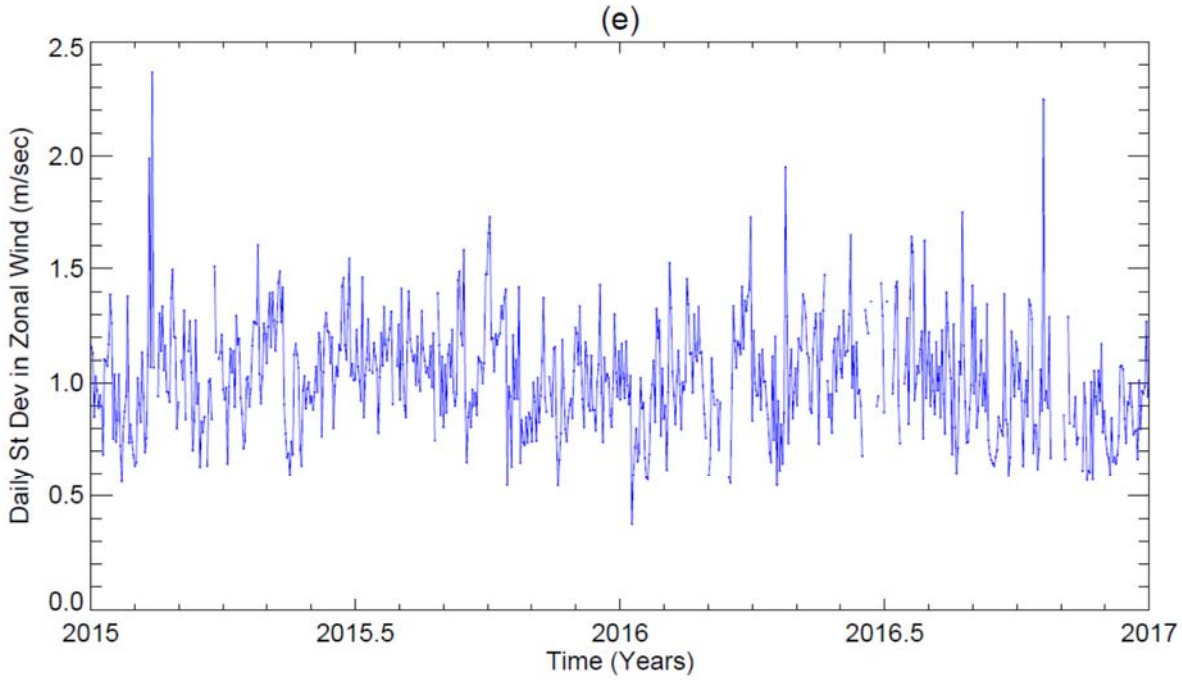
(e)
Daily St Dev in Zonal Wind (m/sec)
2.5
2.0
1.5
1.0
0.5
0.0
2015
2015.5
2016
2016.5
2017
Time (Years)

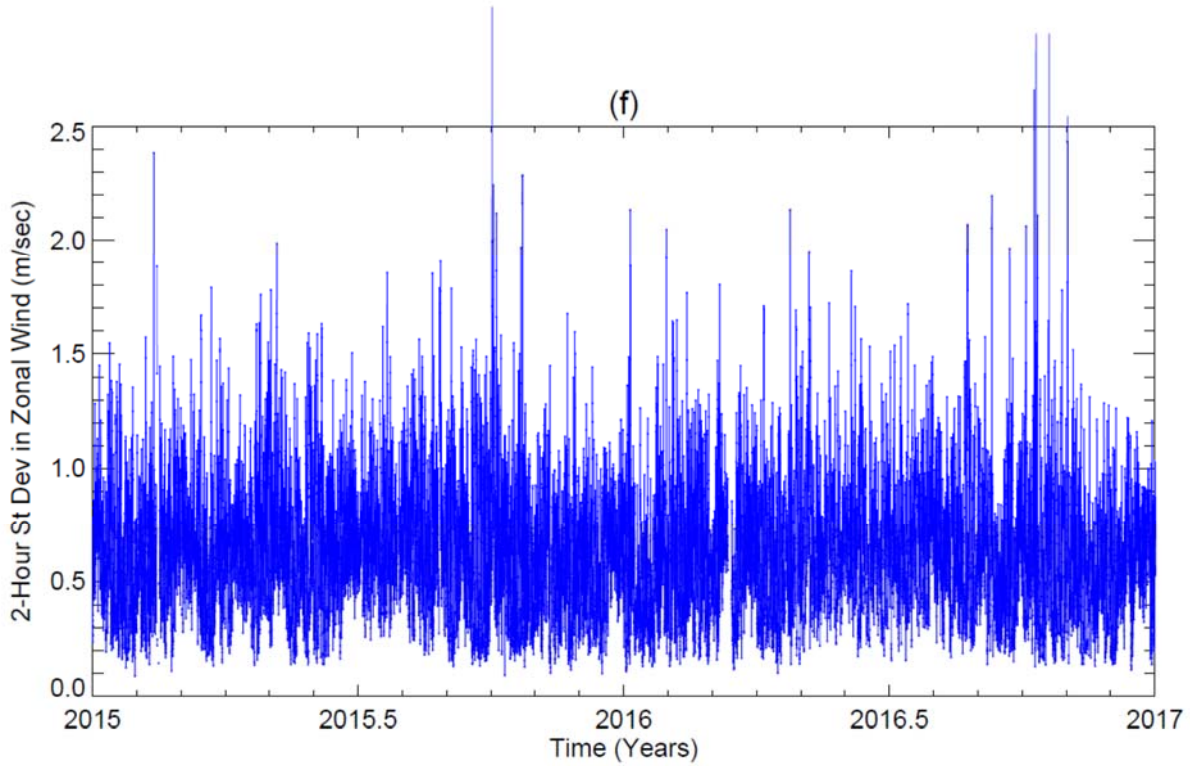

Figure SM2.1 (d) Daily mean zonal wind speed (m/sec) from the meteorological station at Charlotte Amalie. (e) Standard deviation of 6-minute zonal wind speed at Charlotte Amalie during each day. (f) Standard deviation of 6-minute zonal wind speed within 2-hour windows centred on each hour.

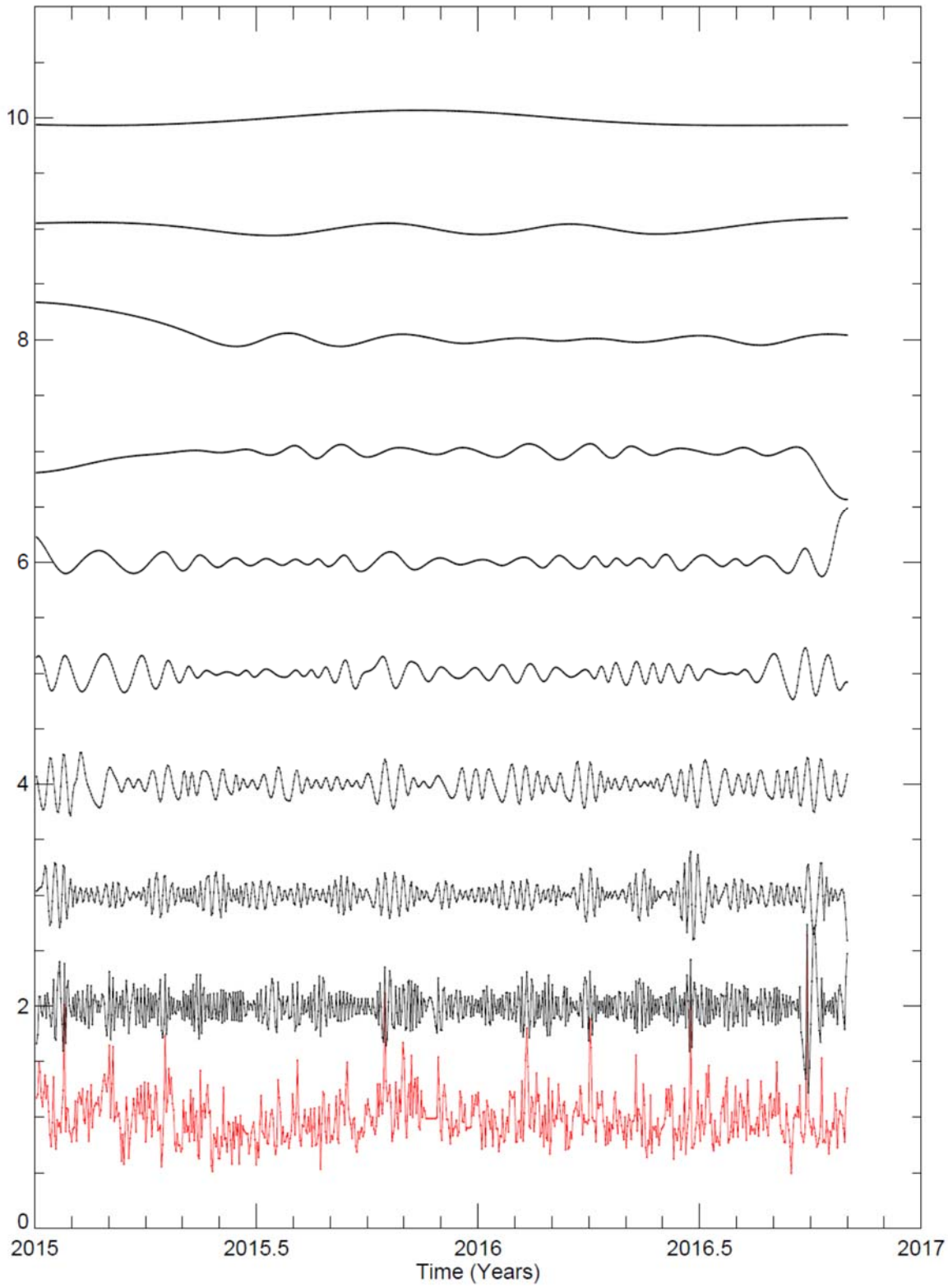

Figure SM3.1 (a) The record of σ_n for Le Robert (red), decomposed into intrinsic mode functions (IMFs) with average periods 3, 6, 11, 20, 30, 67, 191, 223 and 669 days shown bottom to top. Each IMF is offset by 1 unit for plotting.

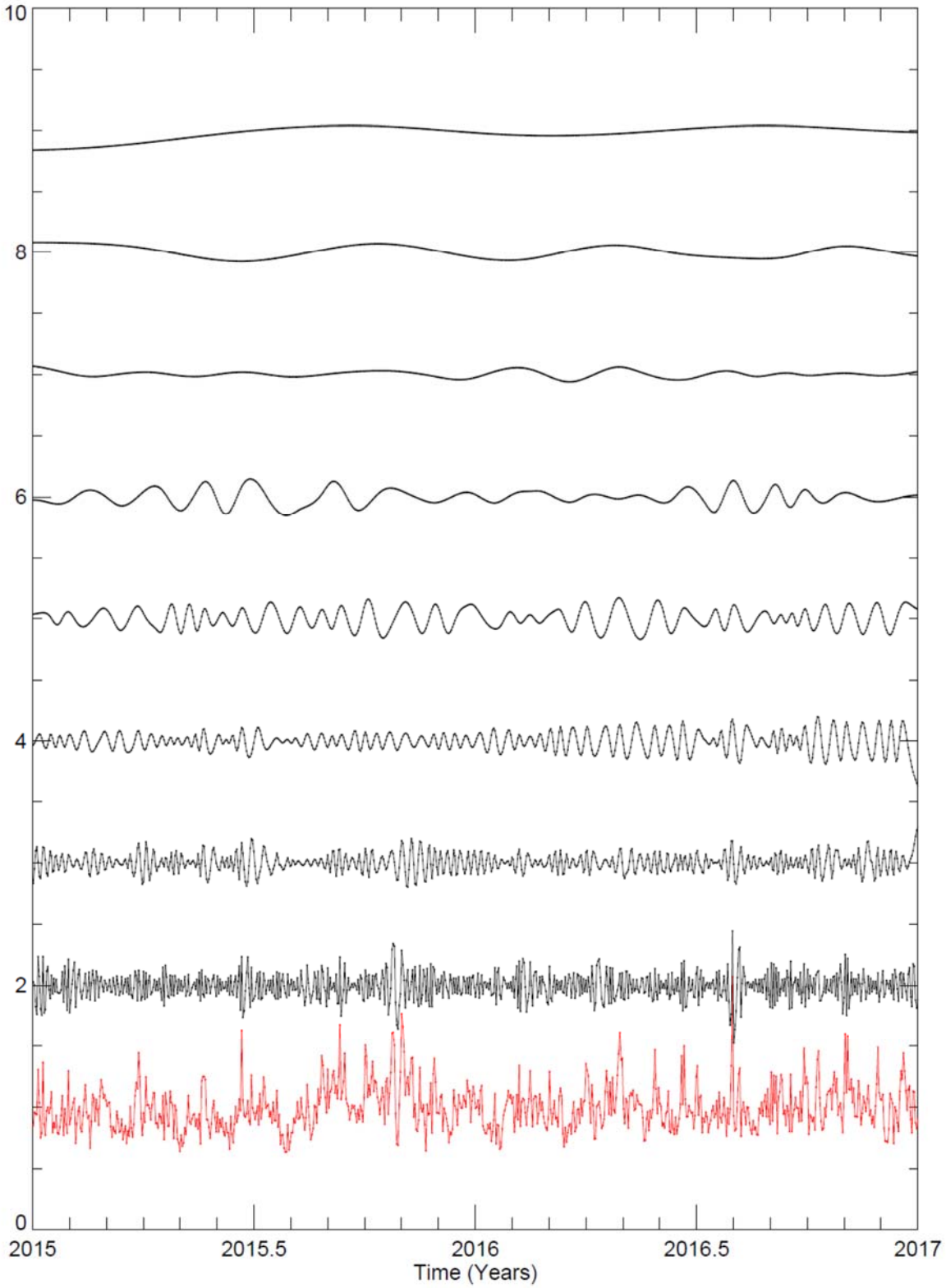

Figure SM3.1 (b) The corresponding average record of σ_n for the northern group, decomposed into IMFs with average periods 3, 6, 10, 22, 47, 81, 209 and 487 days shown bottom to top. Each IMF is offset by 1 unit for plotting.

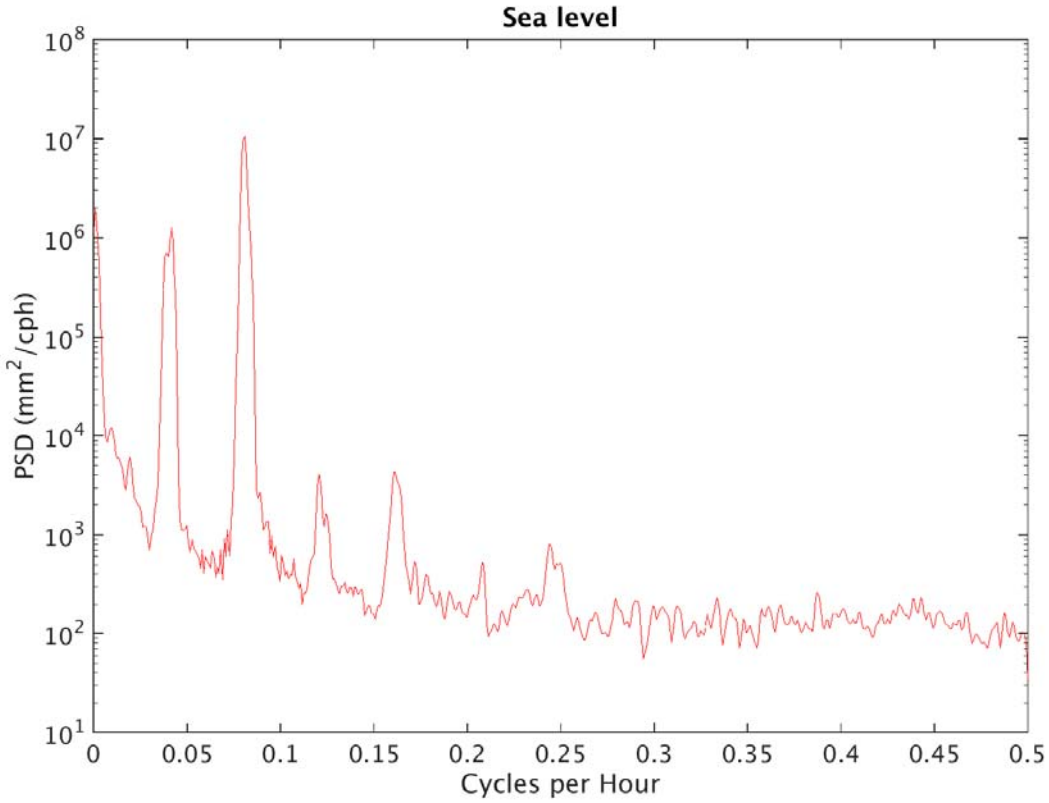

Figure SM4.1 Power spectral density (PSD) from Bridgetown, Barbados obtained from 6 months of hourly data from 1995 provided by the University of Hawaii Sea Level Center.